The primordial origin and dynamical sculpting of close-in planetary system architectures

Thesis by

Christopher Spalding

In Partial Fulfillment of the Requirements for the
degree of
Doctor of Philosophy in Planetary Science

CALIFORNIA INSTITUTE OF TECHNOLOGY
Pasadena, California

2018
Defended February 13, 2018

Christopher Spalding
ORCID: 0000-0001-9052-3400

"Adapt what is useful, reject what is useless, and add what is specifically your own."

– Bruce Lee

ACKNOWLEDGEMENTS

Throughout my academic career, I have been incredibly fortunate to have received the support, love, guidance, mentorship and much else aside from the remarkable people around me. I will begin by thanking my advisor, friend and lead singer of our rock band, Konstantin Batygin. I cannot adequately formulate my gratitude for his mentorship into words. He was a postdoc at Harvard when I first requested to begin graduate work with him. It would have been very easy for him to ask me to wait a year – I am very thankful that he did not. Konstantin has taught me too many things to list. He taught me celestial mechanics, how to write a paper, inspired me to write my own songs and increased my self-confidence by orders of magnitude. Concisely put, he has been instrumental in letting me become the person I wanted to be. Thank you for everything, and I look forward to a long and enjoyable friendship.

Konstantin is my advisor on paper, but the unsung hero of my graduate school experience is undoubtedly Woody Fischer. I always dreamed of studying topics spanning all the way from astrophysics to biology. I thought this was a pipe dream, until I asked Woody if a lowly astrophysicist could play any role in his work on the history of life on Earth. He didn't simply "let" me – he jumped at the chance. I soon realised that he shared my passion for cross-disciplinary exploration. We ended up bringing my idealistic picture to reality, with the publication of my first biology-focused paper. Woody, you made one my dreams come true – if you didn't already know how much that meant to me, I am telling you here. I hope we can continue our quasi-random walk through the disciplines in the years to come.

I would like to thank the other members of my thesis advisory committee, Dave Stevenson, Heather Knutson and Mike Brown. You have each played a key role in guiding my path through grad school. In addition to the faculty on my committee I have had the privilege of interacting with many inspiring individuals at Caltech, be it through course work or simply chance encounters. Particularly in my first couple of years, Andy Thompson and Jess Adkins showed me a spectacular sea of knowledge regarding Earth's oceans. I have had many inspiring conversations with each of you. Andy Ingersoll showed me the wonders of how atmospheres work, including how pressure scales with altitude during a couple of enjoyable nearby hikes we shared.

Science is done best when it is collaborative. I have had the privilege of collaborating with many incredible people during my work. Seth Finnegan at Berkeley helped keep my mathematical hammer aimed at the nail stuck in reality. Fred Adams from Michigan is a walking, talking physics textbook that keeps self-writing new pages. Charlie Doering and Glenn Flierl helped me break into the field of population ecology, one that has interested me for years.

Special thanks also go to Mitch Aiken, who showed me the many avenues of outreach available at Caltech. Along a similar vein, I am thankful to the volunteer co-ordinators at the Natural History Museum in Los Angeles, especially Elizabeth Andres, for letting me come and tell people about dinosaurs for a few hours every week.

On a personal level, I could not have accomplished the work in this thesis without a number of remarkable people I am lucky to have as friends. Special thanks go to Pushkar Kopparla and Dana Anderson for always being there when I needed support or a friendly ear. Specific thanks go to Mike Wong – if it had not been for your sublime

photography skills, there would be no evidence I did anything except work during grad school.

The list of friends who have helped support me is a long one: Henry Ngo, Patrick Fischer, Ian Wong, Nancy Thomas, Elizabeth Bailey, Peter Buhler, Peter Gao (extra credit for finding my jokes funnier than even I do), Elle Chimiak and Joe O'Rourke. Each of you have augmented my life in your own particular way.

Last but certainly not least, I would like to thank my mum, Rosemary Spalding, and my brother, David Spalding. I don't know what I would have done without your continued support and encouragement over the years. My mum always taught me the importance of following my dreams. Thanks to you, many of them have come true. David has been my best friend as well as my big brother, always there when I need him. I have learned so much from both of you and could not be more grateful.

ABSTRACT

For centuries, planet formation theories were tuned to reproduce the remarkable coplanarity of our solar system. Specifically, the eight planetary orbital planes exhibit mutual inclinations limited to $\sim 1-2$ degrees. Furthermore, the misalignment between the Sun's spin axis and the orbital planes of the planets – the 'spin-orbit misalignment'– is only about 6 degrees. However, observational characterization of close-in extrasolar planetary systems has revealed an abundance of spin-orbit misalignments ranging all the way from 0 to 180 degrees (Winn et al. 2010). Particularly among the hot Jupiters (giant planets with orbital periods shorter than $\sim$ 1 week), spin-orbit misalignments are more prevalent in systems hosted by stars with effective temperatures exceeding about 6200 K. Previous work has suggested that these misalignments arose from violent dynamical interactions that excited planets onto inclined and eccentric orbits, with subsequent tidal circularization generating the observed population (Albrecht et al. 2012). This hypothesis has had great difficulty explaining misaligned multi-planet systems, and misaligned orbits of planets that are too distant from their host stars for tidal circularization to act over a sufficiently short timescale. A new mechanism is required.

In chapters II-VI, I present a theoretical framework referred to as "disk-torquing," whereby spin-orbit misalignments arise through the tilting of protoplanetary disks themselves (Batygin 2012, Spalding & Batygin 2014, 2015). In this picture, gravitational torques from a companion star lead to the precession of the protoplanetary disk. When the disk is young and massive, gravitational star-disk coupling quenches misalignments between the stellar spin axis and disk plane. However, as the disk dissipates, a secular resonance is encountered that

impulsively excites large stellar obliquities, ranging between 0 and 180 degrees, in accordance with the observations. In addition, I computed the magnetic torques between the star and disk, finding that a dipole field strength of ∼1 kGauss is sufficiently strong to realign the star and disk within typical disk lifetimes (∼ 3 million years). Magnetic fields of this magnitude are observed to persist throughout the disk-hosting stage only for stars less massive than ∼1.2 solar masses (Gregory et al. 2012), corresponding to a main sequence effective temperature of 6200 K, i.e., coincident with the observed break between aligned and misaligned hot Jupiters. Cumulatively, the disk-torquing framework exhibits qualitative consistency with the observed dependence of spin-orbit misalignments upon stellar mass, leaving the theory ripe for a statistical comparison to observations within future work.

The final three chapters change focus from spin-orbit misalignments toward the excitation of mutual inclinations between planetary orbits – orbit-orbit misalignments. Evaluation of the relative numbers of single to multi-transiting planetary systems within the Kepler space telescope's dataset has revealed a dichotomy whereby there exist two populations of planetary system – one with low orbit-orbit inclination, and a second that either possesses a single planet, or possesses multiple planets with large mutual inclinations, leaving only one detectable via transit (Johansen et al. 2012, Ballard & Johnson 2016). In separate but related observational work, it has become apparent that transiting hot Jupiters often appear without co-transiting, close-in planetary companions, wheres warm Jupiters often do (Steffen et al. 2012, Huang et al. 2016). I showed that both of these observations can naturally arise owing to secular perturbations from the host star (Spalding & Batygin 2016, 2017). Specifically, young stars rotate fast, becoming oblate. If the star's spin axis is misaligned with respect

to the orbits of a multi-planet system, its quadrupole moment can disrupt the coplanarity of the system. Indeed, the stellar perturbations are often sufficient to completely destabilize the system (Chapter VI). In addition to constituting an entirely new mechanism of planetary instability, the origin of the required spin-orbit misalignment relates directly back to the discussion above – spin-orbit misalignments may drive the seemingly unrelated Kepler dichotomy.

Finally, I tied in the observation that hot Jupiters appear lonely by demonstrating that stellar contraction can give rise to a secular resonance that tilts exterior companions of hot Jupiters, taking them out of transit. Crucially, this resonance is encountered at an earlier time in systems hosting warm Jupiters, precisely owing to their slightly increased orbital distance. I found that the demarcation between a system undergoing secular tilting, and one where the disk quenches the tilting, coincides well with the relatively arbitrary dividing line between hot and warm Jupiters, usually set at orbital periods of about a week.

In summary, I showed that spin-orbit misalignments and orbit-orbit misalignments, measured across a range of planetary size classes, can arise primordially owing to interactions with the host star and binary companions. The importance of the central star had most likely been missed in the previous literature owing to our solar system's peculiarly wide inner edge at ~ 0.4 AU, as opposed to the more typical ~ 0.1 AU within a galactic setting. In reality, through the wider lens of our Galactic planetary census, a true understanding of planet formation demands a look at star-planet interactions wholly unknown from centuries of solar system exploration.

PUBLISHED CONTENT AND CONTRIBUTIONS

Spalding, C. and Batygin, K., (2014). "Early excitation of spin-orbit misalignments in close-in planetary systems". In: *The Astrophysical Journal* 790.1, p. 42. DOI: 10.1088/0004-637X/790/1/42.

C. S. contributed in a conceptual evaluation of the project's goals, performed calculations and numerical simulations to generate the results, and participated in writing the manuscript. This work was adapted to constitute Chapter II.

Spalding, C., Batygin, K. and Adams, F., C. (2014). "Alignment of protostars and circumstellar disks during the embedded phase". In: *The Astrophysical Journal Letters*. 797.2, p. L29. DOI: 10.1088/2041-8205/797/2/L29.

C. S. contributed to the conception of the project, performed calculations and numerical simulations to generate results, and led the writing of the manuscript. This work was adapted to constitute Chapter III.

Spalding, C. and Batygin, K., (2015). "Magnetic origins of the stellar mass-obliquity correlation in planetary systems". In: *The Astrophysical Journal*, 811.2, p. 82. DOI: 10.1088/0004-637X/811/2/82.

C. S. contributed to the conception of the project, performed calculations and numerical simulations to generate results, and led the writing of the manuscript. This work was adapted to constitute Chapter IV.

Spalding, C. and Batygin, K. (2016). "Spin-orbit misalignment as a driver of the *Kepler* dichotomy". In: *The Astrophysical Journal*. 830.1, p. 5. DOI: 10.3847/0004-637X/830/1/5

C. S. conceived of the project's primary objectives, performed

simulations to generate results, and led the writing of the manuscript. This work was adapted to constitute Chapter V.

Spalding, C., Marx, N., W. and Batygin, K. (2018) "The resilience of Kepler systems to stellar obliquity", *The Astronomical Journal*, *in press.* preprint found at arXiv: 1803.01182

C. S. conceived of the project's primary objectives, performed simulations and calculations, and wrote the manuscript, in addition to mentoring high school student N. W. M in setting up and running some of the simulations. This work was adapted to constitute Chapter VI.

Spalding, C. & Batygin, K. "A Secular Resonant Origin for the Loneliness of Hot Jupiters". In: *The Astronomical Journal*, 154.3, p. 93. DOI: 10.3847/1538-3881/aa8174.

C. S. conceived of the project's primary objectives, carried out the computations and simulations, and wrote the manuscript. This work was adapted to constitute Chapter VII.

TABLE OF CONTENTS

LIST OF ILLUSTRATIONS

Number *Page*

LIST OF TABLES

Chapter 1

INTRODUCTION

1.1 From planetary to exo-planetary science

The term "planet" comes from the Greek "to wander," recapitulating the original realization that the motion of planets across the sky deviates from the simple east to west motion of the stars. Even to the naked eye, planets stand apart from stars in that they do not twinkle, Mars has a red hue, and with the aid of a small backyard telescope, the phases of Venus are revealed, in resemblance to those of the moon. Humans have written myths, legends, and creative masterpieces inspired by the planets. But the reality, as is so often the case, goes beyond the imagination of even the most whimsical of tales.

Up until 1995, an extensive literature had been written in the quest to understand the origin of our own solar system. Laplace and Kant had independently come to the correct conclusion that the planets' birthplace consisted of a disk of gas (Kant, 1755; Laplace, 1796). This idea was motivated by the coplanar arrangement of the planetary orbits, and has been spectacularly confirmed by relatively recent images from the Hubble Space Telescope.

In later work, it was noted that a giant planet such as Jupiter, if placed within such a disk, would gravitationally interact with it in such a way as to undergo inward, radial migration (Goldreich and Tremaine, 1980), and indeed signs of a similar process were evident in Saturn's rings. Furthermore, the current model of our own solar system's history supposes that Jupiter migrated inwards, then outwards in a celestial manoeuvre colloquially referred to as the "Grand Tack"

(Walsh et al., 2011).

Given the prose above suggesting inward migration, perhaps it should not have been the paradigm-shattering event that it was when the first planet discovered around a Sun-like star, 51 Pegasi b, was a giant planet residing 20 times closer to its host star than the Earth sits in its orbit (Mayor and Queloz, 1995). These planets, known as "hot Jupiters" feature heavily in the following chapters. In order to form such a titan within a disk of gas, a core of solids must first be constructed totalling over 10 Earth masses (Stevenson, 1982; Pollack et al., 1996), such that its gravity attracts a significant amount of gas towards it. This so-called "core accretion" framework was thought impossible within the hot, inner regions of the natal disk. The reason is that water would have evaporated, leaving a lower solid surface density which, together with a reduced cohesiveness between dust particles, would inhibit the growth of larger cores. Consequently, the requisite cores must have formed at distances more similar to Jupiter, before migrating inwards. However, whereas our Jupiter "tacked" and moved back out (because of interactions with Saturn), the hot Jupiters continued their inward march to the inner edge of the disk.

Disk-driven migration constitutes a viable hypothesis for the migration of hot Jupiters. However, there is a second method of migration that may feasibly account for these objects' close-in orbits. The so-called "high-eccentricity" pathway of migration (Wu and Murray, 2003) supposes that the planet formed at a distance similar to Jupiter, but did not migrate whilst the disk was present (i.e., the first $1 - 10$ million years: Haisch Jr, Lada, and Lada 2001). Rather, dynamical perturbations arising from nearby planets or stars increased the eccentricity of the orbit – a measure of the difference between closest and furthest approach from the parent body (the star in this case). These eccentric-

ities bring the closest approach of the planet's orbit close enough to the host star for tidal deformation to become significant. These tides, raised on the planet, dissipate the orbital energy, reduce the orbital distance, and turn the "cold" Jupiter into a "hot" Jupiter.

As I discuss further below, this second pathway is essentially unique to hot Jupiters, and thus if true would constitute an entirely separate formation history for hot Jupiters than for almost all other planets known. Despite this apparent special place for hot Jupiters, the literature has tended toward favouring the high-eccentricity pathway.

1.2 The hot Jupiter debate

For the past 15 years, most of the literature investigating the *formation* pathway of hot Jupiters has been focused primarily upon deducing their *migration* pathway. However, since then, numerous other types of close-in planets have come to light. For example, the so-called "warm Jupiters" are giant planets, like hot Jupiters, but instead of possessing week-long orbits, their orbits last between weeks and months. These objects still reside too close-in to have formed via core accretion, but they are too far from the star for tides to have circularized their orbits within a sufficiently short amount of time. In other words, they still must have migrated, but can only have done so owing to interactions with the natal disk.

The most common close-in planets are the so-called "super Earths" (Fulton et al., 2017) – planets between Earth and Neptune in size. There is no consensus over whether these objects migrated or formed where we see them, but the point is that it is extraordinarily unlikely that they formed through high-eccentricity migration. The reasons are multiple, but principally these objects are too small to dissipate sufficient tidal energy, and secondarily, these bodies are frequently

found as members of multiple-planet systems – a delicate configuration (see Chapter V) that probably would not have survived the violent events required to excite sufficiently high eccentricities.

With the above discussion highlighting the suspected importance of disk-driven migration for other types of planets, it appears odd that hot Jupiters arrive through an extra formation pathway, one not shared by the warm Jupiters, not shared by the super Earths, and not shared by our own solar system. Before the completion of the work contained within this thesis, two pieces of evidence in particular strongly suggested that this special place was appropriate for the hot Jupiters. These were:

1) Hot Jupiters exhibit significant spin-orbit misalignments – misalignments between the perpendicular to the orbit and the spin axis of the host star (Winn, Fabrycky, et al., 2010; Albrecht et al., 2012).

2) Hot Jupiters are almost never found to possess close-in companion planets within the same system. (Steffen et al., 2012; Huang, Wu, and Triaud, 2016)

Spin-orbit misalignments

With regard to 1), the literature typically assumed that the solar-system's aligned configuration is overwhelmingly the most likely initial condition for planet formation (Winn and Fabrycky, 2015). In other words, stars and disks were assumed to begin their lives in an aligned configuration. With that picture in mind, the only way to tip stars over with respect to the orbital planes of their planets is through perturbations occurring subsequent to the disk-hosting phase – the high-eccentricity pathway satisfies this requirement well.

Despite consistency at first look, the high-eccentricity pathway suf-

fers in numerous respects upon closer inspection. Specifically, the framework predicts a small but significant population of planets “on the way" towards becoming hot Jupiters. However, fewer such objects are detected than would be predicted form the hypothesis (Dawson, Murray-Clay, and Johnson, 2014). Furthermore, under reasonable assumptions, the orbital energy deposited within the giant planet during its tidal dissipation is potentially enough to unbind the entire planet (Gu, Lin, and Bodenheimer, 2003). In any case, the process itself is difficult to thoroughly test because it depends upon the abundance of encounters likely to excite sufficient orbital eccentricities. Nevertheless, estimates typically conclude that under half of hot Jupiters may form this way, though the fraction of misaligned hot Jupiters explained may be larger (Naoz, Farr, and Rasio, 2012).

Given the theoretical difficulty in explaining the properties of hot Jupiters with high-eccentricity migration, in this thesis (Chapters II-VI), I will challenge the above premise that stars and disks form in an initially coplanar configuration. If true, the concerns regarding the high-eccentricity framework are circumvented, as the planetary orbits become misaligned with the central star from the outset. Furthermore, as we shall see, tilting a disk with respect to its central star’s spin axis naturally results from the presence of a gravitationally bound, stellar mass companion (Chapter II). Though empirical estimates differ, a fraction of stars close to unity originate in gravitationally-bound multiples (Sadavoy and Stahler, 2017). Accordingly, with the theory developed in this thesis, disk-star misalignments aren’t simply *possible*, they are *expected*.

A subtlety in the observations is that hot Jupiters orbiting stars more than about 1.2 times the Sun’s mass are significantly more misaligned than those orbiting lower-mass stars (Winn, Fabrycky, et al., 2010).

The previous, leading hypothesis to explain this trend was that misalignments occurred around stars of all masses, but that the large convective envelope possessed by the lower-mass stars enhanced tidal dissipation, realigning the star and the planet over time (Winn, Fabrycky, et al., 2010; Lai, 2012; Dawson, 2014). Unfortunately, this idea required questionable assumptions to be made regarding the pathway toward tidal dissipation. Specifically, one needs to require that inclination damps faster than semi-major axis, or any model correcting inclinations would remove the planet from orbit. Furthermore, though more distant planets show a slight trend toward larger misalignments, as expected from a tidal mechanism, the trend occurs too far out to be indisputably tidal in nature (Li and Winn, 2016).

In the thesis, I postulate an alternative idea, one that, like the tilting of the disk itself, plays out during the first few million years of planet formation. Specifically, not tides, but magnetic torques between the young star and its disk realign the lower-mass stars (Chapter IV: Spalding and Batygin 2015). This idea was motivated by observations suggesting a roughly order of magnitude reduced dipole field strength of disk-hosting, high mass stars relative to their lower mass counterparts (Gregory, Donati, et al., 2012). This picture is by no means complete, largely owing to uncertainties stemming from the physics of star-disk magnetic interactions. Nevertheless my work here demonstrates its feasibility, and bypasses the poorly-constrained nature of tidal models.

Orbit-orbit misalignments

Considering 2) above, the absence of close-in companion planets to hot Jupiters, in contrast to a $\sim$ 50% abundance of such companions in warm Jupiter-hosting systems, has been noted by numerous authors

(Steffen et al., 2012; Huang, Wu, and Triaud, 2016). Almost ubiquitously, the proposed mechanism is that the dynamically violent nature associated with the high-eccentricity migration has removed any close-in planetary companions that may once have existed. Whereas if indeed hot Jupiters form through such a pathway, they would be expected to cast out companion planets, the above concerns regarding high-eccentricity migration suggest an alternative hypothesis may be required.

The alternative model presented in this thesis considers the dynamical consequences of forming a close-in companion exterior to a hot Jupiter. In brief, that the gravitational perturbations associated with the contracting, central star initiate resonant dynamics between the two planets. These interactions cause a tilting of the lower-mass planet's orbit out of the plane of the hot Jupiter (Batygin, Bodenheimer, and Laughlin, 2016; Spalding and Batygin, 2017). Given the preponderance of transit data used to infer these patterns, this tilted configuration would be observed as a hot Jupiter without any companion planets. Warm Jupiters escape this resonant tilting because, owing to their larger orbital distances, the stellar oblateness weakens before the disk dissipates. Consequently, the disk anchors the planets within the same plane, despite the resonance, allowing warm Jupiters to coexist with close-in companion planets.

A first-order prediction of the above picture is that "lonely" hot Jupiters should possess inclined, lower-mass companion planets (Batygin, Bodenheimer, and Laughlin, 2016). However, this framework is in need of a more detailed modeling approach to fully delineate a set of testable predictions. Specifically, in Chapters V and VI of the thesis, I model systems of multiple, coplanar planets and subject them to the gravitational influence of a tilted, oblate star. I show that such a configuration

often leads to dynamical instability, and many of the planets are lost. I have not yet combined these two frameworks. Is an inclined companion to a hot Jupiter dynamically stable over billions of years? If not, it would not be detected, meaning that different observational tests are required.

An observational test suggested in this thesis is of a more statistical nature (Chapter VII). In particular, knowing the orbital properties of a giant planet, and its potential exterior companions, we can construct a theoretical parameter-space where the proposed resonant tilting should occur. If exterior planets are frequently found in that region, the model needs to be reconsidered. Only 4 examples exist of close-in giants with exterior companions (Huang, Wu, and Triaud, 2016; Spalding and Batygin, 2017). Whereas they are all consistent with my proposed framework, the number is still too small to derive any significant statistical conclusions.

Implications

The two observations above are consistent with a violent formation history, and apparently inconsistent with a system arising within a flat disk and remaining undisturbed for billions of years. This thesis challenges the latter assumption. That is to say, this thesis shows that formation within a disk naturally leads to spin-orbit misalignments, and as the host star subsequently contracts, gravitational perturbations within the giant planet-hosting system lead to the removal of close-in companions to hot Jupiters, as the observations have shown. Cumulatively, this body of work demonstrates that disk-driven migration as a dominant formation pathway for hot Jupiters is not falsified by the current observations, and provides a new set of predictions, readily testable by upcoming planet-finding missions.

The picture conceived by Kant and Laplace was correct in many ways. However, binary stars, the spinning down of planet-hosting stars, and the numerous gravitational perturbations felt within the early stages of the formation of a planetary system all conspire to disrupt coplanarity akin to our solar system in numerous other instances. How might our solar system's history have been different if the Sun was tilted over? Perhaps it was early on, but the stellar magnetic field righted the system. Potentially, if our system, like most others, possessed close-in super Earth planets the resulting star-planet interactions would have destabilised the solar system.

This thesis introduces and analyses numerous new concepts that have helped to understand how the architectures of planetary systems are sculpted, and why the sculptures differ from system to system. Only by considering our solar system within such a galactic context can we truly understand our own planetary system's place within the universe.

Chapter 2

EARLY EXCITATION OF SPIN-ORBIT MISALIGNMENTS IN CLOSE-IN PLANETARY SYSTEMS

ABSTRACT

Continued observational characterization of transiting planets that reside in close proximity to their host stars has shown that a substantial fraction of such objects posses orbits that are inclined with respect to the spin axes of their stars. Mounting evidence for the wide-spread nature of this phenomenon has challenged the conventional notion that large-scale orbital transport occurs during the early epochs of planet formation and is accomplished via planet-disk interactions. However, recent work has shown that the excitation of spin-orbit misalignment between protoplanetary nebulae and their host stars can naturally arise from gravitational perturbations in multi-stellar systems as well as magnetic disk-star coupling. In this work, we examine these processes in tandem. We begin with a thorough exploration of the gravitationally-facilitated acquisition of spin-orbit misalignment and analytically show that the entire possible range of misalignments can be trivially reproduced. Moreover, we demonstrate that the observable spin-orbit misalignment only depends on the primordial disk-binary orbit inclination. Subsequently, we augment our treatment by accounting for magnetic torques and show that more exotic dynamical evolution is possible, provided favorable conditions for magnetic tilting. Cumulatively, our results suggest that observed spin-orbit misalignments are fully consistent with disk-driven migration as a dominant mechanism for the origin of close-in planets.

2.1 Introduction

Nearly two decades after the celebrated radial velocity detection of a planet around 51 Peg (Mayor and Queloz, 1995; Marcy and Butler, 1996), the orbital histories of hot Jupiters, (giant planets that reside within ~ 0.1 AU of their host stars) remain poorly understood. Conventional planet formation theory (Pollack et al., 1996) suggests that in-situ formation of hot Jupiters is unlikely, implying that these objects formed beyond the ice-lines of their natal disks (at orbital radii of order $\sim$ a few AU) and subsequently migrated to their present locations. The nature of the dominant migration mechanism, however, remains somewhat elusive.

Broadly speaking, the proposed theoretical mechanisms responsible for delivery of hot Jupiters to close-in radii fall into two categories. The smooth migration category essentially argues that large-scale transport of giant planets is associated with viscous evolution of the disk (Lin, Bodenheimer, and Richardson, 1996; Morbidelli and Crida, 2007). More specifically the envisioned scenario suggests that newly-formed giant planets clear out substantial gaps in their protoplanetary disks (Goldreich and Tremaine, 1980; Armitage, 2011) and, having placed themselves at the gap center (where torques from the inner and outer parts of the disk instantaneously cancel), drift inwards along with the gas.

A dramatically different story is foretold by the class of violent migration mechanisms. Within the context of this group of descriptions, giant planets initially residing at large orbital radii first attain near-unity eccentricities and eventually get tidally captured onto tighter orbits. The necessary orbital excitations are expected to stem from dynamical processes such as planet-planet scattering (Ford and Rasio, 2008; Nagasawa, Ida, and Bessho, 2008; Beaugé and Nesvorný,

2012), Kozai resonance with a perturbing binary star (Wu and Murray, 2003; Fabrycky and Tremaine, 2007; Naoz, Farr, Lithwick, et al., 2011), and secular chaotic excursions (Lithwick and Wu, 2012).

From a purely orbital stand point, there appears to be observational evidence for both sets of processes. That is, the existence of a substantial number of (near-) resonant giant exoplanets (Wright et al., 2011) and direct observations of gaps in protoplanetary disks (Andrews, Wilner, Espaillat, et al., 2011; Hashimoto et al., 2012) imply that smooth disk-driven migration is an active process. Simultaneously, the existence of highly eccentric planets such as HD80606b (Laughlin, 2009) hint at violent migration as a viable option (see however Dawson, Murray-Clay, and Johnson 2014).

In the recent years, observations of the Rossiter-McLaughlin effect (Rossiter, 1924; McLaughlin, 1924), which inform the projected angle between the stellar spin axis and the planetary orbit (Fabrycky and Winn, 2009), have placed additional constraints on the hot Jupiter delivery process. Particularly, the data shows that spin-orbit misalignments are generally common within the hot Jupiter population, and the individual angles effectively occupy the entire possible range. Interpreted as relics of hot Jupiter dynamical histories (see however Rogers, Lin, and Lau 2012 for an alternative view), these observations seemed to strongly favor the category of violent migration mechanisms over disk-driven migration, as spin-orbit misalignments are a natural outcome of the former.

However, a more thorough theoretical analysis shows that spin-orbit alignment is not a necessary feature of disk-driven migration, because a primordial correspondence between the stellar spin axis and the disk angular momentum vector is not in any way guaranteed. To this

end, Bate, Lodato, and Pringle (2010) hypothesized that stochastic external forces that act on newly formed protoplanetary disks may give rise to spin-orbit misalignment, while Lai, Foucart, and Lin (2011) showed that a mismatch between the stellar magnetic axis and the disk orbital angular momentum vector can be further amplified by magnetic torques.

In a separate effort, Batygin (2012) showed that owing to enhanced stellar multiplicity in star-formation environments (Ghez, Neugebauer, and Matthews, 1993; Kraus et al., 2011; Marks and Kroupa, 2012), secular gravitational perturbations arising from binary companions may torque protoplanetary disks out of alignment with their host stars. This study was subsequently extended by Batygin and Adams (2013), who also considered the dissipative effects of accretion and magnetic modulation of stellar rotation as well as the physical evolution of the star and the disk on the excitation of spin-orbit misalignment. Importantly, the latter study demonstrated that the acquisition of stellar obliquity occurs impulsively, via a passage through a secular spin-orbit resonance.

A distinctive prediction made by the disk-torquing model is the existence of coplanar planetary systems, whose orbital angular momentum vectors differ from the spin axes of the host stars. This prediction was recently confirmed observationally by Huber et al. (2013) in the Kepler-56 system. Moreover, the statistical analysis of Crida and Batygin (2014) has shown that the expected spin-orbit misalignment distribution of the disk-torquing model is fully consistent with the observed one.

Given the aforementioned successes of the the disk-torquing mechanism in resolving the discrepancy between disk-driven migration and

spin-orbit misalignments, a thorough examination of the physical process behind the excitation of inclination is warranted. This is the primary aim of the study at hand. Specifically, in this work, we analyze the passage of the star-disk system through a secular spin-orbit resonance, under steady external gravitational perturbations and magnetically-facilitated tiling of the star. The paper is organized as follows. In section 2, we describe the construction of a perturbative model that approximately captures the relevant physics. In section 3, we describe the characteristic behavior exhibited by the model. We conclude and discuss our results in section 4.

2.2 Model

In order to complete the specification of the problem, we must delineate the various ingredients of the model we aim to construct. In particular, these include formulations of the physical evolution of the disk and the central star (section 2.1), magnetically-facilitated tilting of the stellar-spin axis (section 2.2), gravitational interactions between the disk and the binary companion, as well as the gravitational interactions between the central star and the disk (section 2.3). In this work, we opt to neglect the dissipative effects of accretion, as they have been studied within the context of the same problem elsewhere (i.e., Batygin and Adams 2013) and have been found to be unimportant.

We describe our parameterization of the relevant processes below. In interest of minimizing confusion, we adopt the following convention for identically named variables: quantities referring to the disk are primed, those referring to the central star are marked with a tilde, and those referring to the companion star are labeled by an over-bar. Throughout the paper, an emphasis is placed on simplicity inherent to (semi-)analytical approximations, as opposed to precise yet perplexing

numerical calculations.

Physical Evolution of the Protoplanetary Disk and the Stellar Interior

Typically quoted lifetimes of protoplanetary disks fall in the range $\sim 1 - 10$ Myr and almost certainly depend on various parameters such as the host stellar mass (Williams and Cieza, 2011). We adopt several approximations for the physical evolution of the star and disk, which are specific to Sun-like stars, which host the best observationally characterized hot Jupiters. While generally difficult to accurately parameterize, the disk mass can be taken to evolve as (Laughlin, Bodenheimer, and Adams, 2004):

$$M_{\rm disk} = \frac{M^0_{\rm disk}}{1 + t/\tau_{\rm disk}}. \tag{2.1}$$

Interpreting the time derivative of $M_{\rm disk}$ to represent the accretionary flow, following Batygin and Adams (2013) we find that the initial disk mass, $M^0_{\rm disk} = 5 \times 10^{-2} M_\odot$ and evaporation timescale $\tau_{\rm disk} = 5 \times 10^{-1}$ Myr provide an acceptable match to the observations (Hartmann, 2008; Herczeg and Hillenbrand, 2008; Hillenbrand, 2008).

For simplicity, we model the interior structure of the central star with a polytrope of index $\xi = 3/2$ (appropriate for a fully convective object; Chandrasekhar 1939). A polytropic body of this index is characterized by a specific moment of inertia $I = 0.21$ and a Love number (twice the apsidal motion constant) of $k_2 = 0.14$. Because T-Tauri stars derive a dominant fraction of their luminosity from gravitational contraction, we adopt the following expression for the radiative loss of binding energy (Hansen, Kawaler, and Trimble, 2012):

$$-4\pi R_\star^2 \sigma T_{\rm eff}^4 = \left(\frac{3}{5-\xi}\right) \frac{G M_\star^2}{2 R_\star^2} \frac{dR_\star}{dt}. \tag{2.2}$$

Equation (2.2) effectively dictates the process of Kelvin-Helmhotz contraction, and is satisfied by the solution:

$$R_\star = (R_\star^0)\left[1 + \left(\frac{5-\xi}{3}\right)\frac{24\pi\sigma T_{\rm eff}^4}{GM_\star (R_\star^0)^3}t\right]^{-1/3}. \tag{2.3}$$

A good match to the numerical evolutionary track of Siess, Dufour, and Forestini (2000) for a $M_\star = 1M_\odot$ star can be obtained by assuming an initial radius of $R_\star^0 \simeq 4R_\odot$ and an effective temperature of $T_{\rm eff} =$ 4100K.

Magnetic Torques

In order to model the magnetic disk-star interactions, we consider a T Tauri star possessing a pure dipole magnetic field, whose north pole is aligned with the stellar spin axis. In the region of interest (i.e., in the domain of the disk), the field is current-free and can be expressed as a gradient of a scalar potential:

$$\vec{B}_{\rm dip} = -\vec{\nabla}V. \tag{2.4}$$

To retain generality, we take the field to be tilted at an angle β_i with respect to the disk plane into a direction specified by an azimuthal angle $\tilde{\phi}_i$:

$$\begin{aligned} V = B_\star R_\star\left(\frac{R_\star}{r}\right)^2\Bigg[&P_0^1(\cos(\tilde{\theta}))\cos(\beta_i) \\ &- \sin(\beta_i)\Big(\sin(\tilde{\phi}_i)\sin(\tilde{\phi}) \\ &+ \cos(\tilde{\phi}_i)\cos(\tilde{\phi})\Big)P_1^1(\cos(\tilde{\theta}))\Bigg], \end{aligned} \tag{2.5}$$

where $B_\star$ is the stellar surface field and P_l^m are associated Legendre polynomials.

If we assume the disk to be circular and Keplerian, there exists a radius, $a'_{\rm co} = (G\,M_\star/\omega^2)^{1/3}$ at which the mean motion of the disk material,

n', equals the spin rate of the stellar magnetic field, ω. At larger and smaller radii, Keplerian shear will give rise to relative fluid velocity with respect to the stellar rotation. Accordingly, as a result of thermal ionization of alkali metals in the disk (Draine, Roberge, and Dalgarno, 1983), the magnetic field will be dragged azimuthally by differential rotation, whilst slipping backwards diffusively (Livio and Pringle, 1992). Following Armitage and Clarke (1996) we parameterize the magnitude of the azimuthally-induced field B_ϕ as a fraction, $\gamma = B_\phi / B_z$, of the vertical component of the dipole field B_z.

As shown by Agapitou and Papaloizou (2000) and Uzdensky, Königl, and Litwin (2002), beyond a critical value of $\gamma \simeq 1$, field lines are stretched to a sufficient degree to reconnect and transition from a closed to an open topology. Thus, the condition $|\gamma| \lesssim 1$ defines a magnetically-connected region within the disk with $\hat{a}'_{\rm in} < a' < \hat{a}'_{\rm out}$. Outside of this region, we assume there to be no appreciable magnetic coupling to the disk.

The radial profile of γ is determined by the magnetic diffusivity of the disk, which in turn may be represented by the dimensionless parameter (Matt and Pudritz, 2004):

$$\zeta = \frac{\alpha}{P_m} \frac{h}{a'}, \tag{2.6}$$

where $\bar{\alpha}$ is the disk viscosity parameter introduced by Shakura and Sunyaev (1973), P_m is the Magnetic Prandtl number, and h is the scale height of the disk. As argued by Matt and Pudritz (2004) and Matt and Pudritz (2005), any realistic choice of parameters yields $\zeta \leq 10^{-2}$, which is the value we adopt throughout our work here. In terms of ζ, a steady state magnetic twist angle may be expressed as (Uzdensky,

Königl, and Litwin, 2002)

$$\gamma = \frac{(a'/a'_{\rm co})^{3/2} - 1}{\zeta}. \tag{2.7}$$

For our adopted value of ζ this so-called magnetically-connected region does not diverge from the corotation radius by more than $\sim$ 1%.

The above discussion highlights a crucial aspect of the magnetic star-disk interaction, which is discussed in detail by Matt and Pudritz (2004) and Matt and Pudritz (2005). If the disk is truncated at $a'_{\rm in} > \hat{a}'_{\rm out}$, then there is no magnetically-connected region within the disk. The picture is slightly more complicated for the case where $a'_{\rm in} < \hat{a}'_{\rm in}$, as one may speculate that magnetic effects arising from differential rotation outside $a'_{\rm co}$ may cancel those associated with differential rotation inside $a'_{\rm co}$ to first order. In all of the following work, we circumvent these issues by assuming a disk-locked condition (Shu, Najita, et al., 1994; Mohanty and Shu, 2008) where $a'_{\rm in} = a'_{\rm co}$, but add a cautionary note that this assumption may lead to somewhat overly favorable results.

In order to derive the analytical form of the torques, we take a similar approach to that of Lai, Foucart, and Lin (2011), and assume the disk to be razor thin. The disk current loops are envisioned to follow the magnetic field lines in a force-free fashion (see, e.g., Krasnopolsky, Shang, and Li 2009; Zanni and Ferreira 2013) and connect onto the stellar surface. Accordingly, the induced azimuthal magnetic field arises from a radial current within the disk (Lai, 1999).

The magnitude of the radial current is calculated using Ampère's Law (Jackson, 1998) in the form:

$$\int_C \vec{B} \cdot d\vec{l} = \mu_0 \int \int_A \vec{J} \cdot d\vec{S}, \tag{2.8}$$

where $d\vec{l}$ is a vector path length, $d\vec{S}$ is a vector area element and C is a loop encompassing the surface A. $\vec{J}$ is the (induced) current density within the disk. Because the induced field is entirely toroidal, we can integrate the left hand side along an azimuthal loop around the disk. This yields:

$$4\pi a' B_\phi = 2\pi \mu_0 a' K_r, \tag{2.9}$$

where $K_r = \int J_r dz = 2B_\phi/\mu_0$ is the inward radial surface current.

Combining this expression with equation (2.7), we obtain:

$$K_r = \frac{2B_z}{\mu_0}\left[\frac{(a'/a'_{\rm co})^{3/2} - 1}{\zeta}\right]. \tag{2.10}$$

With an expression for the induced current at hand, we immediately arrive at an expression for the associated Lorentz torque, considering the induced current to interact only with the stellar dipole field:

$$\vec{\tau}_L = (a'\,\hat{\vec{\rho}}\,) \times (K_r\,\hat{\vec{\rho}} \times \vec{B}_{\rm dip}). \tag{2.11}$$

In the above expression, $\hat{\rho}$ is the radial unit vector in the plane of the disk.

At this point, in order to cast the magnetic torques into a usable form, we project $\vec{\tau}_L$ onto each of the Cartesian axes in the disk's frame and subsequently integrate over the entire magnetically-connected region:

$$\tau_{i'} = \int_0^{2\pi} \int_{a'_{\rm co}}^{\hat{a}'_{\rm out}} \vec{\tau}_L \cdot \hat{\vec{x}}_{i'}\, \rho\, d\rho\, d\phi, \tag{2.12}$$

where the subscript i' represents the Cartesian axes in the disk's frame. With the variables and parameters given above, these torques evaluate to:

$$\tau_{x'} = \left(\frac{2\pi B_\star^2 R_\star^6\, \zeta\, \sin(\beta_i)\, \cos(\beta_i)}{3\mu_0(1+\zeta)^2 (a'_{\rm co})^3}\right) \cos(\tilde{\phi}_i) \tag{2.13}$$

$$\tau_{y'} = \left(\frac{2\pi B_\star^2 R_\star^6 \zeta \sin(\beta_i) \cos(\beta_i)}{3\mu_0 (1+\zeta)^2 (a'_{\rm co})^3} \right) \sin(\tilde{\phi}_i) \tag{2.14}$$

$$\tau_{z'} = \left(\frac{4\pi B_\star^2 R_\star^6 \zeta \cos^2(\beta_i)}{3\mu_0 (1+\zeta)^2 (a'_{\rm co})^3} \right). \tag{2.15}$$

Note that for $\beta_i > \pi/2$, the star and disk spin in opposite directions, rendering $a'_{\rm co}$ meaningless. In such a regime, there is no magnetically connected region of the form described above. Indeed, it is unclear how the magnetic field would interact with the disk in this case. For the purposes of our model, we incorporate this loss of a magnetically connected region by artifically forcing the torques to equal zero for angles of $\beta_i > \pi/2$. Mathematically, this is done by multiplying the torques by an approximation to a step function $\mathcal{S}(\beta_i)$ given by:

$$\mathcal{S}(\beta_i) = 1 - \left(\frac{\pi/2 + \arctan\left(\frac{\beta_i - \pi/2}{\ell}\right)}{\pi} \right), \tag{2.16}$$

where $\ell = 10^{-4}$. The importance of such a term becomes apparent once the torques are coupled to gravity and inclinations above 90 degrees are naturally attained.

Angular momentum transport among neighboring annuli of the disk is facilitated by propagation of bending waves (Foucart and Lai, 2011) as well as disk self-gravity (Batygin, Morbidelli, and Tsiganis, 2011) and generally occurs on a much shorter timescale than magnetic tilting of the host star. Taking advantage of this, in our analyses we assume that the effective moment of inertia of the disk around all axes is much greater than that of the star, allowing us to ignore any torques from the star on the disk and to consider $-\tau_{i'}$ as a back-reaction on the star's dynamics.

As will become apparent below, it is beneficial to carry out all calculations in the frame of a distant, binary companion to the central star.

As such, we follow the approach of Peale et al. (2014) and define Euler angles within the binary frame related to the nutation, precession and rotation of the rigid body while assuming exclusively principal axis rotation (this is an excellent approximation for a T-Tauri star, spinning at a period of 1-10 days). Specifically, $\tilde{\beta}$ is the angle between the central star's spin axis and the binary orbit normal; $\tilde{\Omega}$ is the longitude of ascending node of the star in the binary frame where $\tilde{\Omega} = 0$ implies collinear disk and stellar lines of nodes; and the third Euler angle φ is the angle through which the star rotates as it spins (φ only enters the equations as a rate of change: $\dot{\varphi} = \omega$).

The equations for the evolution of $\tilde{\beta}$ and $\tilde{\Omega}$, adapted from Peale et al. (2014) are:

$$\frac{d\tilde{\beta}}{dt} = -\frac{1}{\omega}\Bigg[\cos(\tilde{\beta})(-N_{\bar{x}}\sin(\tilde{\Omega}) + N_{\bar{y}}\cos(\tilde{\Omega})) + N_{\bar{z}}\sin(\tilde{\beta}))\Bigg], \tag{2.17}$$

$$\frac{d\tilde{\Omega}}{dt} = -\frac{1}{\omega\ \sin(\tilde{\beta})}\Bigg[N_{\bar{x}}\cos(\tilde{\Omega}) + N_{\bar{y}}\sin(\tilde{\Omega})\Bigg], \tag{2.18}$$

where $N_{\bar{i}}$ are projected torques. Note that by fixing the disk's longitude of ascending node at $\Omega' = 0$, we have implicitly placed ourselves into a frame coprecessing with the disk's angular momentum vector. The effect of precession shall be included within the gravitational part of the equations and we need not retain it here.

Throughout the pre-main-sequence, we assume a constant rotation rate of the host star. Although stellar rotation is almost certainly modulated by the presence of the disk (Herbst, n.d.; Affer et al., 2013; Bouvier, 2013), the present lack of detailed understanding of the physical processes behind rotational breaking render this assumption reasonable (see Gallet and Bouvier 2013).

The projected quantities $N_{\bar{i}}$ are directly related to the torques calculated above, although the components of the torques in the disk frame, $-\tau_{i'}$, must first be projected onto the Cartesian axes in the binary frame. Such a projection constitutes a simple rotation of co-ordinates because, as discussed below, the disk-binary inclination is a constant of motion. The rotation angle is fixed at some prescribed angle, β', anti-clockwise about the x-axis. As such, the components, $N_{\bar{i}}$ are given in terms of τ_i by:

$$N_{\bar{x}} = -\tau_{x'}/(IM_\star R_\star^2), \tag{2.19}$$

$$N_{\bar{y}} = -(\cos(\beta')\tau_{y'} - \tau_{z'}\sin(\beta'))/(IM_\star R_\star^2), \tag{2.20}$$

$$N_{\bar{z}} = -(\cos(\beta')\tau_{x'} + \tau_{y'}\sin(\beta'))/(IM_\star R_\star^2). \tag{2.21}$$

The above equations can be used to analyze the dynamics of the central star owing to its magnetic field interacting with its protoplanetary disk. It is noteworthy that we have made no mathematical assumption of small angles, but physically, we have not taken into account the changes in the parameterized geometry of the problem that arise when mutual disk-star inclinations approach $\beta_i \longrightarrow \pi/2$.

Gravitational Torques

Binary Star - Disk Interactions

In this section, we calculate the gravitational response of a disk to a distant, binary companion, whose orbit is taken to lie in the reference plane. We derive a Hamiltonian for the disk subject to perturbations from the companion, working under the secular approximation. In other words, we assume that the disk's outer radius $a'_{\rm out}$ is sufficiently small compared to the binary orbit's semi-major axis $\bar{a}$ that no meaningful commensurabilities between the orbital motions exist.

The Gaussian averaging method (see Ch. 7 of Murray and Dermott 1999) dictates that in the aforementioned regime, the (orbit-averaged) treatment of the gravitational interactions of the disk-companion system is mathematically equivalent to considering the companion to be a circular ring with line density $\lambda = \bar{M}/(2\pi\bar{a})$ and the disk as an infinite series of annular wires at every radius between $a'_{\rm in}$ and $a'_{\rm out}$ (Murray and Dermott, 1999; Morbidelli, Tsiganis, et al., 2012).

It is well known that within the secular framework, the semi-major axes are constants of motion (Morbidelli, 2002). Consequently, the Keplerian contribution to the Hamiltonian can be dropped, rendering the Hamiltonian of this set up, simply the total gravitational potential energy $\mathcal{U}$ possessed by the disk in the field of the companion ring:

$$\mathcal{U} = -\int_{\rm disk}\int_{\rm ring} \frac{G}{r}\, dM_{\rm disk}\, dM_{\rm ring}, \tag{2.22}$$

where r is the separation between two mass elements $dM_{\rm ring}$ (companion), and $dM_{\rm disk}$ (disk). The integral is carried out over all angles ($\bar{\phi}$) within the ring and over all radii (a') and angles (ϕ') in the disk. The evaluation of $r(\phi', a', \bar{\phi})$ is a purely geometric problem and can be simplified by approximating $a'_{\rm out}/\bar{a} \ll 1$. Under such an approximation, we expand r to second order in equation (2.22) (first order terms are axisymmetric and therefore cancel out).

In order to compute the integral (2.22), we must specify the disk surface density profile, Σ. For definitiveness, in this work we shall follow (Mestel, 1963; Batygin, 2012) and adopt

$$\Sigma = \Sigma_0\left(\frac{a'_0}{a'}\right), \tag{2.23}$$

where Σ_0 is the surface density at semi-major axis a'_0. We note that the passive disk model of Chiang and Goldreich (1997) is characterized by a very similar power-law index: $\Sigma \propto (a')^{-15/14}$ (Rafikov, 2012).

With this prescription, equation (2.22) becomes:

$$\mathcal{U} = -\int_{a'_{\rm in}}^{a'_{\rm out}} \int_0^{2\pi} \int_0^{2\pi} \frac{G}{r} \Sigma_0 \, a'_0 \, \frac{\bar{M}}{2\pi} \, d\bar{\phi} \, d\phi' \, da'. \tag{2.24}$$

Noting that $a'_{\rm in} \ll a'_{\rm out}$, we arrive at the expression for the Hamiltonian.

Switching to canonically conjugated variables, we introduce the scaled Poincaré action-angle coordinates:

$$Z' = 1 - \cos(\beta') \qquad z' = -\Omega'. \tag{2.25}$$

This definition of the coordinates differs from the standard definition (see Ch. 2 of Murray and Dermott 1999) in that at each disk annulus, the standard definition multiplies Z' by $d\Lambda = dm'\sqrt{GM_\star a'}$, where $dm' = 2\pi\Sigma_0 a'_0 da'$ is the mass of the annulus. Thus, for the variables (4.4) to remain canonical, we must also scale the Hamiltonian itself in a corresponding manner:

$$\begin{aligned} \breve{\mathcal{U}} &= \frac{\mathcal{U}}{2\pi \int_{a'_{\rm in}}^{a'_{\rm out}} \Sigma_0 a'_0 \sqrt{GM_\star a'} da'} \\ &= \frac{3n'_{\rm out}}{8} \frac{\bar{M}}{M_\star} \left(\frac{a'_{\rm out}}{\bar{a}}\right)^3 \left[Z' - \frac{Z'^2}{2}\right]. \end{aligned} \tag{2.26}$$

This expression agrees with the fourth-order Lagrange-Laplace expansion of the disturbing function (Murray and Dermott, 1999), where Laplace coefficients are replaced with their leading order hypergeometric series approximations (Batygin and Adams, 2013).

The crucial result here is that $\breve{\mathcal{U}}$ does not depend on z', meaning that the disk inclination is exactly preserved in the binary frame:

$$\frac{dZ'}{dt} = -\frac{\partial \breve{\mathcal{U}}}{\partial z'} = 0 \tag{2.27}$$

while the precession rate depends on both the companion semi-major axis and mass. As shown by Batygin (2012) via a different approach,

the constancy of disk-star inclination holds even if an eccentric companion is considered. In this case, however, the precession rate is enhanced by a factor of $(1 + 3\bar{e}/2)$.

Disk - Central Star Interactions

As already mentioned above, the spin rates of classical T-Tauri stars fall within the characteristic range of $1 - 10$ days (Herbst, n.d.; Bouvier, 2013). This results in substantial rotational deformation of young stars. To an excellent approximation, the dynamical response of a spheroidal star to the gravitational potential of the disk can be modeled by considering an inertially equivalent orbiting ring of mass

$$\tilde{m} = \left[\frac{3M_\star^2\omega^2R_\star^3I^4}{4Gk_2}\right]^{1/3}, \tag{2.28}$$

and semi-major axis

$$\tilde{a} = \left[\frac{16\omega^2k_2^2R_\star^6}{9I^2GM_\star}\right]^{1/3}. \tag{2.29}$$

Within the context of this picture, the standard perturbation techniques of celestial mechanics can be applied (Murray and Dermott, 1999; Morbidelli, 2002).

In the exploratory study of Batygin and Adams (2013), the gravitational torques were computed using a low mutual inclination approximation to the true potential. This simplification is limiting, especially on the quantitative level, as it forces the topology of the dynamical portrait to be that of the second fundamental model for resonance (Henrard and Lemaitre, 1983), for all choices of parameters. In this work, we shall place no restrictions on the mutual inclination and adopt the series of Kaula (1962) as a representation of the potential, which utilizes the semi-major axis ratio $(\tilde{a}/a')$ as an expansion parameter. Provided the smallness of the semi-major axis ratio inherent to

our problem ($\tilde{a}/a' \lesssim O(10^{-1})$), an octupole-order expansion suffices our needs.

Written in terms of scaled canonical Poincaré action-angle coordinates (4.4), the Hamiltonian that governs the dynamics of the stellar spin-axis[1] under the gravitational influence of an infinitesimal wire of mass dm' reads:

$$\begin{aligned} d\mathcal{H} &= \frac{1}{16}\sqrt{\frac{GM_\star}{a'^3}}\frac{dm'}{M_\star}\left(\frac{\tilde{a}}{a'}\right)^{3/2}\Bigg[\left(2-6\tilde{Z}+3\tilde{Z}^2\right) \\ &\times \left(2-6Z'+3Z'^2\right)+12\left(\sqrt{\tilde{Z}(2-\tilde{Z})}-\sqrt{\tilde{Z}^3(2-\tilde{Z})}\right) \\ &\times \left(\sqrt{\tilde{Z}(2-\tilde{Z})}-\sqrt{\tilde{Z}^3(2-\tilde{Z})}\right)\cos(\tilde{z}-z') \\ &+ 3\tilde{Z}Z'\left(\tilde{Z}-2\right)\left(Z'-2\right)\cos\left(2(\tilde{z}-z')\right)\Bigg]. \end{aligned} \tag{2.30}$$

As above, to obtain an expression for the Hamiltonian that incorporates the effect of the entire disk, we imagine the disk to be composed of a series of such aforementioned wires and integrate:

$$\mathcal{H} = \int d\mathcal{H}. \tag{2.31}$$

Recalling that the mass of each individual wire comprising the disk is $dm' = 2\pi\Sigma_0 a_0' da'$, we note that the integral (2.31) runs with respect to the disk semi-major axis.

Because of the stiff dependence of equation (2.30) on a', the integral (2.31) is only sensitive to the disk's total mass, and not the location of its outer edge, provided that the latter is substantial (i.e., 10s of AU; Anderson, Adams, and Calvet 2013). On the contrary, the disk's mass is predominantly set by the disk's size, $a'_{\rm out}$:

$$M_{\rm disk} = 2\pi\int_{a'_{\rm in}}^{a'_{\rm out}} a'\Sigma_0\left(\frac{a'_0}{a'}\right)da' \simeq 2\pi\Sigma_0 a'_0 a'_{\rm out}. \tag{2.32}$$

[1] In unanimity with the above treatment, the back-reaction of the star onto the disk is ignored.

In addition to the disk's physical properties, we must also prescribe its dynamical behavior to complete the specification of the problem. As already mentioned above, because the Hamiltonian (4.5) is independent of the angles (i.e., is a Birkhoff normal form), the disk inclination with respect to the binary orbital plane (and therefore Z') is conserved, while the disk's nodal precession rate, $\nu = dz'/dt$, is given by

$$\nu = \frac{\partial \breve{\mathcal{U}}}{\partial Z'} = \frac{3n'_{\rm out}}{8}\frac{\bar{M}}{M_\star}\left(\frac{a'_{\rm out}}{\bar{a}}\right)^3\left[1 - Z'\right]. \tag{2.33}$$

Consequently, $\mathcal{H}$ represents a non-autonomous one degree of freedom system.

Because the time-dependence inherent to the problem at hand is particularly simple ($z' = \nu t$), $\mathcal{H}$ can be made autonomous by employing a canonical transformation arising from the following generating function of the second kind (Goldstein, 1950):

$$\mathbb{G}_2 = (\tilde{z} - \nu t)\Phi, \tag{2.34}$$

where $\phi = (\tilde{z} - \nu t)$ is the new angle and the new momentum is related to the old one through:

$$\tilde{Z} = \frac{\partial \mathbb{G}_2}{\partial \tilde{z}} = \Phi. \tag{2.35}$$

Accordingly, the Hamiltonian itself is transformed as follows (Lichtenberg and Lieberman, 1992):

$$\mathcal{K} = \mathcal{H} - \frac{\partial \mathbb{G}_2}{\partial t}. \tag{2.36}$$

Having removed explicit time dependence, we additionally scale the Hamiltonian by ν, which introduces a single dimensionless number $\tilde{\delta}$ that encompasses the physical properties of the system.

Following the transformations described above, the Hamiltonian takes on the following form:

$$\begin{aligned}\mathcal{K} &= -\Phi + \frac{\tilde{\delta}}{12}\Big[3\big(\Phi-2\big)\Phi - 3\big(2+3(\Phi-2)\big)\Phi\cos^2(\beta') \\ &+ 6\sin(2\beta')\big(\Phi-1\big)\sqrt{(2-\Phi)\Phi}\cos(\phi) + 3\sin^2(\beta') \\ &\times \big(\Phi-2\big)\Phi\cos(2\phi)\Big]. \end{aligned} \tag{2.37}$$

Accordingly, the explicit expression for the resonance proximity parameter reads:

$$\tilde{\delta} = \frac{3}{8}\left(\frac{n'^2_{\rm in}}{\omega\nu}\frac{M_{\rm disk}}{M_\star}\frac{a'_{\rm in}}{a'_{\rm out}}\right). \tag{2.38}$$

2.3 Results

With a theoretical model in place, let us begin our exploration of the acquisition of spin-orbit misalignments in an idealized limit. That is, we begin by neglecting magnetic torques and assuming adiabaticity.

Purely Gravitational Excitation

Although the Hamiltonian (4.10) does not exhibit explicit time-dependence, it does possess implicit time-dependence through the evolution of resonance proximity parameter, $\tilde{\delta}$. As discussed in Batygin and Adams (2013), the time-dependent variation in $\tilde{\delta}$ is primarily brought about as a result of disk mass loss and the physical evolution of the host star (via $\tilde{n}$). While both of these processes can be quite complex, for our purposes, it suffices to note that for any reasonable choice of parameters, $\tilde{\delta} \longrightarrow 0$ as the system approaches main sequence.

What are the consequences of the changes in the value of $\tilde{\delta}$? Preliminary progress towards understanding this question can be made by studying the equilibria of the Hamiltonian (4.10). To do so, it is

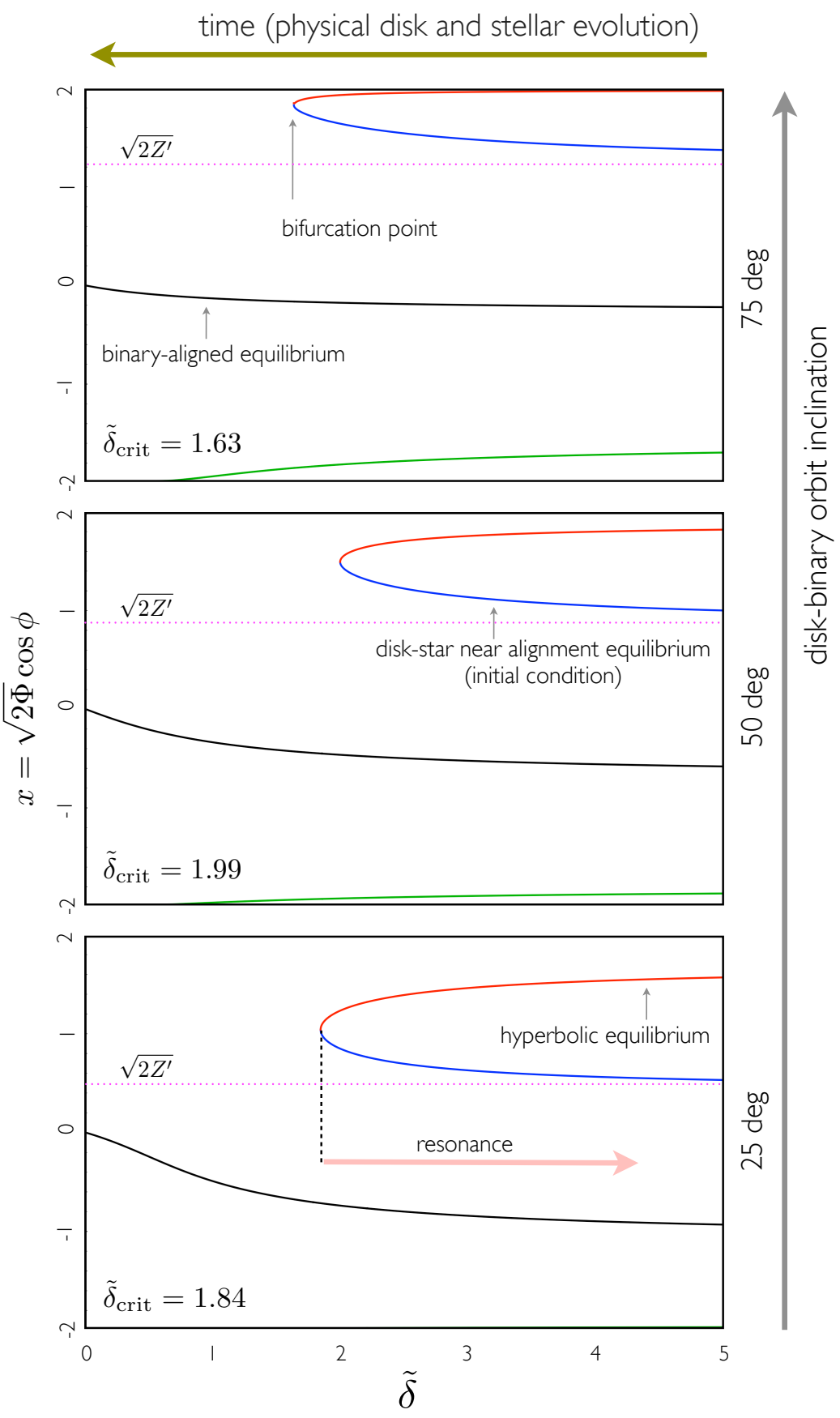

Figure 2.1: Equilibria of the Hamiltonian (4.10) as a function of the resonance proximity parameter $\tilde{\delta}$. The three panels correspond to different choices of disk-binary inclination, namely $\beta' = 25$ deg, $\beta' = 50$ deg, and $\beta' = 75$ deg. The equilibria

particularly convenient to switch to cartesian coordinates defined as

$$x = \sqrt{2\Phi}\cos(\phi) \qquad y = \sqrt{2\Phi}\sin(\phi). \tag{2.39}$$

The angular dependence of $\mathcal{K}$ shows that all equilibria will have $\phi = 0$, also implying $y = 0$ (Murray and Dermott, 1999). The equilibrium values of x are shown as functions of $\tilde{\delta}$ in Figure (2.1) for three choices of disk-binary orbit inclination.

Depending on the value of $\tilde{\delta}$, the Hamiltonian $\mathcal{K}$ possesses between two and four fixed points. Generally, for $\tilde{\delta} < 1$ two stable (elliptic) fixed points exist (shown in black and green), while four fixed points (one of which is stable (shown in blue) and the other is unstable, i.e., hyperbolic (shown in red)) are guaranteed for $\tilde{\delta} > 2$. There exists a critical bifurcation value $1 \leqslant \tilde{\delta}_{\rm crit} \leqslant 2$ where the number of fixed points is three and the stable and unstable fixed points merge into a single unstable equilibrium (Henrard and Lemaitre, 1983; Peale, 1986). As shown in Figure (2.1), $\tilde{\delta}_{\rm crit}$ depends on the disk-binary orbit inclination: it changes smoothly from $\tilde{\delta}_{\rm crit} = 1$ at $\beta' = 0\,$deg to $\tilde{\delta}_{\rm crit} = 2$ at $\beta' = 45\,$deg, and back to $\tilde{\delta}_{\rm crit} = 1$ at $\beta' = 90\,$deg.

Physically, $\tilde{\delta}$ represents the ratio of the characteristic precession rates of the star's and disk's angular momentum vectors. It is generally safe to assume that this ratio is well above unity at the epoch when the system emerges from the embedded stage (see, e.g., Williams and Cieza 2011). Moreover, it can be argued that dissipative processes such as accretion will force the stellar spin axis to evolve towards the equilibrium point closest to alignment with the disk's angular momentum vector (see Batygin and Morbidelli 2011 for a related discussion). Provided that the changes in $\tilde{\delta}$ are slow compared to the characteristic precession period of the star, adiabatic theory dictates that the (null) phase-space area (i.e., the adiabatic invariant $\mathcal{J}$) associated with the

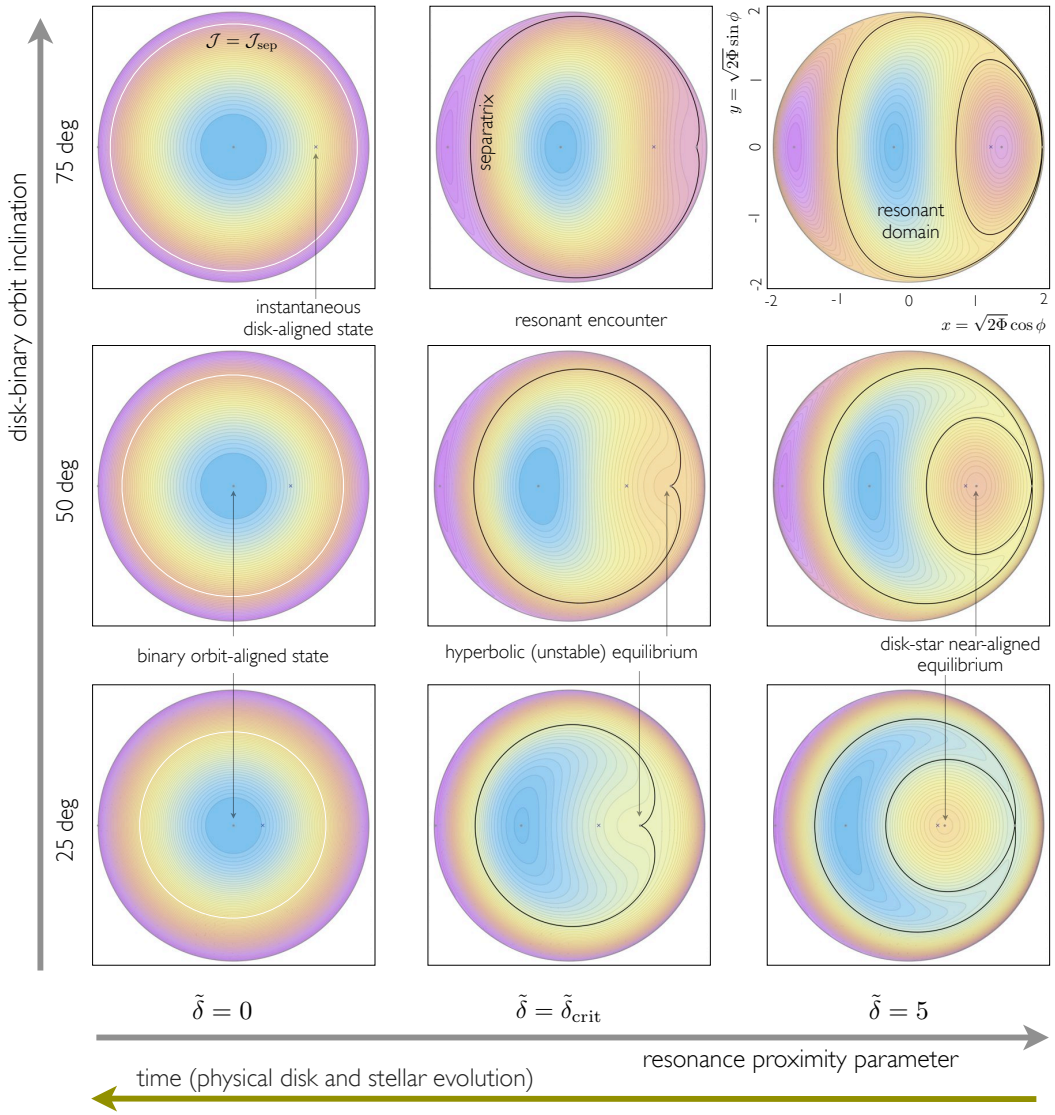

Figure 2.2: Phase-space portraits of the Hamiltonian (4.10) at different values of the resonance proximity parameter $\tilde{\delta}$ and disk-binary inclination. The colors represent the value of the Hamiltonian at each contour. In all panels, the equilibria of the Hamiltonian are shown as gray dots. The instantaneous disk aligned state is depicted with a small $\times$ symbol. Note that for $\tilde{\delta}$ well above $\tilde{\delta}_{\rm crit}$, there exist an equilibrium point in close proximity (but not exactly corresponding to) the disk aligned state. The separatrix is shown as a black curve for $\tilde{\delta} \geqslant \tilde{\delta}_{\rm crit}$. On panels corresponding to $\tilde{\delta} = 0$, a white circular orbit that occupies the same phase-space area as the separatrix at $\tilde{\delta} = \tilde{\delta}_{\rm crit}$ is shown.

orbit of the stellar spin axis must be approximately conserved (Henrard, 1982): $\mathcal{J}_{\rm eq} = 0$. Consequently, as $\tilde{\delta}$ decreases in time the stellar spin axis will reside on the equilibrium solution shown in blue on Figure (2.1). However, once the evolutionary track of the system reaches $\tilde{\delta} = \tilde{\delta}_{\rm crit}$, the associated equilibrium becomes unstable.

To understand the dynamical evolution of the stellar spin axis beyond the aforementioned adiabatic trailing phase, it is useful to consider the geometry of the Hamiltonian. For the three choices of inclination depicted in Figure (2.1), Figure (2.2) shows a series of phase-space portraits of $\mathcal{K}$ in cartesian coordinates. Specifically, the panels of the Figure (2.2) depict snap-shots of the Hamiltonian flow at $\tilde{\delta} = 5$, $\tilde{\delta} = \tilde{\delta}_{\rm crit}$, and $\tilde{\delta} = 0$. Here, the equilibrium points of $\mathcal{K}$ are shown as gray dots, while the separatrix (i.e., homoclinic orbit) associated with the secular spin-orbit resonance is depicted as a black curve where it exists (i.e., $\tilde{\delta} \geqslant \tilde{\delta}_{\rm crit}$).

Qualitatively, the following picture holds. As long as $\tilde{\delta} > \tilde{\delta}_{\rm crit}$, the system remains adiabatically frozen on the equilibrium point contained in the inner circulation zone of the separatrix. As $\tilde{\delta} \to \tilde{\delta}_{\rm crit}$, the phase space area associated with the inner circulation zone shrinks and eventually the equilibrium point on which the stellar spin-axis resides is invaded by the separatrix. Because the separatrix is characterized by an infinite period, the adiabatic principle inevitably breaks down and the conservation of $\mathcal{J}$ is momentarily violated. However, immediately after the encounter, the separatrix turns into a regular circulatory orbit and the system returns into the realm of adiabatic theory (Borderies and Goldreich, 1984; Henrard, 1991; Batygin and Morbidelli, 2013). As such, for all subsequent evolution, the value of the adiabatic invariant remains equivalent to that of the separatrix, evaluated at the critical resonance proximity parameter (Peale, 1986).

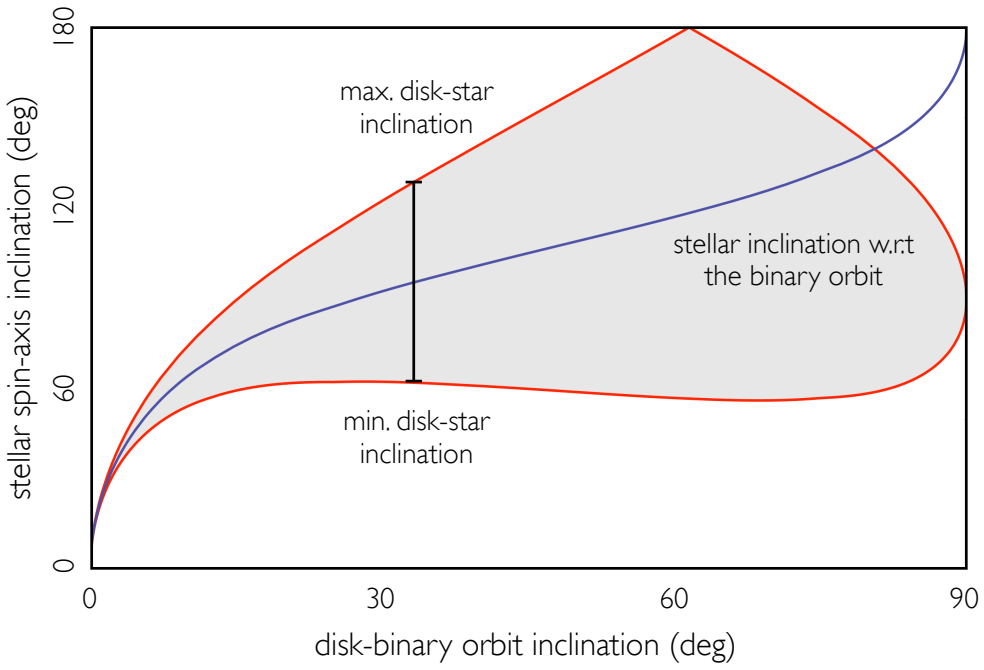

Figure 2.3: Resonant excitation of spin-orbit misalignment. Post-resonant encounter stellar inclination of the star (measured in a frame coplanar with the binary orbit) as a function of disk-binary inclination is shown as a purple curve. Corresponding maximal and minimal spin-orbit misalignments between the stellar and the disk's angular momentum vectors, attained over a precession cycle are depicted as red curves. Note that the entire possible range of spin-orbit misalignments is attainable with a disk-binary inclination $\beta' \leqslant 65\,\mathrm{deg}$.

Ultimately as the disk dissipates, $\tilde{\delta}$ approaches zero and the Hamiltonian (4.10) becomes a trivial one, whose flow is represented by concentric circles on the phase plane. Accordingly, the post-encounter inclination can be calculated from the definition of the adiabatic invariant:

$$\mathcal{J} = 2\pi(1 - \cos(\tilde{\beta})) = \left[\oint \Phi_{\mathrm{separatrix}} d\phi\right]_{\tilde{\delta}_{\mathrm{crit}}}, \tag{2.40}$$

where the separatrix equation at critical $\tilde{\delta}$ can be obtained by substituting the value of $\mathcal{K}$ corresponding to the unstable equilibrium point into equation (4.10). A noteworthy property of the solution (2.40) is that it depends exclusively on Z'. In other words, *in the adiabatic regime,*

the excitation of spin-orbit misalignment is independent of all system parameters except the primordial disk-binary plane inclination.

Using the approach delineated above, we have mapped out the relationship between the primordial disk-binary inclination and the final (post-encounter) stellar inclination (also with respect to the binary orbital plane). This function is shown as a purple curve on Figure (2.3). In the decoupled $\tilde{\delta} = 0$ regime, both the stellar and the disk's inclinations, measured with respect to the binary orbit, are preserved. However, because of differential precession, the mutual disk-star inclination undergoes cyclical variations (Batygin, 2012). The maximal and minimal mutual inclinations are obtained when the stellar orbit crosses the $y = 0$ line with a negative and a positive values of x respectively. The associated range of mutual inclinations is depicted in Figure (2.3) with red lines. As shown in the Figure, a broad array of spin-orbit angles, ranging from perfectly disk-aligned states to perfectly disk-anti-aligned star states can be produced as a consequence of passage through the secular spin-orbit resonance.

Magnetic and Gravitational Excitation

As pointed out by Lai, Foucart, and Lin (2011) (see also Lai 1999) and rehashed in section 2.2 of this paper, a finite disk-star misalignment can be amplified by magnetic disk-star interactions. Within the context of the picture outlined above, it is tempting to assume that magnetic torques will be of no consequence prior to the encounter with the separatrix, since adiabatic invariance ensures alignment between the disk and the star. However, a more thorough examination shows that the equilibrium on which the star is envisioned to reside at $\tilde{\delta} > \tilde{\delta}_{\rm crit}$ deviates away from the exact disk-aligned state by a small amount[2].

[2]This misalignment refers to the forced component of the inclination vector (see Ch.7 of Murray and Dermott 1999)

Consequently, the seed misalignment needed for the magnetic tilting process to become active is ensured to exist from purely gravitational considerations. The amplitude of this equilibrium misalignment is shown as a function of $\tilde{\delta}$ in Figure (2.4) for the three choices of inclination considered above. Note that even for high values of $\tilde{\delta}$, the misalignment can be consequential (e.g., $\sim 0.5 - 5$ deg).

The extent to which the purely gravitational picture outlined above will be altered by the incorporation of magnetic fields depends on the assumed parameters inherent to the system. This can be gathered immediately by considering the characteristic magnetic tilting timescale:

$$\tau_B = \left[\frac{\zeta}{3} \frac{B_\star^2}{\mu_0} \frac{R_\star^4}{I M_\star \Omega_\star a'^3_{\rm in}} \right]^{-1} . \tag{2.41}$$

Evaluated using the physical parameters quoted in section 2, a stellar rotation period of ~ 5 days (Affer et al., 2013; Bouvier, 2013), and a surface field of $B_\star \simeq 1.5$ kGauss (Johns-Krull, 2007; Gregory, Donati, et al., 2012), this timescale (either assuming a constant surface field or a constant magnetic dipole moment in time), along with the characteristic stellar precession timescale, and a typical disk precession timescale are plotted over a maximal disk lifetime in Figure (2.5).

Owing to gravitational contraction, if an evolutionary track with a constant surface field is assumed, the cumulative effect of the magnetic torque is smaller than that if a constant dipole moment is assumed. The former situation is easily tractable within the context of the picture outlined above. First, let us imagine that system parameters are such that the secular resonance is encountered later than ~ 0.5 Myr after the birth of the star (i.e., after the characteristic magnetic tilting timescale becomes considerably longer than the disk lifetime). Under

this assumption, the magnetic and gravitational acquisitions of disk-star misalignment occur on separate timescales and can be treated sequentially.

It is worth recalling that the neighborhood of the (nearly) disk-aligned equilibrium of $\mathcal{K}$ (shown on Figure 2.2) is foliated in elliptical circulatory trajectories. This means that the system can acquire a non-zero value of $\mathcal{J}$ well before resonance crossing. Consequently, as $\tilde{\delta}$ approaches $\tilde{\delta}_{\rm crit}$, the trajectory will encounter the separatrix at at a moment when the phase-space area occupied by the inner branch of the critical curve matches that of the orbit. In other words, the resonant encounter will take place at $\tilde{\delta} > \tilde{\delta}_{\rm crit}$. As a consequence, the resonant excitation of spin-orbit misalignment will occur earlier in the disk's evolution and the acquired misalignment will be somewhat different. However, blunt evaluation shows that barring unreasonable estimates, the quantitative correction is essentially negligible and is of little interest (especially given the substantial uncertainties in other, more essential parameters such as ν).

Considerably more interesting dynamical behavior can be observed if a constant magnetic moment is assumed. As shown in Figure (2.5), in this case the magnetic tilting timescale is comparable to the disk torquing time. Thus, rather than reasoning through the evolution within the framework of adiabatic theory, we resort to direct numerical integration of equations of motion, accounting for both, magnetic torques (equations 4.31) and gravitational torques arising from Hamiltonian (4.10).

We initialize the system at the gravitational equilibrium point discussed above. The orbit is evolved for 10 Myr, adopting the same choices of disk-binary inclination as before, in addition to an almost

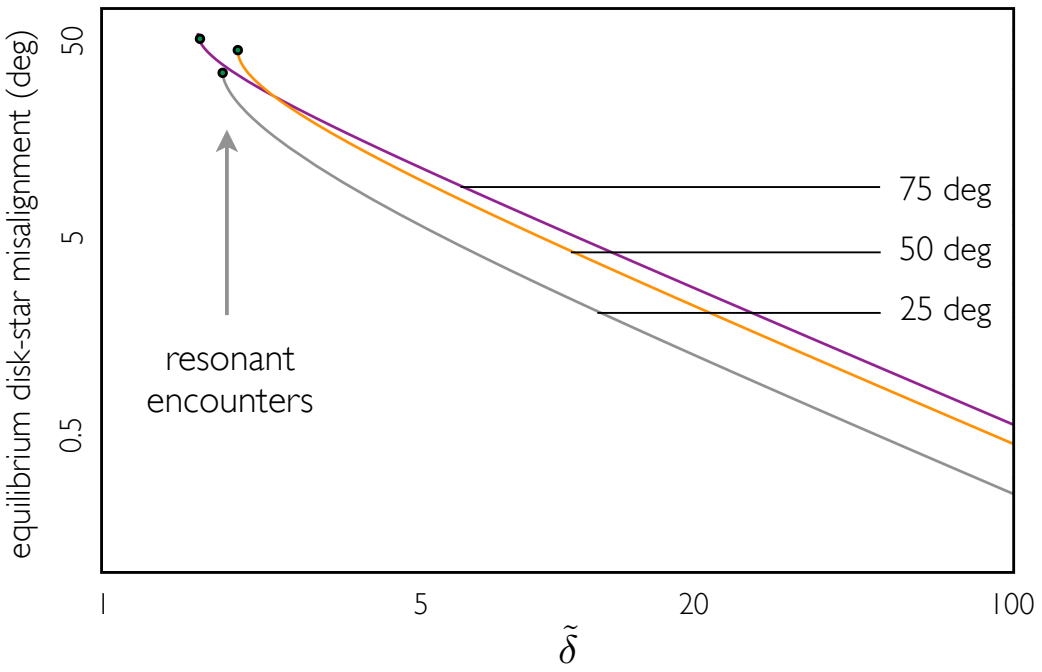

Figure 2.4: Gravitationally enforced misalignment between an equilibrium point (i.e., initial condition) of the Hamiltonian (4.10) and the disk-aligned state as a function of the resonance proximity parameter $\tilde{\delta}$ for various disk-binary inclinations. The fact that the gravitational equilibrium does not lie directly on a disk-aligned state provides a seed inclination for magnetic torques to operate.

orthogonal configuration with $\beta' = 85$ deg. Finally, for a more candid comparison, we ignore the dependence of ν on β' and assume a disk precession period of $2\pi/\nu = 1$ Myr for all simulations. The physical evolutions of the star and the disk are assumed to proceed as described in section 2.1.

The results of the integrations are shown in Figure (2.6), where the full integrations are plotted in red and solutions that only account for gravitational torques are plotted in gray for comparison. Immediately, a number of interesting features can be observed. First, in all simulations, the magnetically facilitated growth of $\mathcal{J}$ is evident, and the impulsive excitation of spin-orbit misalignment occurs substantially earlier when magnetic tilting is taken into account.

For lower inclinations (i.e., $\beta' = 25$ deg and $\beta' = 50$ deg), it is clear that magnetic tilting complicates the trajectory, although the qualitative behavior of the dynamical evolution is similar to that of the purely gravitational calculation. That is to say that the orbit evolves towards a quasi-circular state (in phase-space) as the disk dissipates. However, unlike the purely gravitational case, here the value of $\mathcal{J}$ continues to grow, even after separatrix crossing. This is largely due to magnetic torques and arises from the fact that a fraction of the orbit resides at $\beta < 90$ deg. The plots of stellar inclination relative to the disk give a physical picture of the above process.

When star-disk inclinations reach values of $\beta_i \geq 90$ deg, the magnetic contribution in our model becomes null and the only effect is that of secular gravitational interactions. This remains true until the oscillatory trajectory brings the star-disk inclination to $\beta_i \leq 90$ deg. At this point, the magnetic influence returns and repels the stellar inclination back to values of $\beta_i \geq 90$ deg. This causes the inclination to oscillate in a similar fashion to the purely gravitational case, but with its trajectory is eventually excluded from $\beta_i \leq 90$ deg. It is worth noting that a quantitative description of this effect would be significantly altered if there is in fact some magnetic influence (not considered here) for $\beta_i \geq 90$ deg.

The evolution at higher inclinations is qualitatively different, as the orbit evolves towards a fixed point (characterized by a balance between gravitational and magnetic torques) after crossing the separatrix. The $\beta' = 85$ deg case is particularly striking, as the phase-space plot depicts an initial condition that behaves as a repeller of the trajectory and the binary aligned equilibrium point serves as an attractor. It is interesting to note that similar behavior can be obtained by augmenting the Hamiltonian evolution with dissipative effects of accretion (see

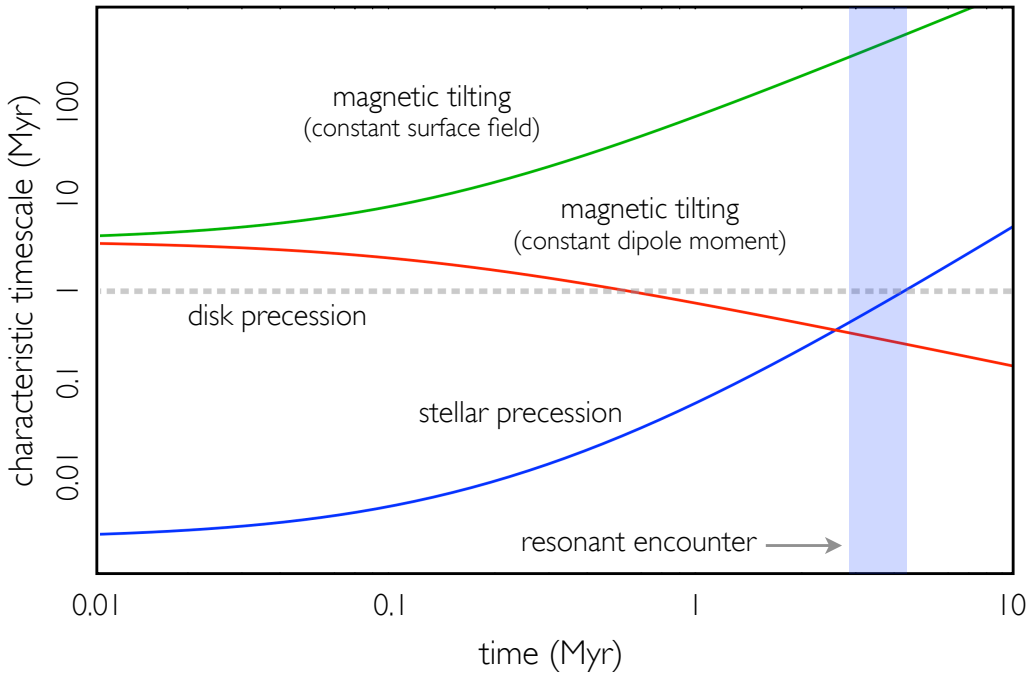

Figure 2.5: Characteristic timescales as functions of disk age. Taking into account the physical evolution of the star and the disk, the stellar precession timescale is shown as a blue line, while magnetic tilting timescales assuming a constant surface field and a constant dipole moment are shown as green and red curves respectively. The disk precession timescale is nominally chosen to be 1 Myr, as in the numerical simulations discussed in the text. The time interval at which the resonant encounter will take place (depending on β') is highlighted in blue.

Batygin and Adams 2013 for an in-depth discussion).

These results imply that provided an advantageous prescription for the ingredients inherent to the magnetic torquing part of the calculation, the dynamical evolution of the system can be qualitatively altered. However, it is important to note that magnetic effects do not obstruct the acquisition of spin-orbit misalignment within the framework of the disk-torquing model but instead act to accelerate it. In turn, gravitational effects provide the root inclination needed for the magnetic torques to operate. Consequently, it seems reasonable to conclude that the magnetic torquing mechanism proposed by Lai, Foucart, and Lin (2011) may play an important, but nevertheless secondary role in

explaining observed hot Jupiter spin-orbit misalignments.

2.4 Discussion

In this work, we have considered the excitation of spin-orbit misalignment within the context of disk-torquing theory (Batygin, 2012), taking into account magnetically-facilitated tilting of the star (Lai, Foucart, and Lin, 2011). While this study builds on the previous work of Batygin and Adams (2013), it differs in two important ways. First, the treatment of gravitational torques employed in this work does not assume small inclinations and allows us to self-consistently explore the process of secular spin-orbit resonant encounters. Second, this work includes additional physics stemming from magnetic disk-star interactions (Lai, 1999). Cumulatively, the results of our work can be summarized as follows.

Taking advantage of the separation of dynamical and physical evolution timescales inherent to the problem, we utilized adiabatic theory (Henrard, 1991) to analytically compute the impulsive excitation of spin-orbit misalignment during resonant encounters. The attained results prove that *the entire possible range of spin-orbit misalignments can be produced exclusively by the disk-torquing mechanism given a disk-binary orbit inclination* $\beta' \leqslant 65\,\mathrm{deg}$. Moreover, as long as the resonant encounter takes place in an adiabatic regime, the attained inclination depends only on β'.

The inclusion of magnetic effects complicates the purely gravitational picture on a quantitative level. Primarily, magnetic perturbations drive the system through secular spin-orbit resonance at an earlier epoch, thereby leading to somewhat enhanced disk-star inclinations. At high disk-binary orbit inclinations, magnetic torques may also drive the system towards an equilibrium that corresponds to a near-alignment

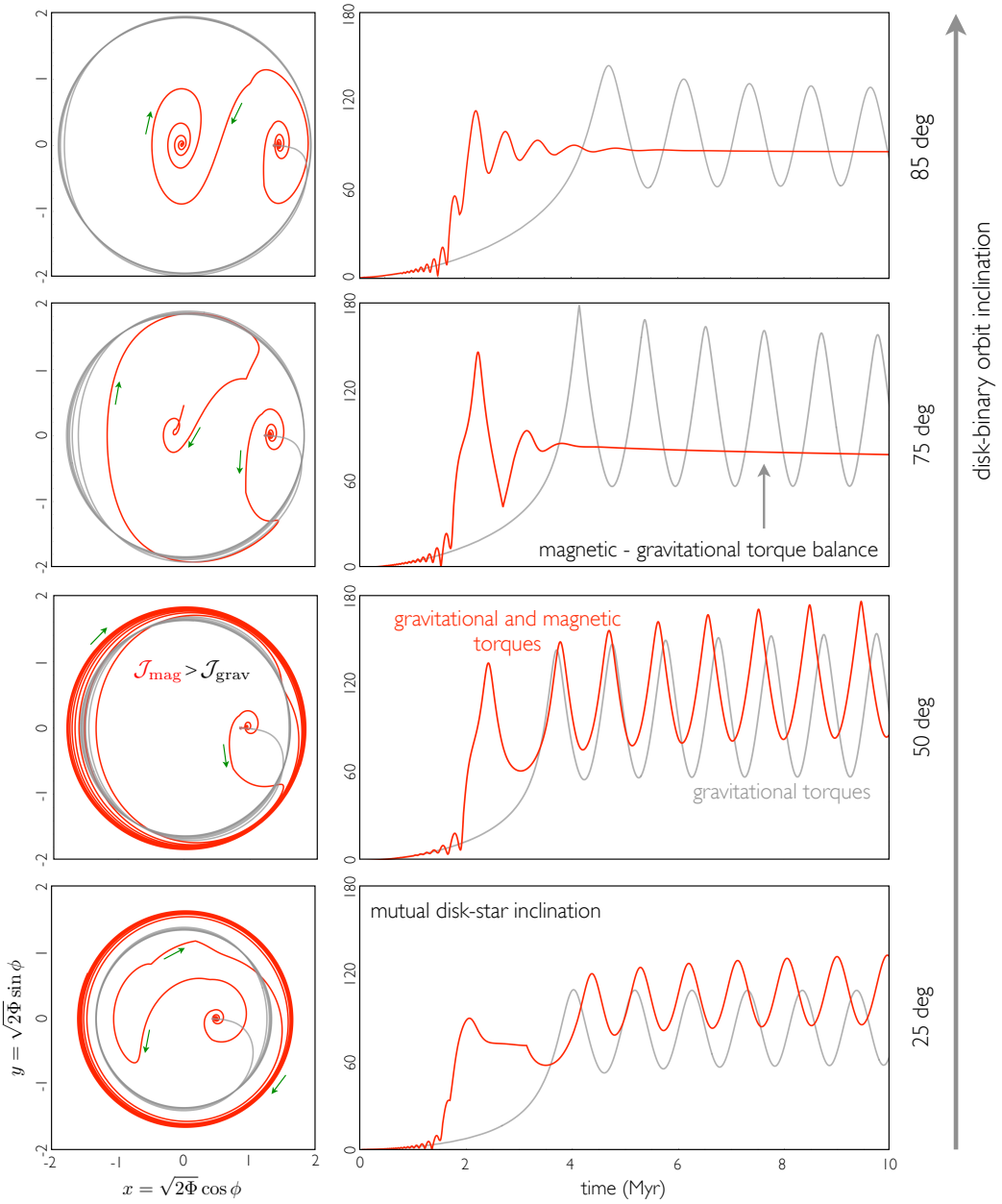

Figure 2.6: The results of numerical integration of equations of motion. The right panels show mutual disk-star inclination as functions of time, while the left panels show the phase-space trajectories of the stellar spin axis. The red curves denote solutions that account for gravitational and magnetic torques, assuming a constant dipole moment. Meanwhile, the gray curves show solutions where only gravitational torques have been retained. While the latter adhere to the analytic solutions obtained within the framework of adiabatic theory, the former show qualitative deviations from purely conservative behavior.

between the stellar spin-axis and and the binary orbit angular momentum vector. However, we note that in order to obtain significant deviations away from a purely gravitational solution, we made favorable (and perhaps unrealistic) assumptions about the strength of the field (Donati et al., 2010; Gregory, Jardine, et al., 2010) and the disk truncation radius (Matt and Pudritz, 2004). Consequently, it may be true that the aforementioned corrections are not too relevant in reality. Either way, the capacity of the disk-torquing model to explain the origins of spin-orbit misalignments of hot Jupiters, within the context of smooth disk-driven transport is not hindered by the inclusion of additional physics.

An obligatory property of the disk-torquing model considered in this work is the prevalence of stellar companions during the early epochs of planet formation.This constraint is not as stringent as that inherent to (for example) the Kozai migration model (Wu and Murray, 2003; Fabrycky and Tremaine, 2007; Naoz, Farr, Lithwick, et al., 2011) which requires longer-lived binaries than the model presented here. As such, we would expect the disk-torquing scenario to play out more frequently across a sample of planetary systems than Kozai migration owing to the expectation that longer-lived binaries are rarer than the short-lived types that torque the disk. Enhanced stellar multiplicity in star-forming environments is nevertheless a requirement of the disk torquing model (Batygin, 2012). Although a significantly elevated fraction of multi-stellar systems in young star clusters is observationally established (Ghez, Neugebauer, and Matthews, 1993; Kraus et al., 2011), it seems natural to additionally expect a corresponding correlation between hot Jupiter spin-orbit misalignments and the existence of present-day wide-orbit companions.

To this end, the observational survey of Knutson et al. (2014) has not

found a statistically significant parallel between the two measurements. However, in interpreting these results, it is important to keep in mind that the dynamics of stellar clusters can be extremely complex (see, e.g., Malmberg et al. 2007; Adams 2010), and dissolution of multi-stellar systems as well as binary exchange reactions will act to obscure a direct relationship between primordial and present (i.e., cluster-processed) field stellar multiplicity. However, such interactions may well be specific to high density clusters (Duchêne and Kraus 2013) and so additional computational effort is required to determine whether the theory presented here is consistent with observations of stellar multiplicity. This issue should be examined in detail as an integral component of a future study.

An observational trend that our model does not explicitly account for is the dependence of hot Jupiter misalignments on the effective temperature of their host stars (Winn, Fabrycky, et al., 2010). Although, an explanation that invokes the mass-dependence of tidal dissipation for why predominantly hotter stars ($T_{\rm eff} \gtrsim 6250$K) are characterized by large obliquities has been presented (Winn, Howard, et al., 2011; Lai, 2012; Albrecht et al., 2012). Within the context of the envisioned scenario, all hot Jupiters originate with high orbital obliquities, and spin-orbit misalignments are subsequently erased by tidal dissipation preferentially in low-mass stars.

Generally, the disk torquing model discussed in this work does not preclude subsequent, additional effects owing to tidal dissipation. However, in light of the recent criticism of this narrative by Rogers and Lin (2013), it may be worthwhile to speculate about an alternative scenario. As already mentioned above, if disk-driven migration is the dominant mode of early orbital transport, the generation of spin-orbit misalignments requires a wide-spread existence of binaries in

birth clusters. It has been noted observationally that stellar binarity (and the stellar orbital distribution) are both strong functions of stellar mass (Kraus et al., 2011). Consequently, a handle on the observed misalignment-$T_{\rm eff}$ correlation may conceivably be obtained by further examining the tally and the longevity of multi-stellar systems in star-formation environments as a function of their mass. While a potentially fruitful avenue of reasoning, additional observational and modeling efforts will be required to definitively evaluate this possibility.

Chapter 3

ALIGNMENT OF PROTOSTARS AND CIRCUMSTELLAR DISKS DURING THE EMBEDDED PHASE

ABSTRACT

Star formation proceeds via the collapse of a molecular cloud core over multiple dynamical timescales. Turbulence within cores results in a spatially non-uniform angular momentum of the cloud, causing a stochastic variation in orientation of the disk forming from the collapsing material. In the absence of star-disk angular momentum coupling, such disk-tilting would provide a natural mechanism for production of primordial spin-orbit misalignments in the resulting planetary systems. However, owing to high accretion rates in the embedded phase of star formation, the inner edge of the circumstellar disk extends down to the stellar surface, resulting in efficient gravitational and accretional angular momentum transfer between the star and the disk. Here, we demonstrate that the resulting gravitational coupling is sufficient to suppress any significant star-disk misalignment, with accretion playing a secondary role. The joint tilting of the star-disk system leads to a stochastic wandering of star-aligned bipolar outflows. Such wandering widens the effective opening angle of stellar outflows, allowing for more efficient clearing of the remainder of the protostar's gaseous envelope. Accordingly, the processes described in this work provide an additional mechanism responsible for sculpting the stellar Initial Mass Function (IMF).

3.1 Introduction

In the simplest picture for star and planet formation, the angular momentum vectors for stellar rotation, the circumstellar disk, and the resulting planetary orbits all coincide. However, recent observations showing that planetary orbits are often misaligned with stellar rotation axes (Fabrycky and Winn, 2009; Winn, Fabrycky, et al., 2010) have prompted several authors (e.g., Bate, Lodato, and Pringle 2010; Batygin 2012) to suggest that disks themselves may become misaligned with their parent stars. Any such primordial star-disk misalignment occurring within the embedded phase, during which the star gains most of its mass, has consequences both for future planetary systems and for the impact of protostellar outflows on their surrounding envelopes. In this letter, we construct a model for protostar-disk systems that describes the gravitationally-facilitated precession of the stellar rotation axis about a tilting disk, including dissipative torques owing to accretion.

In spite of enormous progress in our understanding of star formation (from Shu, Adams, and Lizano 1987 to McKee and Ostriker 2007), the final mass of a star still cannot be unambiguously determined from the initial conditions of the original molecular cloud core. Protostellar outflows represent one mechanism that can help separate a newly formed star from its immediate environment (Shu, Adams, and Lizano, 1987), and this mechanism may provide an explanation for the stellar initial mass function (Adams and Fatuzzo, 1996). Although outflows have sufficient mechanical luminosity to reverse the infall (Lada, 1985), one criticism of this picture is that the outflows start with relatively narrow angular extents. However, the opening angles widen with time and precessing outflows can produce outflow cones that are effectively wider than their intrinsic extent, thereby making it

easier for outflows to limit the mass falling onto the central star/disk system. Independent of the efficacy of the outflows in limiting stellar masses, observations show that protostellar jets precess (Eisloffel et al., 1996; Cesaroni et al., 2005) and that circumstellar disks are not always aligned with the plane of binary orbits (Stapelfeldt et al., 1998; Koresko, 1998).

The angular momentum of a circumstellar disk must be obtained from the gradual accumulation of material from a molecular cloud core. Rotation rates of such cores are estimated through measurements of velocity gradients of a given molecular line across the map of the core (e.g., Goodman et al. 1993). The inferred angular velocity vectors *do not point in the same direction over the entire core*; instead they vary in projected direction over a range of $\sim$ 30 degrees within the region encompassing material that is destined to form a star. Moreover, the coherence length λ for the velocity vectors inferred from these emission maps is $\lambda \sim 0.01$ pc (Caselli et al., 2002). As collapse of these core structures proceeds, the infalling material will thus sample cloud layers of differing angular momentum orientation. As the layers fall inward and join the growing star/disk system, the angular momentum vector of the system must vary in direction (as well as magnitude). On a related note, these cores are observed to be turbulent, especially in the outer layers of low-mass cores (Myers and Fuller, 1992) and in more massive cores (Jijina, Myers, and Adams, 1999). The collapse of a turbulent region also produces varying directions for the angular momentum vectors of the forming star/disk systems as the collapse proceeds. Numerical simulations of this process (Bate, Lodato, and Pringle, 2010; Fielding et al., 2015) show that the angular momentum vectors of the disks change as different cloud layers fall inward.

Assuming the star to be decoupled from the disk, star-disk misalign-

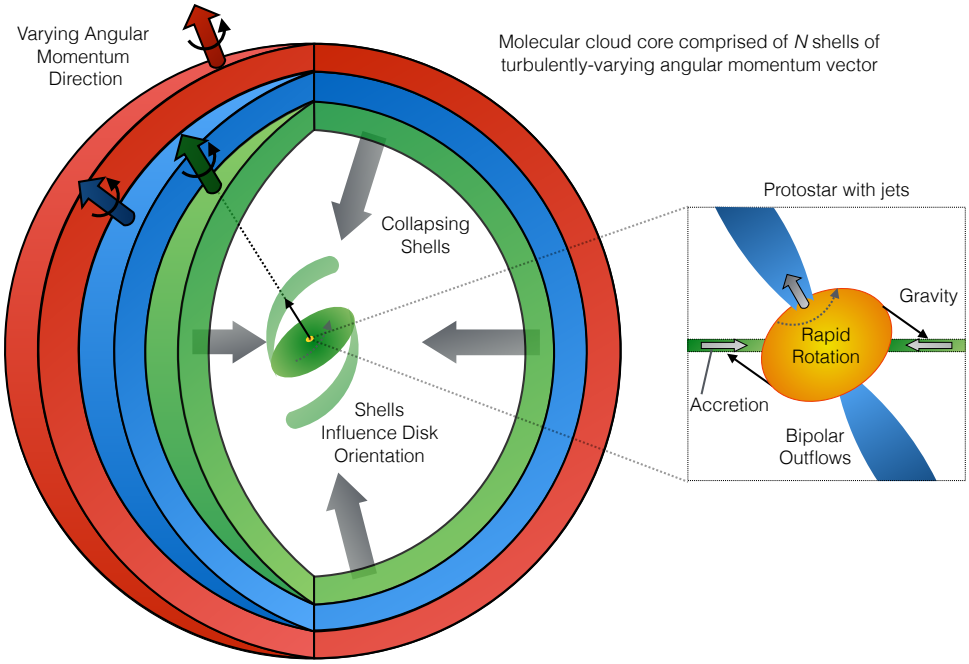

Figure 3.1: A schematic of the process described in the text. Different shells possess different angular momentum vectors. In turn, the disk changes its orientation with time. Gravitational and accretional torques act between the star and disk, with bipolar outflows originating from the stellar spin axis.

ment is indeed an expected result of disk-tilting. However, young stars rotate rapidly, becoming oblate. This oblateness leads to a gravitationally-forced precession of the stellar spin axis with respect to the disk (Batygin and Adams 2013) and provides a physical mechanism by which the star's spin axis may trail the disk as it tilts. Additional potential sources of stellar spin-axis evolution include accretion, stellar winds, and magnetic fields. As we are considering the Class 0 phase, accretion is likely to dominate over other effects, as discussed below.

3.2 Model Description

We begin by describing the basic model, illustrated in Figure 3.1, whereby a molecular cloud core collapses to form a star and circumstellar disk. As noted in the Introduction, sequential radii within the

core differ in mean angular momentum direction. Owing to the large angular momentum reservoir of the collapsing material, the disk will in turn adopt a time-varying orientation as the core collapses onto it. Within the physical framework considered here, there exist three relevant timescales. Specifically, these are the shell-shell de-correlation time ($\tau_{\rm dc}$), the characteristic star-disk realignment time ($\tau_{\rm r}$) and the nodal regression period of the stellar spin-axis ($\mathcal{T}$). Let us evaluate these quantities sequentially.

Turbulent Core Collapse

Although the detailed structure of the core is complicated, we assume that the density distribution has the form

$$\rho(r) = \frac{A\, c_{\rm s}^2}{2\,\pi\, G\, r^2}\,, \tag{3.1}$$

where $c_{\rm s}$ is the isothermal sound speed and $A > 1$ is an overdensity factor (Fatuzzo, Adams, and Myers, 2004) that accommodates the fact that cores are not in exact hydrostatic equilibrium (Lee, Myers, and Tafalla, 1999). With the density distribution (3.1), the enclosed mass has the form

$$M(r) = \frac{2\, A\, c_{\rm s}^2\, r}{G}\,. \tag{3.2}$$

Motivated by both observations of emission maps (Caselli et al., 2002) and numerical simulations of collapsing turbulent cores (Bate, Lodato, and Pringle, 2010; Fielding et al., 2015), we assume that different (spherical) shells have different directions for their angular velocity. To be consistent with observed maps and numerical expectations, the shell thickness should be comparable to, but smaller than, the coherence length λ. For the sake of definiteness, we take the shell thickness $\ell = \lambda/2 = 0.005$ pc. With this choice, the formation of a solar type star will involve the collapse of $N = 5 - 10$ shells. The

mass of each shell is given by

$$\Delta m = \frac{2\,A\,{c_{\rm s}}^2}{G}\,\ell \approx 0.10\,M_\odot \left(\frac{c_{\rm s}}{0.2\,{\rm km/s}}\right)^2 \left(\frac{\ell}{0.005\,{\rm pc}}\right). \tag{3.3}$$

Each of these shells is then assumed to have an angular velocity vector with direction chosen randomly within a range 0 – 30 degrees. In this scenario, the mass infall rate is nearly constant with $\dot{M} = m_0\,c_{\rm s}^3/G$, where m_0 is a dimensionless constant of order unity (Shu, 1977). The shell-shell decorrelation time is equal to the corresponding time interval required for a shell to fall inward, given by

$$\tau_{\rm dc} = \frac{2A}{m_0}\frac{\ell}{c_{\rm s}} \approx 25,000\ {\rm yr}\,. \tag{3.4}$$

In order to model angular velocity variation, we define scaled Poincaré action-angle coordinates in terms of inclination angle β and longitude of ascending node Ω:

$$\mathcal{Z} = 1 - \cos(\beta) \qquad z = -\Omega. \tag{3.5}$$

We randomly choose the third Poincaré momentum of shell i from a Gaussian distribution having mean $\mu = \mathcal{Z}_{i-1}$ and standard deviation $\sigma = \mathcal{Z}_{30^\circ}$ where $\mathcal{Z}_{30^\circ} = 1 - \cos(30^\circ)$ is the value of $\mathcal{Z}_{\rm disk}$ corresponding to a 30 degree inclination. Specifically,

$$\mathcal{Z}_{i+1} = \mathcal{R}_{\rm an}\left[\,\exp\left(-\frac{(\mathcal{Z}-\mathcal{Z}_i)^2}{2\mathcal{Z}_{30^\circ}^2}\right)\right], \tag{3.6}$$

where $\mathcal{R}_{\rm an}[]$ symbolises extracting a random number from the distribution within parentheses. Likewise, the canonical angle z of shell i relative to shell $i-1$ is drawn randomly, but from a uniform distribution of $0 \le -z \le 2\pi$. Additional, small-scale turbulence-mediated stochasticity is introduced by way of $100\,N$ smaller shells, each varying in a Gaussian form by a value of 1 degree. Once all shells have been prescribed a value of $\mathcal{Z}$ and z, we smooth the $100\,N$ inclinations

into a continuous function of time by considering the entire star formation process to proceed over a time $\tau_{\rm form} = 2 \times 10^5$ years and thus, for each of the $100\,N$ inclinations to occur within a time interval of $\Delta t = \tau_{\rm form}/100\,N$. Using a 3rd order cubic spline interpolation, we generate a pseudo-random function of time, $\{\mathcal{Z}(t), z(t)\}$, denoting the time-varying angular momentum vector of the collapsing material. Assuming the disk to obtain its angular momentum directly from the envelope, the disk angular momentum vector instantaneously follows that of the collapsing shells.

Realignment Time

The angular momentum of a rotating star is given by the well-known expression

$$\mathcal{L}_\star = I\, M_\star\, R_\star^2\, \omega, \tag{3.7}$$

where I is the dimensionless moment of inertia and ω is the stellar spin. For the purposes of this letter, we shall adopt stellar structure parameters corresponding to $n = 3/2$ polytrope, which corresponds to a fully convective object.

At the earliest stages of stellar evolution, accretion rates of disk material onto the protostellar core can be ubiquitously high with characteristic values of order $\dot{M} \sim 10^{-5}\,M_\odot$/yr (for a $M \sim 1\,M_\odot$ object; see Ward-Thompson 2002). Accordingly, the accretionary ram pressure may in fact be sufficient to overwhelm the magnetic pressure of the protostellar magnetosphere, connecting the disk's inner edge to the stellar surface (Ghosh and Lamb 1978). The critical magnetic field strength, $B_{\rm crit}$, below which this happens can be estimated by setting the magnetospheric disk truncation radius to that of the star (Shu,

Najita, et al. 1994):

$$B_{\rm crit} = \left(\frac{G\, M_\star\, \dot{M}^2\, \xi^7}{R_\star^5} \right)^{1/4}, \tag{3.8}$$

where ξ is a dimensionless constant of order unity (Mohanty and Shu 2008). Given nominal parameters, the critical field evaluates to $B_{\rm crit} \sim 2\,{\rm kG}$, which is above the oft-cited $B_\star \sim 1$ kG fields inherent to young stellar objects (Gregory, Donati, et al. 2012).

In a regime where the inner edge of the disk is physically connected to the stellar surface, the accretionary flow will facilitate a direct and efficient transfer of angular momentum between the disk and the host star (Ghosh and Lamb 1979). While the details of the disk-star coupling in a shearing boundary layer can be complex (Belyaev, Rafikov, and Stone 2013), to leading order the rate of stellar angular momentum accumulation can be written as follows (Armitage and Clarke 1996):

$$\frac{d\mathcal{L}_\star}{dt} \simeq \dot{M}\, \sqrt{\mathcal{G}\, M_\star\, R_\star}. \tag{3.9}$$

With the above equations at hand, we may now define a characteristic timescale for accretion-forced realignment of the stellar spin-axis. Specifically, we have:

$$\tau_{\rm r} \equiv \frac{\mathcal{L}_\star}{{\rm d}\mathcal{L}_\star/{\rm d}t} \sim \frac{I\, M_\star\, R_\star^2\, \omega}{\dot{M}\, \sqrt{\mathcal{G}\, M_\star\, R_\star}} \sim 10^4 \ \text{years}, \tag{3.10}$$

where as an estimate of the stellar spin rate we adopt the break-up rotational velocity $\omega = \sqrt{\mathcal{G} M_\star / R_\star^3}$, leading to $\tau_{\rm r} = I\,(M_\star/\dot{M})$, which is independent of stellar radius, $R_\star$. Note the similarity between $\tau_{\rm r}$ and the shell infall timescale (equation 3.4)

Additional effects can change the alignment. Perhaps most notably, modulation of the stellar spin-axis may arise from magnetic disk-star

coupling (Lai, Foucart, and Lin 2011; Spalding and Batygin 2014). While we have neglected this effect here, the fact that the accretionary flow at early stages of stellar evolution is intense enough to penetrate the stellar magnetosphere suggests that, indeed, the dominant mode of realignment will be facilitated by accretion and not magnetohydrodynamic effects.

Precession

As mentioned above, during the Class 0 epoch of stellar formation, young stellar objects may spin at near-breakup velocities. This naturally leads to significant rotational deformation. The spin-axis dynamics of an oblate spheroid can be modeled using standard techniques of celestial mechanics by replacing the rotational bulge of the star with an inertially equivalent orbiting ring of semi-major axis

$$\chi = \left(\frac{16\,\omega^2\,k_2^2\,R_\star^6}{9\,I^2\,\mathcal{G}M_\star} \right)^3 = R_\star \left(\frac{4\,k_2}{3\,I} \right)^{2/3}, \tag{3.11}$$

where $k_2 = 0.14$ is the Love number[1] (twice the apsidal motion constant). The second equality follows from assuming that the star spins at breakup frequency. In principle, the aforementioned ring has a well-specified mass, however, its value only controls the back-reaction of the stellar quadrupole moment on the disk, which is unimportant.

To complete the specification of the problem, we must characterize the properties of the disk. We take the disk to be axisymmetric, and its surface density to vary inversely with semi-major axis (Andrews, Wilner, Hughes, et al. 2009):

$$\Sigma = \Sigma_0 \left(\frac{a}{a_0} \right)^{-1}, \tag{3.12}$$

[1] This value corresponds to a polytropic body of index $n = 3/2$

where Σ_0 is the surface density at $a = a_0$. Additionally, we take the disk aspect ratio to be $\zeta \equiv h/a = 0.05$, though its actual value likely varies with disk radius up to ~ 0.1 (Armitage 2011). We note that under this prescription,

$$M_{\rm disk} = \int_0^{2\pi} \int_{R_\star}^{a_{\rm out}} \Sigma \, a \, da \, d\phi \simeq 2\,\pi \Sigma_0 \, a_0 \, a_{\rm out}, \tag{3.13}$$

where $a_{\rm out} = 30 - 50$ AU is the physical size of the disk (Kretke et al. 2012; Anderson, Adams, and Calvet 2013).

To compute the dynamical evolution, we make use of classical perturbation theory (Morbidelli 2002). Accordingly, we must first choose the appropriate expansion of the disturbing Hamiltonian. Given that $\chi \approx R_\star$ and the inner boundary of the disk is linked to the stellar surface, an expansion in the semi-major axis ratio (Kaula 1962; Spalding and Batygin 2014) is bound to be slowly-convergent. Therefore, in this work we shall opt for an alternative description that assumes mutual disk-star inclination as a small parameter and places no restrictions on the semi-major axis ratio (Le Verrier 1856, Murray and Dermott 1999).

As a starting step, consider the mutual interaction of a massive hoop representing the stellar rotational bulge and a disk annulus of radial thickness da. It is a well-known result of secular perturbation theory that upon averaging over the orbital phase, the semi-major axes of both rings are rendered constants of motion. Thus, the Keplerian contributions to the Hamiltonian become trivial and can be omitted.

To leading order in mutual inclination, the Lagrange-Laplace disturb-

ing Hamiltonian reads (Batygin and Adams 2013):

$$d\mathcal{H} = \frac{\tilde{b}^{(1)}_{3/2}}{4}\sqrt{\frac{\mathcal{G}\,M_\star}{a^3}}\frac{dm}{M_\star}\sqrt{\frac{\chi}{a}}\left[\mathcal{Z}_{\rm star} - 2\sqrt{\mathcal{Z}_{\rm star}\mathcal{Z}_{\rm disk}}\cos(z_{\rm star} - z_{\rm disk})\right], \tag{3.14}$$

where $dm = 2\pi\,\Sigma_0\,a_0\,da$ is the mass of the perturbing annulus, $\tilde{b}^{(1)}_{3/2}$ is a softened Laplace coefficient (see below for an explicit expression).

To obtain the Hamiltonian governing the interactions between the star and the full disk, we integrate with respect to the semi-major axis ratio $\alpha = \chi/a$:

$$\begin{aligned}\mathcal{H} = &\frac{1}{4\pi}\sqrt{\frac{\mathcal{G}M_\star}{\chi^3}}\frac{M_{\rm disk}}{M_\star}\frac{\chi}{a_{\rm out}} \\ &\times\left(\int_0^{\chi/R_\star}\int_0^{2\pi}\frac{\cos(\psi)}{(1-2\alpha\cos(\psi)+\alpha^2+\zeta^2)^{3/2}}\,d\psi\,d\alpha\right) \\ &\times\left[\mathcal{Z}_{\rm star} - 2\sqrt{\mathcal{Z}_{\rm star}\mathcal{Z}_{\rm disk}}\cos(z_{\rm star} - z_{\rm disk})\right].\end{aligned} \tag{3.15}$$

Note that in this formulation of the problem, we are not explicitly solving for the dynamical evolution of the disk using the above Hamiltonian. Instead, the time-varying variables $(\mathcal{Z}_{\rm disk}, z_{\rm disk})$ constitute prescribed functions of time, as described above. Suitably, the only equations of motion we derive from equation (3.15) are those corresponding to the $(\mathcal{Z}_{\rm star}, z_{\rm star})$ degree of freedom.

Although the inclination, i, and the longitude of ascending node, Ω, are measured in an inertial reference frame, the inherent assumption of the Lagrange-Laplace secular theory is that the *mutual* disk-star inclination remains small (Morbidelli, Tsiganis, et al. 2012). Thus,

it is important to understand that any solution obtained within the framework of this description is only trustworthy if it dictates a low disk-star inclination for the entirety of the time-span of interest. Conversely, if mutual disk-star inclination is to increase to an appreciable value, one must default to the much more computationally expensive, but ultimately precise Gaussian averaging method (Touma, Tremaine, and Kazandjian 2009).

To obtain the precession rate of the stellar spin axis in the frame of the disk, we may envision that the disk remains stationary at $\beta = 0$ (this assumption will be lifted later), meaning that $\mathcal{Z}_{\rm disk} = 0$. This puts the amplitude of the harmonic part of the Hamiltonian (3.15) to zero, such that $\mathcal{H}$ governs pure rotation in $z_{\rm star}$. Accordingly, we have:

$$\mathcal{T} = 2\pi \left(\frac{\partial \mathcal{H}}{\partial \mathcal{Z}_{\rm star}} \right)^{-1} \simeq 130 \left(\frac{0.01 M_\odot}{M_{\rm disk}} \right) \left(\frac{M_\star}{1 M_\odot} \right) \text{ years.} \tag{3.16}$$

For all reasonable choices of parameters, the precession timescale of the stellar spin-axis (which acts as the dynamical timescale of the problem at hand) is substantially shorter than both the accretionary realignment timescale and the shell-shell decoherence timescale. This feature is of crucial importance to understanding the results that follow, as it effectively guarantees that the dynamical evolution occurs within the *adiabatic* regime, within which the star trails the disk's orientation.

3.3 Numerical Simulations

Equations of motion arising from Hamiltonian (3.15), as formulated in terms of action-angle coordinates (3.5) contain a coordinate singularity at $\mathcal{Z}_{\rm star} = 0$. This complication can be removed with a canonical change of variables. Specifically, we introduce a complex coordinate

$$\eta = \sqrt{\mathcal{Z}} \cos(z) + \imath \sqrt{\mathcal{Z}} \sin(z), \tag{3.17}$$

where $\imath = \sqrt{-1}$. The Hamiltonian now reads:

$$\mathcal{H} = \mathcal{S}\left(\eta_{\rm star}\eta^*_{\rm star} + \eta_{\rm star}\eta^*_{\rm disk} + \eta^*_{\rm star}\eta_{\rm disk}\right), \tag{3.18}$$

where $\mathcal{S} = 2\pi/\mathcal{T}$ is the coefficient on the first line of equation (3.18) and the asterisk denotes a complex conjugate.

In addition to the dynamical evolution governed by $\mathcal{H}$, it is important to account for the dissipative effects originating from the realigning influence of accretionary torques, in the equations of motion. For tractability, it is sensible to parameterize such realignment as an exponential decay of the action[2] $\mathcal{Z}_{\rm star}$. Cumulatively, the relevant equation of motion takes the form:

$$\begin{aligned}\frac{d\eta_{\rm star}}{dt} &= \imath\left(\frac{\partial\mathcal{H}}{\partial\eta^*_{\rm star}}\right) + \left(\frac{d\eta_{\rm star}}{dt}\right)_{\rm r} \\ &= \imath\,\mathcal{S}\left(\eta_{\rm star} + \eta_{\rm disk}\right) - \frac{\eta_{\rm star}}{2\tau_{\rm r}},\end{aligned} \tag{3.19}$$

where $(d\eta_{\rm star}/dt)_{\rm r}$ describes the dissipative term, which acts to damp any misalignment. Without the dissipative term, equation 3.19 describes conservative, gravitational precession of the stellar spin axis about a time-varying disk angular momentum vector.

To complete the specification of the problem, we prescribe the time evolution of a $1\,{\rm M}_\odot$ star as

$$M_{\rm star}(t) = {\rm M}_\odot\left(\epsilon + \frac{t}{\tau_{\rm form}}\right), \tag{3.20}$$

where $\epsilon = 0.01$ represents a small initial 'seed' mass onto which shells collapse. Additionally, the circumstellar disk mass ($M_{\rm disk}$) grows proportionally to that of the star such that

$$M_{\rm disk}(t) = 0.1\,M_{\rm star}(t), \tag{3.21}$$

[2]Introduction of such terms into the equations of motion tends to transform nearby elliptical fixed points into attractors (see, e.g., Batygin and Morbidelli 2011).

with the 0.1 prefactor corresponding approximately to the upper limit for dynamical stability (Armitage 2011). We consider a constant stellar radius of $R_\star = 4\,\mathrm{R}_\odot$ throughout (Stahler, Shu, and Taam 1980).

3.4 Results & Discussion

In Figure 3.2 we present the paths followed by the stellar and disk angular momentum vectors in the purely gravitational regime, i.e., zero accretion. As is immediately obvious, the two paths are indistinguishable, meaning that even in the absence of accretionary realignment, no significant star-disk misalignment can result from turbulent core collapse. Accretionary torques simply act to reduce the already-miniscule misalignments (Figure 3.3) and so are dynamically unimportant to the problem at hand. As such, the first crucial result is that *the hypothesis that turbulent core-collapse leads to primordial spin-orbit misalignments is inconsistent with the framework presented here*. Spin-orbit misalignments must be obtained at a later evolutionary stage, such as during the main phase of planet formation (Lai, Foucart, and Lin 2011; Batygin 2012; Batygin and Adams 2013; Spalding and Batygin 2014) or after the disk has dispersed (e.g., Wu and Lithwick 2011; Beaugé and Nesvorný 2012; Albrecht et al. 2012).

Class 0 and Class I protostars possess collimated bipolar jets with sufficient mechanical luminosity to reverse the infall of core material. Such jets have been observed to 'wiggle' in such a way as to suggest time evolution of the jet direction (Eisloffel et al. 1996; Cesaroni et al. 2005). Previous pictures considering only disk motion do not necessarily account for jet wiggles, as the jets are collimated along the stellar spin axis through the action of magnetic fields (Shu, Najita, et al. 1994). Thus the jet itself is unlikely to move significantly if the star itself is not changing orientation. As noted by Shu, Adams, and

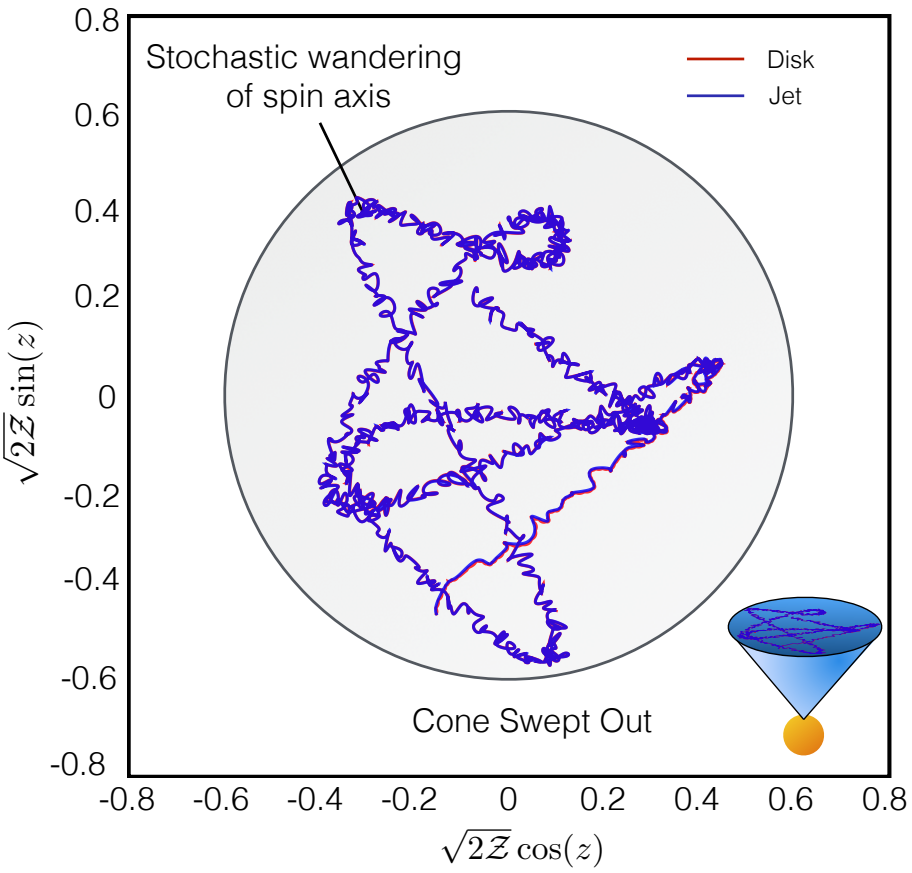

Figure 3.2: The paths traced out by the angular momentum vectors of the disk (red) and star (blue) plotted in canonical Cartesian co-ordinates (see text). Notice that the red and blue paths almost exactly overlap. The shaded region approximately inscribes the cone of gas cleared out by stellar spin axis-aligned jets.

Lizano (1987), a star breaks free of its enshrouding molecular envelope once outward pressures owing to stellar winds and jets exceed the ram pressure of infalling gas. Stellar outflows contribute significantly to such outward pressures and thus may in part determine the final mass of the forming star. Here we find that the stellar outflows carry out a random walk (Figure 3.2), leading to an effectively wider opening angle of the outflow. Accordingly, the wandering outflows may help separate the newly formed star/disk system from its environ-

ment earlier than would a stationary outflow. Such a physical process adds an important correction onto previous theories of star formation (e.g., Adams and Fatuzzo 1996) which propose that the IMF may be determined in part by outflows.

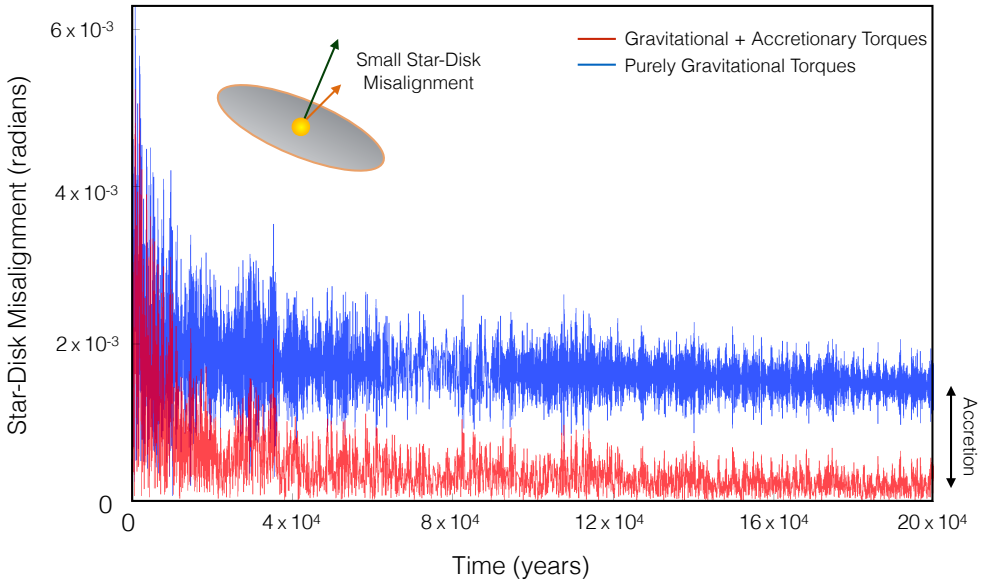

Figure 3.3: The misalignment between star and disk angular momenta plotted as a function of time. Gravitational interactions alone (blue) are sufficient to suppress significant misalignment. Accretionary torques (red) further reduce the misalignment to near-zero values.

Here, we considered a constant mass infall rate of $\dot{M} \approx 10^5\ M_\odot\ \mathrm{year}^{-1}$ over the entire star formation process. Strictly speaking, this assumption contradicts the non-steady nature of turbulent collapse. In principle, sufficiently violent episodic mass infall may lead to more rapid variations in disk angular momentum than considered here. However, owing to the vast separation of timescales between shell-shell decorrelation ($\tau_{\mathrm{dc}} \sim 10^4$ years) and stellar precession ($\mathcal{T} \sim 10^2$ years) the star shall trail the disk under almost any reasonable collapse conditions. Additionally, the mass infall and accretion rates fall by about an order of magnitude over a longer timescale, between the Class 0 and Class I phases of star formation (Ward-Thompson 2002). Such a

drop in infall rate is not included in our model but during the Class I phase, most of the mass is in the star-disk system (by definition) and so, combined with a drop in infall rate, disk tilting is likely to become significantly lower in amplitude. Accordingly, the star should remain even more tightly coupled to the disk, despite reduced accretionary torques, which we determined to be dynamically unimportant.

This letter presents a simple model for star/disk formation in molecular cloud cores possessing non-uniform angular momentum directions. We find that outflows change direction substantially, but stars and disks remain nearly aligned. Future work should develop more detailed models for all aspects of this problem, including the initial conditions, disk formation, wandering of outflow directions, and misalignment between star and disk.

Chapter 4

MAGNETIC ORIGINS OF THE STELLAR MASS-OBLIQUITY CORRELATION IN PLANETARY SYSTEMS

ABSTRACT

Detailed observational characterization of transiting exoplanet systems has revealed that the spin-axes of massive ($M \gtrsim 1.2\,\mathrm{M}_{\odot}$) stars often exhibit substantial misalignments with respect to the orbits of the planets they host. Conversely, lower-mass stars tend to only have limited obliquities. A similar trend has recently emerged within the observational dataset of young stars' magnetic field strengths: massive T-Tauri stars tend to have dipole fields that are $\sim$10 times weaker than their less-massive counterparts. Here we show that the associated dependence of magnetic star-disk torques upon stellar mass naturally explains the observed spin-orbit misalignment trend, provided that misalignments are obtained within the disk-hosting phase. Magnetic torques act to realign the stellar spin-axes of lower-mass stars with the disk plane on a timescale significantly shorter than the typical disk lifetime, whereas the same effect operates on a much longer timescale for massive stars. Cumulatively, our results point to a primordial excitation of extrasolar spin-orbit misalignment, signalling consistency with disk-driven migration as the dominant transport mechanism for short-period planets. Furthermore, we predict that spin-orbit misalignments in systems where close-in planets show signatures of dynamical, post-nebular emplacement will not follow the observed correlation with stellar mass.

4.1 Introduction

Of all ideas in planetary science, few have stood the test of time better than the "Nebular Hypothesis", originally proposed in the 18th century by Kant and Laplace (Kant, 1755; Laplace, 1796). The impetus for such a model was the near-aligned configuration of the planetary orbits with each other and with the Sun's spin axis; the net angular momentum of the the planets differs in direction from the Sun's spin by about 7 deg[1] (Beck and Giles, 2005). Centuries of refinement (with help from astronomical observations) have resulted in the modern picture whereby a dense molecular cloud core collapses under its own self gravity (Shu, Adams, and Lizano, 1987; McKee and Ostriker, 2007) to form a star encircled by a disk of gas and dust.

The earliest descriptions of molecular core collapse were naturally the most simplistic, supposing that the star and its disk both inherit similar angular momentum directions. More recent work (Goodman et al., 1993; Caselli et al., 2002; Bate, Lodato, and Pringle, 2010) has added a layer of complexity to the story by noting that turbulence in collapsing cores implies that the last bits of material falling onto the disk do not necessarily share the same angular momentum direction as the star. Despite this apparent tendency towards slight misalignment, the mutual gravitational torque between star and disk is likely strong enough during the earliest stages to stave off any significant star-disk misalignment arising from core turbulence (Spalding, Batygin, and Adams, 2014).

Long before the first exoplanetary detections (Mayor and Queloz, 1995; Marcy and Butler, 1996), the theory behind protoplanetary disks was already fairly mature (e.g., Goldreich and Tremaine 1979; Goldreich and Tremaine 1980; Lin and Papaloizou 1986; Ward 1986).

[1] Of course, 7 deg is very different from zero and so is still in need of an explanation.

An early prediction from this field was that angular momentum exchange between disks and their embedded planets should give rise to planetary migration towards shorter-period orbits. More recent work has subjected this idea to extensive numerical (Nelson, Papaloizou, et al., 2000; Rice, Armitage, and Hogg, 2008) and analytic (Tanaka, Takeuchi, and Ward, 2002) analyses, with the general picture of migration holding up as an expected outcome (for a recent review, see Kley and Nelson 2012). Sure enough, the earliest days of exoplanet-hunting revealed a considerable population of hot Jupiters, planets with about the mass of Jupiter but with orbital periods of a few days. Conventional planet formation theory (Pollack et al., 1996) suggests that these planets must form at several AU, beyond the snow line, and must have migrated towards their present-day orbits. Accordingly, disk-driven migration seemed an attractive mechanism by which giant planets may be delivered to close-in orbits.

Until recently, it was impossible to tell whether these systems, supposed to migrate through a planar disk, were aligned or misaligned with their stars. This property, referred to variably as obliquity or spin-orbit misalignment, has now fallen within the observational capabilities of exoplanetary astronomy by way of the Rossiter-McLaughin effect (Rossiter, 1924; McLaughlin, 1924; Winn, Noyes, et al., 2005). Currently, measurements of misalignments are most common for the orbits of hot Jupiters, wherein the findings have revealed that a substantial fraction of such planets follow orbits with significant obliquities (Winn, Fabrycky, et al., 2010; Albrecht et al., 2012). Indeed, misalignments range all the way from prograde aligned to retrograde anti-aligned. However, the degree of misalignment exhibits a clear dependence on stellar mass, with the most extreme, retrograde (circular) orbits only appearing around stars with mass greater than $M \gtrsim 1.2\,\mathrm{M}_{\odot}$

(Figure 4.1).

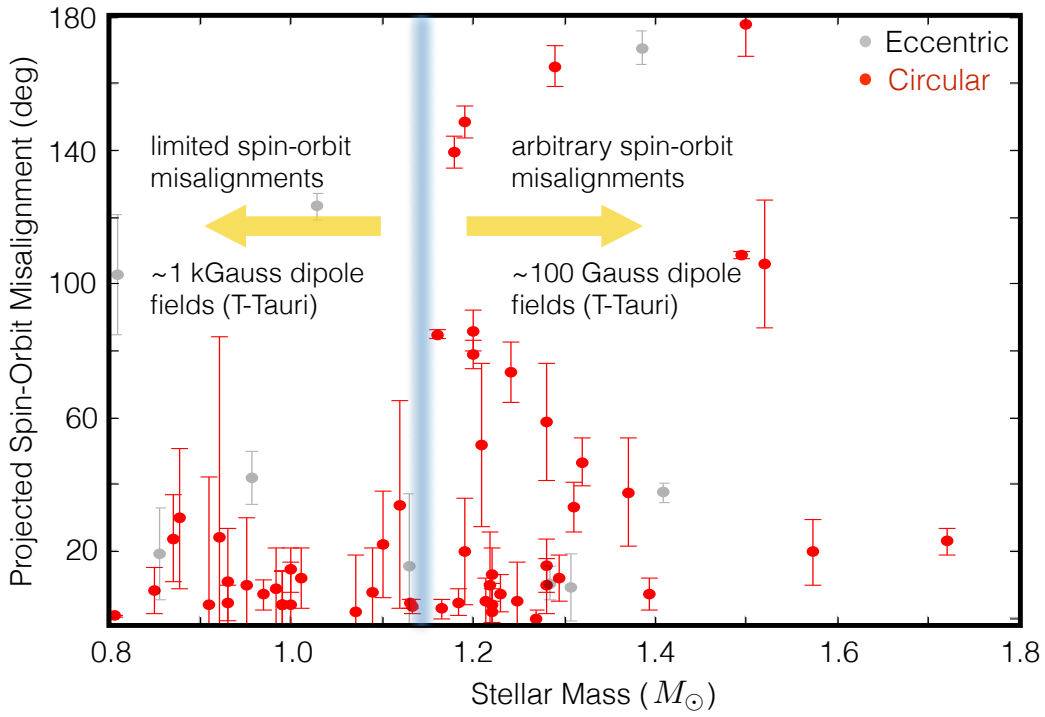

Figure 4.1: The observed projected angle between the stellar spin axis and orbital plane of circular planetary orbits ($e \leq 0.1$; red, solid points) and eccentric orbits ($e > 0.1$; black, faint points) for stars of given masses. There exists a clear distinction between low-mass stars ($M \lesssim 1.2\,M_\odot$), which display moderate-to small misalignments (especially among circular systems), and the more massive stars ($M \gtrsim 1.2\,M_\odot$), which exhibit misalignments ranging all the way from retrograde-aligned to prograde-aligned. Measurements of magnetic field strengths (Gregory, Donati, et al., 2012) have revealed that, among T-Tauri stars, lower-mass stars (similarly, corresponding to $M \lesssim 1.2 - 1.4\,M_\odot$) possess a much stronger surface dipole field than do their higher-mass counterparts. Specifically, low-mass stars possess fields of ~1 kGauss in contrast to more modest ~0.1 kGauss for higher-mass T-Tauri stars. The misalignments data were obtained from `exoplanets.org` and follow the discussion of Albrecht et al. (2012).

In light of the existence of significant obliquities, many authors (e.g., Albrecht et al. 2012; Lai 2012; Dawson, Murray-Clay, and Johnson 2014; Storch, Anderson, and Lai 2014; Petrovich 2015a) have sought alternatives to disk-driven migration as a production mechanism for inclined hot Jupiters. Specifically, in contrast to the 'smooth' picture

of disk-driven migration, there exists a separate class of migration mechanisms which occur after the dissipation of the protoplanetary disk. Post-disk migration must invoke dynamical interactions to excite near-unity eccentricities, bringing the periastron close enough to the central star such that tidal forces may take over and circularize the orbit (Ford and Rasio, 2006). The necessary perturbations are hypothesized to arise from processes such as planet-planet scattering (Ford and Rasio, 2008; Nagasawa, Ida, and Bessho, 2008; Beaugé and Nesvorný, 2012), Kozai resonance with a perturbing companion (Wu and Murray, 2003; Fabrycky and Tremaine, 2007; Naoz, Farr, Lithwick, et al., 2011) or secular chaotic excursions (Lithwick and Wu, 2012).

Despite the natural tendency of dynamical interactions to excite inclinations, their occurrence rate appears to be insufficient to explain the current data (Dawson, Murray-Clay, and Johnson, 2014). Conversely, disk-driven migration is expected to be almost ubiquitous but has long been assumed to give rise to low-obliquity systems because of the tendency for an isolated collapsing core to form an aligned star-disk system. However, stars do not form in isolation. On the contrary, binary fraction probably lies somewhere between half and unity during the early, disk-hosting stage of stellar evolution (Ghez, Neugebauer, and Matthews, 1993; Kraus et al., 2011; Marks and Kroupa, 2012; Duchêne and Kraus, 2013). The potential for neighbouring stars to influence disk orientation has actually been recognized for some time (e.g., Larwood et al. 1996), but it was first suggested as an explanation for spin-orbit misalignments by Batygin (2012). In this scenario, the gravitational torque exerted by a distant companion star causes the disk to precess about the plane of the binary system. Observations suggest that binary planes do not correlate with disk orientation (Stapelfeldt et al., 1998; Koresko, 1998; Jensen and Akeson, 2014) and so the

disk-precession tends to torque the star and disk out of alignment.

We recently advanced the so-called "disk-torquing" framework by taking into account the gravitational torques communicated between the star and its disk (Spalding and Batygin, 2014). Specifically, the star tends to precess about the disk's plane at a rate that decreases with time owing both to stellar contraction and disk mass-loss. In the earliest stages, the star is well enough coupled to the disk to adiabatically trail the disk as it precesses. However, once the precession rate of the star about the disk is roughly commensurate with that of the disk about the binary plane, a secular resonance is encountered which is capable of exciting star-disk misalignments occupying the entire observed range. Such a picture has been independently corroborated in other work and appears to be a robust result across various levels of approximation (Batygin and Adams, 2013; Lai, 2014; Xiang-Gruess and Papaloizou, 2014).

From the above discussion, it appears that spin-orbit misalignments may arise naturally out of either class of proposed migrationary scenario. What is less obvious is how to reconcile the migration pathway with the mass-dependence of the obliquity distribution (Figure 4.1). Previous attempts to explain the trend (Winn, Fabrycky, et al., 2010; Lai, 2012) have largely focused on the violent migration pathway. Specifically, it has been proposed that dynamical encounters misalign orbits, after which, strong tidal coupling between low-mass stars and their planets (owing to an extended convective region) re-aligns the orbits. These hypotheses rest upon a number of assumptions, one of which being that the tidal damping rate of obliquity greatly exceeds that of orbital semi-major axis (Lai, 2012). Additionally, the presence of misaligned multi-transiting systems (Huber et al., 2013) has yet to be given a viable explanation within the violent framework.

The disk-torquing mechanism is expected to misalign all planets in the system by a similar amount, at least in the inner disk. However, to date, the mass-misalignment trend has not been given an adequate explanation. Here, we provide such an explanation by utilizing an additional piece of evidence in the form of the magnetic field strengths of young, disk-hosting stars. Specifically, recent observations (Gregory, Donati, et al., 2012) have revealed that low-mass T-Tauri stars possess dipole field strengths of order $\sim 1\,\mathrm{kG}$, an order of magnitude greater than their higher-mass counterparts ($\sim 0.1\,\mathrm{kG}$). This trend appears to continue into the more massive Herbig AeBe class of star-disk systems ($M \sim 1.5 - 8\,\mathrm{M}_\odot$) (Alecian et al., 2012), suggesting the dipole strength to be a robust mass-dependent feature, intrinsically connected to PMS evolution. Crucially, the transition from weaker to stronger fields occurs at a similar mass to that defining the mass-misalignment trend ($\sim 1.2\,\mathrm{M}_\odot$). In this work, we suggest that the two trends are causally linked: *stronger magnetic fields of low-mass stars erase primordial misalignments that their higher-mass, weaker-field counterparts retain*.

In order to test this idea, we must first quantify the torques communicated between a tilted dipole and a disk. We are not the first to suggest that magnetic torques might influence misalignments (Lai, Foucart, and Lin, 2011) but our goal is to couple the star-disk magnetic torques to the full disk-torquing picture, i.e., a freely precessing star-disk system. Consequently, we develop a more complete picture of the various torques involved using semi-analytic methods, whilst taking advantage of the conclusions of various numerical studies (mostly on aligned disks, e.g., Ghosh and Lamb 1978; Armitage and Clarke 1996; Uzdensky, Königl, and Litwin 2002). Highly sophisticated numerical models exist for the study of star-disk interactions (e.g., Romanova

et al. 2012), however, detailed simulations must be integrated in full throughout each stellar rotation period. Even at the current state-of-the-art, full 3D calculations can only be carried out within a reasonable length of computer time for $\sim$ 1000 orbital timescales (depending upon the precision). In contrast, we seek to model the global evolution of the star-disk system, including time-dependent disk mass and stellar contraction, over multi-Myr timescales. Considering also that current observations only constrain the topologies of T-Tauri field strengths to within an order of magnitude or so, we shall construct our model such that the level of detail is commensurate with that of the observations.

In this paper, we begin with a description for the time evolution of the star and disk. Next we provide a re-hashing of the purely gravitational torques as derived in Spalding and Batygin (2014), derive the various magnetic torques communicated between the disk and star, and subsequently present the results obtained through numerical integration of the star-disk system, complete with gravitational and magnetic torques. We conclude by discussing the implications of the result for the acquisition of spin-orbit misalignments within the disk-torquing framework.

4.2 Model

Our goal is to describe the spin-axis dynamics of a star, possessing a dipolar field that is encircled by a protoplanetary disk. We suppose the star-disk system to be orbited by a companion star. In what follows, we derive the analytical forms of the various torques inherent to the system. Throughout the entire calculation, we assume a hierarchical configuration. Specifically, we assume that the central star and binary companion do not influence each other directly. Rather, the companion torques the disk (gravitationally), which in turn interacts with the

central star (gravitationally and magnetically). In order to improve clarity, we adopt the following convention for variables with identical symbols: quantities referring to the disk are primed, those referring to the central star are marked with a tilde, and those referring to the companion star are given an over-bar (e.g., semi-major axes will be defined as a', $\tilde{a}$, and $\bar{a}$, respectively).

The binary companion is prescribed a mass $\bar{M}$ and an orbit with semi-major axis $\bar{a}$ which is much greater than the outer disk edge $a'_{\rm out} \approx 30\,{\rm AU}$. The resulting gravitational torques acting upon the disk cause it to precess at a frequency that depends upon the mass of the companion, its semi-major axis and its inclination relative to the disk-plane (Spalding and Batygin, 2014). In the absence of star-disk interactions, the precession of the disk would simply cause it to tilt out of alignment with its host star. However, the central star can interact with its disk by way of several physical processes. Specifically, young stars rotate rapidly enough to possess a considerable centrifugal bulge at their equators. This bulge allows for gravitational coupling between the disk and star, the dynamics of which having been derived in detail elsewhere (Batygin and Adams, 2013; Spalding and Batygin, 2014). In addition, observations of young stars have revealed the presence of significant magnetic fields (Johns-Krull, 2007; Gregory, Donati, et al., 2012) which facilitate angular momentum transfer between star and disk in addition to the gravitational influences.

Our ultimate goal is to develop a theoretical framework by which we may test the hypothesis that differences in stellar magnetic field between high and low-mass stars is the dominant driver of the observed mass-misalignment trend in the current Rossiter-McLaughlin dataset (Winn, Fabrycky, et al., 2010; Albrecht et al., 2012). We follow a semi-analytic, parameterized framework in deriving the relevant

equations.

As the system ages, the star contracts and the disk loses mass. Accordingly, before calculating the star-disk torques, we must first provide formulations of the physical evolution of the disk and the central star. Within such a framework we then describe our calculations of magnetically-facilitated tilting of the stellar-spin axis and star-disk gravitational coupling. Torques arising from accretion are neglected in this work because their influence within a similar physical framework has been examined elsewhere (Batygin and Adams, 2013) and found to be insignificant.

Physical Evolution of the Protoplanetary Disk and the Stellar Interior

Typically quoted lifetimes of protoplanetary disks fall in the range $\sim 1 - 10\,\mathrm{Myr}$, with some recent evidence in support of longer-lived systems (Haisch Jr, Lada, and Lada, 2001; Williams and Cieza, 2011; Bell et al., 2013). We parameterize disk mass evolution as (Laughlin, Bodenheimer, and Adams, 2004):

$$M_{\rm disk} = \frac{M^0_{\rm disk}}{1 + t/\tau_{\rm disk}}. \tag{4.1}$$

The time derivative of $M_{\rm disk}$ approximately represents the accretionary flow. Following Spalding and Batygin (2014), we note that observations (Hartmann, 2008; Herczeg and Hillenbrand, 2008; Hillenbrand, 2008) are best matched by adopting an initial disk mass, $M^0_{\rm disk} = 5 \times 10^{-2}\,\mathrm{M}_\odot$ and dissipation timescale $\tau_{\rm disk} = 5 \times 10^{-1}\,\mathrm{Myr}$.

For simplicity, we approximate the central star with a polytrope of index $\xi = 3/2$ (appropriate for a fully convective object; Chandrasekhar 1939). A polytropic body of this index possesses a specific moment

of inertia $I = 0.21$ and a Love number (twice the apsidal motion constant) of $k_2 = 0.14$. In contracting along their respective Hyashi Tracks, T-Tauri stars derive most of their luminosity from the release of gravitational potential energy. We describe the radiative loss of such binding energy as (Hansen, Kawaler, and Trimble, 2012):

$$-4\pi R_\star^2 \sigma T_{\rm eff}^4 = \left(\frac{3}{5-\xi}\right)\frac{GM_\star^2}{2R_\star^2}\frac{dR_\star}{dt}, \tag{4.2}$$

with a solution,

$$R_\star = (R_\star^0)\left[1 + \left(\frac{5-\xi}{3}\right)\frac{24\pi\sigma T_{\rm eff}^4}{GM_\star (R_\star^0)^3}t\right]^{-1/3}. \tag{4.3}$$

For definiteness, we match the numerical evolutionary track of an $M_\star = 1\,{\rm M}_\odot$ star (Siess, Dufour, and Forestini, 2000) by assuming an initial radius of $R_\star^0 \simeq 4R_\odot$ and an effective temperature of $T_{\rm eff} = 4100\,{\rm K}$.

Disk-Binary Gravitational Interactions

The binary companion interacts with the disk through gravitational torques alone. To capture the long-term behaviour of the angular momentum exchange, we utilize the secular approximation (Murray and Dermott, 1999; Morbidelli, 2002) whereby the torques exerted by the companion on the disk are equivalent to those communicated by a massive wire sharing the companion's orbital elements. As a consequence of self-gravity and hydrodynamic pressure forces, the disk retains coherence under the influence of such torques, acting as a rigid body (Larwood et al., 1996; Batygin, Morbidelli, and Tsiganis, 2011; Xiang-Gruess and Papaloizou, 2014). Additionally, we neglect any dynamical influence of disk-warping.

We adopt a Hamiltonian framework in describing the dynamics. The gravitational torques acting between a star, disk, and companion have already been comprehensively derived and discussed elsewhere (Spalding and Batygin, 2014). Accordingly, here we provide only a brief outline of the corresponding computation.

To begin, we introduce the scaled Poincaré action-angle coordinates, defined in terms of the disk-star mutual inclination β' and the disk's argument of ascending node Ω',

$$Z' = 1 - \cos(\beta') \qquad z' = -\Omega'. \tag{4.4}$$

The appropriate Hamiltonian describing the companion's influence upon the disk is then

$$\mathcal{U} = \frac{3n'_{\rm out}}{8}\frac{\bar{M}}{M_\star}\left(\frac{a'_{\rm out}}{\bar{a}}\right)^3\left[Z' - \frac{Z'^2}{2}\right], \tag{4.5}$$

where $n_{\rm out}$ is the mean motion of the gas at the outer edge of the disk. Crucially, $\mathcal{U}$ contains no explicit dependence on z'. Therefore, *the disk-binary inclination is a constant of motion*. Appropriately, in our analysis, we carry out our simulations within a reference frame co-precessing with the disk, at a rate $\nu = dz'/dt$, given by

$$\nu = \frac{\partial \mathcal{U}}{\partial Z'} = \frac{3n'_{\rm out}}{8}\frac{\bar{M}}{M_\star}\left(\frac{a'_{\rm out}}{\bar{a}}\right)^3\left[1 - Z'\right]. \tag{4.6}$$

Boosting into such a frame is equivalent to subtracting νt from the argument of ascending node of the disk.

Owing to the arbitrary nature of choosing the companion's orbital parameters, we prescribe ν and Z' in our problem independently. It is

worth noting that the picture whereby a single companion remains on a circular orbit throughout the entire disk lifetime is highly idealized. In reality there may exist multiple companions and/or companions might be gained and lost throughout the pre-main sequence. Of course, these complications will lead not only to a time-dependent ν, but also to secular variations in Z'. This point is not crucial to the problem at hand, so we leave analysis of such dynamic processes to future work and maintain a constant ν and Z' throughout.

Disk-Star Interactions: Gravity

Having prescribed the secular evolution of the disk owing to the companion (constant, rigid-body precession), we now describe the processes by which torques are communicated between the star and the disk. Observations of T-Tauri stars have revealed that they spin with periods ranging between $\sim 3 - 10$ days (Herbst, n.d.; Littlefair et al., 2010; Bouvier, 2013). Such high spin rates (~within a factor of ten of break-up rotation) lead to the development of a significant centrifugal bulge on the stellar equator. When the star and disk are misaligned, this bulge results in gravitational torques that force a precession of the stellar spin pole about the disk plane (analogous to a top spinning on a planar table).

The dynamics of a spheroidal star and the gravitational influence arising from its rotationally-derived equatorial bulge may be approximated to high precision by considering the inertially-equivalent picture of a wire with mass $\tilde{m}$ in circular orbit with semi-major axis $\tilde{a}$ around a point mass. Respectively, the appropriate mass and semi-major axis are given by (Batygin and Adams, 2013)

$$\tilde{m} = \left[\frac{3M_\star^2\omega^2R_\star^3I^4}{4Gk_2}\right]^{1/3},$$
$$\tilde{a} = \left[\frac{16\omega^2k_2^2R_\star^6}{9I^2GM_\star}\right]^{1/3}. \tag{4.7}$$

With this prescription, the standard perturbation techniques of celestial mechanics can be applied to the spheroidal star (Murray and Dermott, 1999; Morbidelli, 2002).

By working in a frame co-precessing with the disk, we introduce a time-dependence to the Hamiltonian resulting in an apparent linear increase in the disk's argument of ascending node of $\nu\, t$. The Hamiltonian can be made autonomous by employing a canonical transformation arising from the following generating function of the second kind (Goldstein, 1950):

$$\mathbb{G}_2 = (\tilde{z} - \nu t)\,\Phi, \tag{4.8}$$

where $\phi = (\tilde{z} - \nu t)$ is the new angle and the new momentum is related to the old one through:

$$\tilde{Z} = \frac{\partial \mathbb{G}_2}{\partial \tilde{z}} = \Phi. \tag{4.9}$$

In addition to removing explicit time dependence, we scale the Hamiltonian by ν. Following the transformations described above, the Hamiltonian takes on the following form:

$$\begin{aligned}\mathcal{H} = -\Phi + \frac{\tilde{\delta}}{12}\Big[&3\big(\Phi-2\big)\Phi \\ &- 3\big(2+3(\Phi-2)\big)\Phi\cos^2(\beta') \\ &+ 6\sin(2\beta')\big(\Phi-1\big)\sqrt{(2-\Phi)\Phi}\cos(\phi) \\ &+ 3\sin^2(\beta')\big(\Phi-2\big)\Phi\cos(2\phi)\Big],\end{aligned} \tag{4.10}$$

where

$$\tilde{\delta} \equiv \frac{3}{8}\left(\frac{n'^2_{\rm in}}{\omega\nu}\frac{M_{\rm disk}}{M_\star}\frac{a'_{\rm in}}{a'_{\rm out}}\right), \tag{4.11}$$

and $n'_{\rm in}$ is the mean motion at the disk's inner edge.

The purely gravitational dynamics described by the above Hamiltonian (4.10), together with the physical evolution of the star and disk, give rise to the excitement of mutual inclination between the central star and its disk (Spalding and Batygin, 2014). However, additional physical mechanisms must exist in order to explain the mass-misalignment trend. The main hypothesis of our paper is that the dominant driver of such a trend is the mass-dependence of T-Tauri dipole field strengths. Accordingly, next we present our derivations of the magnetic torques and the differential equations used in determining their influence on stellar spin dynamics.

Magnetic Torques

In order to prescribe the magnetic disk-star interactions, we consider a T-Tauri star possessing a purely dipole magnetic field, whose north pole is aligned with the stellar spin axis. A pure dipole is modeled because the octupole component in real systems falls off much faster

with distance ($\propto 1/r^5$) than the dipole ($\propto 1/r^3$). Accordingly, at the position of the inner edge of the disk ($\sim 10\,R_\star$), the octupole components have been attenuated to a factor of $\sim 10^{-5}$ relative to the stellar surface field ($r = R_\star$) as opposed to the $\sim 10^{-3}$ attenuation suffered by the dipole component. Observations constrain the surface octupole field to differ from the dipole field by little more than a factor of 10 (higher or lower) and so the octupole component is almost always negligible when considering disk-star torques. The stronger dipoles of low-mass stars directly lead to a greater magnetic interaction with their disks than for high-mass stars.

In the region of interest (i.e., in the domain of the disk), the stellar field is current-free and can be expressed as the gradient of a scalar potential:

$$\mathbf{B}_{\rm dip} = -\boldsymbol{\nabla} V. \tag{4.12}$$

To retain generality, we take the field to be tilted at an angle β' with respect to a spherical coordinate system $(r\,,\,\theta\,,\,\phi)$ into a direction specified by an azimuthal angle ψ:

$$\begin{aligned} V = B_\star R_\star \left(\frac{R_\star}{r}\right)^2 \Bigg[& P_0^1(\cos(\theta))\cos(\beta') \\ & - \sin(\beta')\Big(\sin(\psi)\sin(\phi) \\ & + \cos(\psi)\cos(\phi)\Big) P_1^1(\cos(\theta))\Bigg], \end{aligned} \tag{4.13}$$

where $B_\star$ is the equatorial stellar surface field and P_l^m are associated Legendre polynomials. Within such a framework, the tilted dipole components are as follows:

$$
\begin{aligned}
B_r &= 2\,B_\star\left(\frac{R_\star}{r}\right)^3\Big(\cos\beta'\cos(\theta) \\
&\quad + \cos(\phi-\psi)\sin(\beta')\sin(\theta)\Big) \\
B_\theta &= B_\star\left(\frac{R_\star}{r}\right)^3\Big(\cos\beta'\sin(\theta) \\
&\quad - \cos(\phi-\psi)\sin(\beta')\cos(\theta)\Big) \\
B_\phi &= B_\star\left(\frac{R_\star}{r}\right)^3\Big(\sin(\beta')\sin(\phi-\psi)\Big),
\end{aligned}
\tag{4.14}
$$

which describe the vector field

$$
\mathbf{B}_{\rm dip} = B_r\hat{\mathbf{e}}_r + B_\theta\hat{\mathbf{e}}_\theta + B_\phi\hat{\mathbf{e}}_\phi. \tag{4.15}
$$

If we assume that the disk material is in Keplerian orbit about the star and for now suppose the star and disk are aligned, there exists a well-known expression for the corotation radius $a'_{\rm co}|_{\beta'=0} = (G\,M_\star/\omega_\star^2)^{\frac{1}{3}}$, the radius at which relative angular velocity between the stellar magnetosphere ($\omega_\star$) and the disk material is zero. Now consider tilting the star with respect to the disk. The azimuthal motion of the stellar magnetosphere at the disk plane becomes reduced in such a way that the corotation radius is modulated as follows:

$$
a'_{\rm co} = \left(\frac{G\,M_\star}{\omega_\star^2\,\cos^2(\beta')}\right)^{\frac{1}{3}}. \tag{4.16}
$$

In other words, *as the star tilts, the proportion of the disk which is effectively super-rotating relative to stellar rotation increases*. At radii greater or smaller than the corotation radius, Keplerian shear results in relative motion between the stellar magnetosphere and the fluid comprising the disk (Figure 4.2).

Owing to thermal ionization of alkali metals within the inner regions of the disk, motion of disk material relative to the stellar magnetosphere 'drags' the field lines, inducing magnetic fields. The evolution of induced fields is governed by the induction equation,

$$\frac{\partial \mathbf{B}}{\partial t} = \nabla \times \Big(\eta \nabla \times \mathbf{B} + \mathbf{v} \times \mathbf{B} \Big), \tag{4.17}$$

where $\mathbf{B}$ is the total magnetic field, η is the magnetic diffusivity and

$$\mathbf{v} = v_K \, \hat{\mathbf{e}}_\phi - \boldsymbol{\omega} \times \mathbf{r} \tag{4.18}$$

is the motion of the disk fluid *in the frame rotating with the stellar magnetosphere*, i.e., we imagine the stellar magnetosphere to be held fixed, with the disk moving within it. The Keplerian velocity v_K is azimuthally-directed whereas stellar rotation, arising from stellar angular velocity $\boldsymbol{\omega}$ has both azimuthal and vertical components.

A full, time-dependent solution of equation (4.17) is computationally difficult and so we adopt an approximate, semi-analytic approach. Specifically, we simplify the picture by noting that the disk fluid velocity $\mathbf{v}$ possesses two separate components in the rotating frame. The first is an azimuthal component, arising from motion of disk material in Keplerian orbit relative to the azimuthal magnetospheric motion from stellar rotation. Second, there is a vertical component, where 'vertical' refers to normal to the disk's plane. Vertical motion occurs owing to the tilt of the star with respect to its disk, which causes the stellar magnetosphere to be dragged vertically through the disk every stellar rotation period (best imagined for a star tilted by 90 deg; red diagram in Figure 4.2). In a frame rotating with the star, this vertical dragging appears as a vertical motion of disk material (a

vertical component to $\mathbf{v}$) and therefore constitutes an additional source of magnetic induction (see section 4.2).

For a small region on either side of the corotation radius, the relative azimuthal motion may be sufficiently small to allow a steady state to exist between magnetic field dragging and slippage (Matt and Pudritz, 2004). However, everywhere outside of this small region (of annular thickness $\sim 0.01\, a'_{\rm co}$), the diffusive timescale is longer than the dragging timescale, leading to the unbounded inflation of magnetic field lines. Such inflation cannot physically continue indefinitely and so some mechanism must act to dissipate magnetic energy on orbital timescales.

Analytic and numerical models of the aligned star-disk configuration find that the most likely dissipative process is magnetic reconnection, whereby the magnetic field lines are stretched azimuthally until the induced field is of the same order as the vertical stellar field. At this point the magnetic field lines break and reform (Livio and Pringle, 1992; Uzdensky, Königl, and Litwin, 2002). Such a process is intrinsically non-steady, however. Owing to the short timescale of reconnection ($\sim$ the orbital period) compared to disk evolution, we may average over each orbit and consider a steady magnetic torque to result between the star and disk.

We shall proceed by considering separately the fields generated from azimuthal relative motion and those originating from vertical (in the disk's frame) relative magnetospheric motion. The form of equation (4.17) ensures that the fields induced by vertical and azimuthal velocities back-react upon each other (through the $\mathbf{v} \times \mathbf{B}$ term) and so such separation of vertical and azimuthal induction is not strictly accurate. However, as we are seeking an approximate model for the

magnetic star-disk interactions, we proceed with the picture whereby the two components act independently.

Azimuthal Induction

Relative azimuthal disk motion induces an azimuthal field[2] through flux-freezing (Armitage and Clarke, 1996; Agapitou and Papaloizou, 2000). This induced field, $B_{\phi,\mathrm{i}}$ is represented as a fraction (also called a pitch angle), γ of the component of the stellar dipole field perpendicular to the disk's surface. In the case of a thin disk in spherical coordinates, the 'vertical' field is well approximated by the (negative) $\theta-$component of the stellar field, B_θ, at the disk mid plane ($\theta = \pi/2$). Thus, $B_{\phi,\mathrm{i}} = \gamma B_\theta$, where the subscript 'i' refers to 'induced'.

As mentioned above, γ is unable to instantaneously greatly exceed unity, but rather, magnetic reconnection reduces γ to $\gamma \sim 0$ each orbital period, allowing the field to be re-wound. We average over each reconnection timescale and consider the star-disk torque to act equivalently to a steady torque of azimuthal pitch angle $\gamma \sim 1$. The force per unit volume is given by the Lorentz equation

$$\mathbf{f} = \mathbf{J} \times \mathbf{B}. \tag{4.19}$$

In the case of azimuthal induction, the current density $\mathbf{J} = (1/\mu_0)\nabla \times \mathbf{B}_{\mathrm{ind}}$ may be considered to arise from the variation in magnetic field going from outside the disk vertically into the plane of the disk over some length scale δ. In such a case, the current induced is radial and within the plane of the disk. Effectively, this statement is equivalent to setting the ∇ operator equal to a vector of magnitude $1/\delta$ in the

[2]Physically, the motion of the disk material relative to the background field generates a current within the disk. For purely-azimuthal fluid motion, the current is radial. This radial current in turn induces its own an azimuthal magnetic field (in the ideal MHD case), which leads the background field lines to appear stretched.

vertical direction. Assuming $\delta \ll h$, where h is the disk scale height, the final torque per unit area on the disk is obtained approximately by multiplying equation (4.19) by δ, effectively integrating the torque over the vertical dimension.

Angular momentum transport among neighbouring annuli of the disk is facilitated by the propagation of bending waves (Foucart and Lai, 2011), disk viscosity (Larwood et al., 1996) and through disk self-gravity (Batygin, Morbidelli, and Tsiganis, 2011), all of which generally occur over a shorter timescale than does stellar tilting. As a result, the effective moment of inertia of the disk in response to magnetic torques is much greater than that of the star, as was the case above in the gravitational picture. Accordingly, in the calculations which follow, we consider only the back-reaction of the torques, in determining the dynamics of the star (which effectively introduces a minus sign), with the disk's dynamics being forced solely by the perturbing companion.

From considering only the azimuthal field induction, arising from the penetration of stellar flux into the upper and lower surfaces of the disk, a torque per unit area of

$$\boldsymbol{\tau} = -\mathbf{r} \times \left[\gamma B_\theta \hat{\mathbf{e}}_r \times \mathbf{B}_{\rm dip}\big|_{\theta=\pi/2} \right] \tag{4.20}$$

is communicated between the disk and the star. It is appropriate to display these torques in terms of their Cartesian components in the disk frame (i.e., $\hat{\mathbf{e}}_z$ points along the disk angular momentum axis) before integrating over the entire disk. We find that the $\hat{\mathbf{x}}$, $\hat{\mathbf{y}}$, and $\hat{\mathbf{z}}$ torques arising from equation (4.20) within the region interior to corotation ($a < a_{\rm co}$) are given by

$$\tau_x = \frac{2\pi\mathcal{T}}{3}\frac{(a_{\rm co}^3 - a_{\rm in}^3)}{a_{\rm co}^3 a_{\rm in}^3}\sin(\beta)\cos(\beta)\cos(\psi)$$
$$\tau_y = \frac{2\pi\mathcal{T}}{3}\frac{(a_{\rm co}^3 - a_{\rm in}^3)}{a_{\rm co}^3 a_{\rm in}^3}\sin(\beta)\cos(\beta)\sin(\psi)$$
$$\tau_z = \frac{4\pi\mathcal{T}}{3}\frac{(a_{\rm co}^3 - a_{\rm in}^3)}{a_{\rm co}^3 a_{\rm in}^3}\cos(\beta)^2, \tag{4.21}$$

where the variable $\mathcal{T}$, a measure of stellar magnetic moment, is defined for ease of writing as

$$\mathcal{T} \equiv \frac{B_\star^2 R_\star^6}{\mu_0}. \tag{4.22}$$

Analogous torques generated by the region exterior to corotation are similar in functional form but instead of integrating the torques between $a_{\rm in}$ and $a_{\rm co}$, we integrate outwards from $a_{\rm co}$ and note that the outer edge of the disk is sufficiently large as to be approximately equivalent to integration out to $a' \to \infty$. Accordingly, the torques arising from outside of corotation are given by

$$\tau_x = -\frac{2\pi\mathcal{T}}{3}\frac{1}{a_{\rm co}^3}\sin(\beta)\cos(\beta)\cos(\psi)$$
$$\tau_y = -\frac{2\pi\mathcal{T}}{3}\frac{1}{a_{\rm co}^3}\sin(\beta)\cos(\beta)\sin(\psi)$$
$$\tau_z = -\frac{4\pi\mathcal{T}}{3}\frac{1}{a_{\rm co}^3}\cos(\beta)^2. \tag{4.23}$$

It is important to notice that the above torques are null for a star-disk inclination of $\beta = \pi/2$. The torque vanishes in such a scenario because in the picture considered thus far, at $B_\theta = 0$ no flux penetrates the upper and lower surfaces of the disk. In other words, the null

torque arises as an artifact of assuming a razor-thin disk. In reality, the disk possesses a finite scale height h. For small β, most of the stellar magnetospheric flux penetrates the upper and lower surfaces of the disk, validating the razor-thin model. However, as β is increased, more stellar flux penetrates the inner edge of the disk. This flux penetration leads to additional azimuthal twisting of field lines within a small annular region at the disk truncation radius (Figure 4.2).

Whereas the induction considered previously generated a radial current, the induction owing to horizontal penetration of flux in the inner disk wall causes the field strength to vary along the radial direction. By the curl operator in equation (4.17), radial variation loosely translates to the generation of a vertical current. If we again suppose that the induced field is of a similar magnitude to the background stellar field, the current generated is that given by a change in magnetic field strength of $B_r(r = a_{\rm in})$ (the radial stellar field evaluated at the truncation radius) over a radial length scale δ_r. Once again, we integrate over this small region, assuming $\delta_r / a_{\rm in} \ll 1$, to find a torque per unit area (where the area is now the inner face of the disk) of

$$\boldsymbol{\tau}_r = \frac{1}{\mu_0} a_{\rm in} \hat{\mathbf{e}}_r \times \left[- B_r \hat{\mathbf{e}}_\theta \times \mathbf{B}_{\rm dip} \big|_{r=a_{\rm in}} \right]. \tag{4.24}$$

Once again, converting to Cartesian components and integrating, we obtain the torques arising from radial flux penetration in the form,

$$\begin{aligned} \tau_x &= 0 \\ \tau_y &= 0 \\ \tau_z &= \frac{8\,\pi\,\alpha \mathcal{T}}{a_{\rm in}^3} \sin(\beta)^2, \end{aligned} \tag{4.25}$$

where $\alpha \equiv h_{\rm in}/a_{\rm in}$ is the aspect ratio evaluated at the inner edge of the disk. Its value is likely to be about ~ 0.1 (Armitage, 2011), although it may indeed be slightly larger at the inner disk edge as a result of thermal expansion from strong stellar irradiation. For definiteness, we set $\alpha = 0.1$ in our calculations.

Vertical Induction

Many previous works have considered the torques arising from azimuthal field dragging within accretion disks (Ghosh and Lamb, 1978; Livio and Pringle, 1992; Armitage and Clarke, 1996; Agapitou and Papaloizou, 2000; Uzdensky, Königl, and Litwin, 2002; Matt and Pudritz, 2004; Lai, Foucart, and Lin, 2011). However, a feature which has been omitted from previous works is the fact that if a stellar magnetosphere is rotating at an inclination relative to its disk, there exists a component of relative star-disk motion which forces the field lines to be dragged *vertically* through the disk. This process is best imagined in the case of a star inclined by $\pi/2$ to a disk, i.e., spinning on its side. In such a case, consider the situation in a frame co-rotating with the star. In this frame, the disk is being forced to push through and break all stellar field lines each rotation period.

The result is that as the star spins, the field loops are forced to bunch up on one face of the disk and become rarified on the opposed side of the disk (red diagram in Figure 4.2), similarly to how water is pressurized on the leading edge of a boat paddle. Unlike the azimuthal induction, this paddle-like braking occurs over the entire disk as opposed to solely the region orbiting beyond co-rotation. As such, this effect constitutes a significant source of angular momentum loss for the star.

In addition to the intuitive braking torque upon stellar spin rate, the vertical component of magnetic induction leads to an additional torque

affecting stellar orientation. In order to calculate the magnitude of these torques, we take a similar approach to that used within the azimuthal framework above. Specifically, we suppose that the component of the magnetosphere parallel to the disk is built up over half the disk and reduced on the other half to a degree which is of the same order as the stellar magnetosphere. Again, we suppose non-steady reconnection to provide a bound on magnetic field magnitude. Thus, we suppose the field induced by vertical field dragging (with subscript "p") is given by

$$\mathbf{B}_{\rm p} = \zeta(\phi)\left[B_r\,\hat{\mathbf{e}}_r + B_\phi \hat{\mathbf{e}}_\phi\right], \tag{4.26}$$

where $\zeta(\phi) = \sin(\phi - \psi)$. Recalling that ψ is the azimuthal angle of the stellar spin pole direction projected onto the disk plane, this functional form for ζ ensures that field lines bunch up on the faces of the disk where magnetic field lines are being pushed into the disk and the field is rarified on the other faces, where the field is being rotated away from the disk surface[3].

Finally, vertical field motion generates torques which take the form,

$$\begin{aligned}
\tau_x &= -\frac{7\,\pi\,\mathcal{T}}{6\,a_{\rm in}^3}\,\sin(\beta)^2\cos(\psi)\\
\tau_y &= -\frac{7\,\pi\,\mathcal{T}}{6\,a_{\rm in}^3}\,\sin(\beta)^2\sin(\psi)\\
\tau_z &= -\frac{2\,\pi\,\mathcal{T}}{3\,a_{\rm in}^3}\,\cos(\beta)\sin(\beta),
\end{aligned} \tag{4.27}$$

where we have again invoked $a_{\rm out} \gg a_{\rm in}$.

[3]The $\zeta = \sin(\phi - \psi)$ form additionally ensures that $\nabla \cdot \mathbf{B}_{\rm p}$=0.

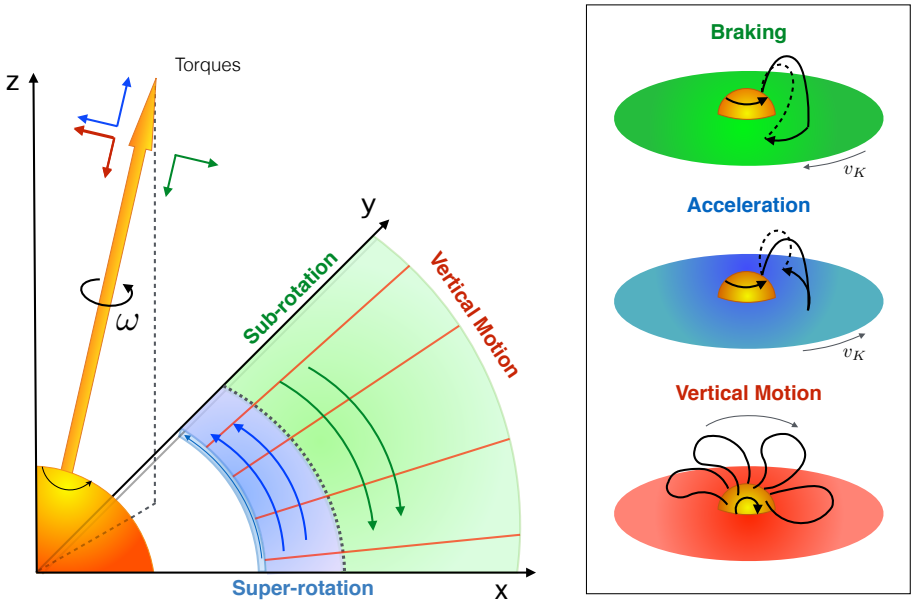

Figure 4.2: A schematic to illustrate the origin of each magnetic torque. The blue region represents the disk material interior to corotation, including the inner wall of the disk, which super-rotates with respect to the stellar spin, acting both to spin the star up and realign its axis with the disk's. The green region is further out and so rotates more slowly, braking the stellar spin and acting to misalign the star. Red lines represent the requirement that the entire magnetosphere must be dragged vertically through the disk once per stellar rotation period if the star and disk are misaligned. A simple illustration of the physical mechanism behind each torque is shown on the right. The colored arrows in the top-left denote the net torque acting upon the stellar spin axis: green regions slow down and misalign the star, blue regions speed the star up and force realignment, whereas red regions act to brake stellar rotation whilst realigning the stellar spin-axis. Summed together, the resultant magnetic effect is usually to realign the disk and star with each other.

We complete the specification of the torques arising from vertical field dragging by noting that if the star spins sufficiently slowly, the field lines will be able to diffuse vertically through the disk within one rotational period. Essentially, this is equivalent to saying that the field lines no longer reconnect and a true steady state is attainable (at least in terms of vertical field dragging). Suppose that the disk's diffusivity is prescribed as

$$\eta = \bar{\alpha}_s h^2 n_K, \tag{4.28}$$

where $\bar{\alpha}_s$ is the Shakura-Sunyaev parameter for disk viscosity (Shakura and Sunyaev, 1973) and n_K is the Keplerian angular velocity. We may suppose that the stellar field lines could diffuse vertically through the disk over a timescale $\tau \approx h^2/\eta = 1/(\bar{\alpha}_s n_K)$. Put another way, if the star is spinning more slowly than about $1/\bar{\alpha}_s$ times the angular velocity of the gas in the disk, we would expect field lines to diffuse through with greatly reduced magnetic induction. The likely value of $\bar{\alpha}_s$ within the inner disk ranges widely, from 10^{-1} to 10^{-3}. Owing to this range, for definiteness we suppose that negligible field is induced if the star rotates less than about 10 times the Keplerian angular velocity of the disk. We include such an effect qualitatively by modulating the torques in equation (4.27) by a factor of $\exp[-(\omega/\epsilon\,\omega_0)^{-2}]$ with $\epsilon = 0.1$ and ω_0 corresponding to an 8 day spin-period.

Summary of Magnetic Torques

The cumulative impact of the magnetic torques derived above is depicted visually in Figure 4.2 and may be summarized as follows. The inner regions of the disk (i.e., $a' < a'_{co}$) rotate faster than the stellar magnetosphere, dragging field lines azimuthally, ahead of the stellar rotation. The result is both an acceleration of the stellar spin rate and a torque that acts to *realign* the disk and stellar spin pole. Note that previous authors have concluded ambiguity over the sense of the tilting component to this torque (Lai, Foucart, and Lin, 2011) largely owing to uncertain parameterizations for the stellar wind. Our analysis here demonstrates that the pure impact of the magnetic torques from the inner disk is realignment. As can be seen from equations (4.25), the

z-component (i.e., disk-aligned) component is always positive, which tends to spin up and realign. The horizontal components, however, are also positive and so tend to misalign, but simply adding the z- and horizontal components in quadrature results in a net realignment torque.

The sense of torques is exactly reversed in the outer disk, i.e., the outer regions have a tendency to misalign. Torques arising from vertical induction tend predominantly to brake the stellar spin rate but they include a small component acting to realign. In order to complete the specification of magnetic torques, we must choose a value for the inner disk radius $a'_{\rm in}$. In our models, we adopt a so-called "disk-locked" configuration (Koenigl, 1991; Mohanty and Shu, 2008), whereby the outer and inner disk torques cancel at some prescribed stellar period (which we set to 8 days; see section (4.2) below). Accordingly, the inner disk truncation radius lies at $\sim 0.8\, a_{\rm co}|_{\beta=0}$, in agreement with more sophisticated numerical simulations (Long, Romanova, and Lovelace, 2005).

Stellar Spin Rate

A complete account of the factors influencing the spin rates of young stars remains elusive (Matt and Pudritz, 2004; Herbst, n.d.; Littlefair et al., 2010). The reason is that if one naïvely assumes a T-Tauri star to contract along its Hyashi track whilst conserving angular momentum, it would be expected to spin up sufficiently quickly such as to reach break-up velocity within the disk lifetime. However, observations clearly demonstrate that the vast majority of T-Tauri stars spin at rates far reduced from their break-up angular velocity. Specifically, most young stellar objects rotate at about 3 – 10 day periods with only a rare few which are indeed close to break-up angular velocity, at periods of

$\sim$ 1 day. The slow spins of such stars is sometimes referred to as the 'stellar angular momentum problem' because stars spin slower than they "should".

It has long been suspected that magnetic star-disk interactions play a key role in modulating the spin rates of T-Tauri stars (see Bouvier et al. (2014) for a recent review). Here, we do not attempt any sophisticated modeling aimed at explaining the stellar spin rates in detail. However, we note that the quasi-periodic twisting and opening of magnetic field lines discussed above provides a conduit through which angular momentum may be lost from the system, by way of stellar and/or disk winds. In addition, the torque arising from vertical field motion, derived above, provides an extremely efficient braking mechanism upon stellar spin, provided the stellar magnetosphere is sufficiently strong. As such, mutual inclination between a star and its disk may give rise to hitherto under appreciated magnetohydrodynamic influences upon stellar spin, especially when considering stars with lower masses ($M \lesssim 1.2\,\mathrm{M}_\odot$) and strong magnetospheres ($\sim$1 kGauss).

Within the framework of our model, we treat spin-rate evolution as follows. We allow the torques prescribed above to act freely on stellar spin rate. In addition, we introduce a relaxation factor, reflecting the reluctance of stars to spin up to break-up, whereby the star seeks the disk-locked spin rate ω_r over a timescale τ_r. The relaxation is prescribed as,

$$\left(\frac{d\omega}{dt}\right)_\mathrm{r} = -\frac{\omega - \omega_0}{\tau_\mathrm{r}}, \tag{4.29}$$

where we choose, for τ_r, the stellar contraction timescale, which may be derived from equation (4.2):

$$\tau_{\rm r} \equiv (\dot{R}/R)^{-1} = \frac{24\pi}{5-\xi}\frac{R_\star^3 \sigma T_{\rm eff}^4}{GM_\star^2}. \tag{4.30}$$

The above timescale changes as the star contracts, but remains of order ~ 1 Myr which is the value we adopt in this work. As already stated above, we choose the equilibrium angular velocity to be within the observed range, $\omega_0 = 2\pi/(8\,\text{days})$.

Frame of Reference

It is beneficial to carry out all calculations in the frame of a distant, binary companion to the central star. As such, we follow the approach of Peale et al. (2014) and define Euler angles within the binary frame related to the nutation, precession and rotation of the rigid body while assuming exclusively principal axis rotation (this is an excellent approximation for a T-Tauri star, spinning at a period of $3-10$ days). Specifically, $\tilde{\beta}$ is the angle between the central star's spin axis and the binary orbit normal; $\tilde{\Omega}$ is the longitude of ascending node of the star in the binary frame where $\tilde{\Omega} = 0$ implies commensurate disk and stellar lines of nodes; and the third Euler angle φ is the angle through which the star rotates as it spins (φ only enters the equations as a rate of change: $\dot{\varphi} = \omega$).

The equations for the evolution of $\tilde{\beta}$, ω, and $\tilde{\Omega}$, adapted from Peale et al. (2014) are:

$$\frac{d\omega}{dt} = -\frac{\omega - \omega_0}{\tau_{\rm r}} + \sin(\tilde{\beta})\Big[N_{\bar{x}}\sin(\tilde{\Omega}) - N_{\bar{y}}\cos(\tilde{\Omega})\Big] + \cos(\tilde{\beta})\,N_{\bar{z}},$$

$$\frac{d\tilde{\beta}}{dt} = -\frac{1}{\omega}\Big[\cos(\tilde{\beta})(-N_{\bar{x}}\sin(\tilde{\Omega}) + N_{\bar{y}}\cos(\tilde{\Omega})) + N_{\bar{z}}\sin(\tilde{\beta}))\Big],$$

$$\frac{d\tilde{\Omega}}{dt} = -\frac{1}{\omega\,\sin(\tilde{\beta})}\Big[N_{\bar{x}}\cos(\tilde{\Omega}) + N_{\bar{y}}\sin(\tilde{\Omega})\Big], \tag{4.31}$$

where $N_{\bar{i}}$ are projected torques. Note that by fixing the disk's longitude of ascending node at $\Omega' = 0$, we have implicitly placed ourselves into a frame co-precessing with the disk's angular momentum vector, as discussed above. The effect of precession was included within the gravitational part of the calculation (equation (4.10)) and so we need not retain it here.

The projected quantities $N_{\bar{i}}$ are directly related to the torques calculated above, although the components of the torques in the disk frame, $-\tau_{i'}$, must first be projected onto the Cartesian axes in the binary frame. Such a projection constitutes a simple geometric rotation of co-ordinates because the disk-binary inclination is a constant of motion. The co-ordinate rotation transformation angle is fixed at some prescribed value, β' to the z-axis and its sense is defined as anti-clockwise about the x-axis. As such, the components, $N_{\bar{i}}$, are given in terms of τ_i by:

$$
\begin{aligned}
N_{\bar{x}} &= -\tau_{x'}/(IM_\star R_\star^2), \\
N_{\bar{y}} &= -(\cos(\beta')\tau_{y'} - \tau_{z'}\sin(\beta'))/(IM_\star R_\star^2), \\
N_{\bar{z}} &= -(\cos(\beta')\tau_{x'} + \tau_{y'}\sin(\beta'))/(IM_\star R_\star^2).
\end{aligned} \tag{4.32}
$$

The above equations can be used to model the dynamics of the central star resulting from its magnetic interactions with its protoplanetary disk whilst the disk itself precesses within the binary frame.

4.3 Results

We motivate the following analysis by considering the timescales over which the magnetic torques act, as derived above. Specifically, magnetic torques increase as $\propto B^2$, meaning that the order-of-magnitude difference in field strengths between high and low-mass stars translates to an enhancement of two orders of magnitude in the torques felt by lower-mass stars. Supposing the star to be set up in a retrograde, anti-aligned state ($\beta = \pi$), we calculate the characteristic realignment timescale $T_{\rm align}$ using the equations derived above:

$$
T_{\rm align} \equiv \frac{\omega}{\dot{\omega}} = \frac{3GM_\star^2 I}{4\pi\omega}\frac{\mu_0}{B_\star^2 R_\star^4}, \tag{4.33}
$$

where $R_\star$ follows the time-dependence described in equation 7.4, giving rise to a time dependent magnetic torquing timescale which we illustrate in Figure 4.3. Taking 1 kGauss as the field strength typical of low-mass stars, under nominal star-disk parameters their absolute re-alignment timescales are of the order of $\sim$ 1 Myr throughout the majority of the disk lifetime. Conversely, the analogous timescale for the 0.1 kGauss fields typical of high-mass stars is closer to $\sim$ 100 Myr (Figure 4.3). These timescales are respectively shorter and longer than the typically-quoted 3 – 10 Myr lifetimes of protoplanetary disks

(Haisch Jr, Lada, and Lada, 2001). Therefore, magnetic interactions only have the potential to wipe out primordial star-disk misalignments in low-mass systems.

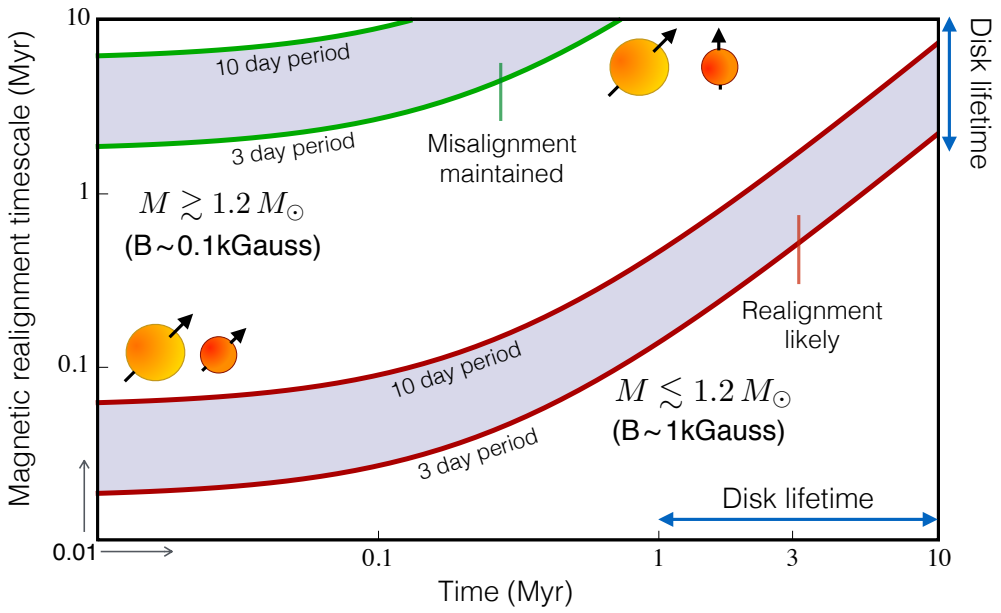

Figure 4.3: The approximate magnetic torquing timescale ($T_{\rm align}$) as a function of disk-star age for four regimes. The green lines apply to high-mass stars with a surface field strength of ~ 0.1 kGauss. Red denotes low-mass stars with a surface field strength of ~ 1 kGuass. In both cases, the upper line considers the timescale relevant to a star which is spinning with a 10 day period whereas the lower line applies to one with a 3 day period. The stellar spin rate is assumed to result from the locking to a circumstellar disk (Koenigl, 1991) and so the faster-spinning cases consider a disk which is truncated at smaller radii, increasing the magnetic influence. Notice that the dominant effect upon magnetic torquing timescale is the magnetic field strength, with timescales proportional to its inverse square. The timescales increase with time because the star contracts, leading to an effectively weaker field at the position of the inner disk. Only for the very earliest stages of protoplanetary disk evolution are high-mass stars' magnetospheres strong enough to significantly alter their orientation whereas low-mass stars remain dynamically influenced by magnetic fields throughout the entire typical disk lifetime of $\sim 1 - 10$ Myr.

A companion inclined by 30 degrees

In order to place magnetic realignment into the disk-torquing context, we integrate the mutual star-disk inclination over a 10 Myr timescale (i.e., an upper bound on typical disk lifetimes; Haisch Jr, Lada, and Lada 2001), adopting the case of a 1 $M_\odot$ massive companion inclined at 30 degrees to the disk plane. We present three cases in Figure 4.4: the purely-gravitational scenario (thick, pink line), the dynamics of a star with a dipole magnetic field strength of 0.1 kG, characteristic of higher-mass stars (thin grey line), and the situation for a dipole field strength of 1 kG, typical of low-mass stars (blue line).

Both the magnetic field-free and 0.1 kG cases look almost identical. In other words, the magnetic fields of higher-mass stars are dynamically unimportant within the disk lifetime, in accordance with the timescale analysis quoted above. The gravitational evolution is then equivalent to that discussed in Spalding and Batygin (2014). Specifically, at the earliest times, the star precesses about the disk plane much faster than the disk precesses about the binary plane (the high-frequency wiggles at time $t \lesssim 0.3$ Myr) and small misalignments are maintained. However, as the star shrinks and the disk loses mass, gravitational star-disk coupling weakens until the two precession timescales are roughly commensurate. This situation causes the system to pass through a secular resonance (Murray and Dermott, 1999; Morbidelli, 2002), facilitating a brief period of extremely efficient angular momentum transfer between the disk and star, resulting in large misalignments.

Importantly, even with the initial companion-disk inclination set to 30 degrees, a retrograde disk may emerge from the secular resonance. It is this non-linearity between disk-binary inclination and resulting misalignment which is the essence of how disk-torquing can account for the entire range of observed misalignments (Spalding and Batygin,

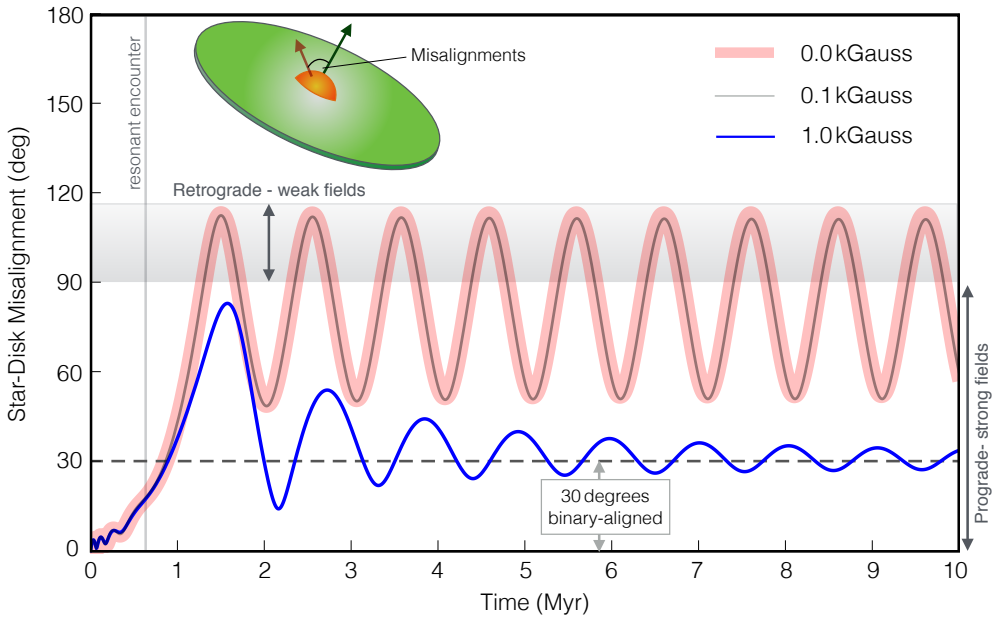

Figure 4.4: The time evolution of mutual star-disk inclination. We consider a binary companion to orbit the system at an inclination of 30 degrees relative the disk (greater angles are displayed in Figure 4.5). The companion is prescribed to cause the disk to precess with a 1 Myr period. The purely gravitational case is shown as a thick, pink line. The thin, black line denotes evolution in the presence of the weak fields of high-mass stars (~ 0.1 kGauss) and the blue line denotes the evolution corresponding to the strong fields of low-mass stars (~ 1 kGauss). As in previous work (Spalding and Batygin, 2014), we find that a secular spin-orbit resonance is encountered as the disk loses mass and the star contracts. However, significant misalignments are inhibited for the stronger magnetic fields characteristic of low-mass stars whereas the fields of high-mass stars make no appreciable difference to the dynamics. Interestingly, the action of magnetic torques takes the star into alignment with the binary plane, not the disk plane, suggesting that small misalignments are indeed a natural outcome of low-mass star evolution, whereas high-mass stars can take on the full range of misalignments, in direct agreement with the observations.

2014).

The same secular resonance is encountered in the 1 kG case, but crucially, the resulting large misalignments are erased within typical disk lifetimes. An important aspect of the dynamics is that the orientation of the star does not converge upon the disk plane, but rather, it converges to 30 degrees, i.e., the binary plane., which may be explained qualitatively as follows. Gravitational systems are conservative, al-

lowing their dynamics to be described as following contours of a scalar function, or Hamiltonian (Morbidelli, 2002). Magnetic torques introduce a dissipative component that acts to turn the elliptical equilibrium points of the Hamiltonian into attractors. In this case, the attractor is the binary-aligned state.

A crucial point to emphasize is that *in aligning with the binary plane, retrograde disks are prohibited*. To see this, note that the companion's gravitational perturbation upon the disk is dynamically equivalent whether the binary orbit is clockwise or counter-clockwise (as defined in some arbitrary frame). Such symmetry arises from approximating the orbit as a massive wire and has the consequence that the equilibrium of the Hamiltonian never lies at a position where the star is tilted by more than 90 deg to the disk.

Sensitivity to Disk-Binary Inclination

For completeness, we investigate the star-disk dynamics over a range of disk-binary inclinations in addition to the 30 deg case above. Specifically, Figure 4.5 illustrates the more extreme cases of 45, 60, and 75 degree inclinations. The picture is very similar across 30, 45 and 60 degrees, i.e., the magnetic fields of low-mass stars are capable of realigning them with the binary plane within the disk lifetime for a broad range of angles. In contrast, even the stronger fields were unable to wipe out retrograde disks when an extreme initial binary-disk inclination of 75 degrees is chosen. As expected, the orientation of the star is almost entirely unaltered by magnetic disk-star interactions for 0.1 kG fields in all cases.

We also present the time evolution of stellar spin resulting from the dynamics. A notable effect of larger binary inclinations is the considerable impact upon stellar spin rate, displayed in Figure (4.6). Though

one should not take the rotation periods displayed in Figure (4.6) too literally, owing to the uncertainties in prescribing rotation rates, an important aspect of the set-up emerges. Specifically, tilted stars will interact with their disks in such a way as to significantly brake stellar rotation, with such braking being more significant for larger star-disk inclinations. The origin of such an effect is in the requirement of a tilted star to drag its entire magnetosphere vertically through the disk once every period[4]. For high binary inclinations, the star is potentially spun down to nearly a stand-still as the system passes through the secular resonance, before being spun-up again in the direction of the disk.

4.4 Discussion

Summary

Prior to this work, a deficiency of the "disk-torquing" model (Batygin, 2012; Batygin and Adams, 2013; Spalding and Batygin, 2014) for the acquisition of spin-orbit misalignments lay in its inability to reproduce the observed mass-dependence of misalignments (Winn, Fabrycky, et al., 2010; Albrecht et al., 2012). Here, we resolved this discrepancy through the addition of a comprehensive set of magnetic star-disk torques on top of the previously-considered gravitational dynamics. Taking account of the recently-observed mass-dependence of T-Tauri dipole field strengths (Gregory, Donati, et al., 2012), the observed trend arises naturally.

We began by deriving analytical expressions describing the magnetic star-disk torques. Many previous authors have contributed to the development of a description of such torques (Ghosh and Lamb, 1978; Livio and Pringle, 1992; Armitage and Clarke, 1996; Agapitou and

[4]Note that ignoring the torques arising from vertical field motion would actually predict spin-*up* of a tilted star owing to the expanded corotation radius.

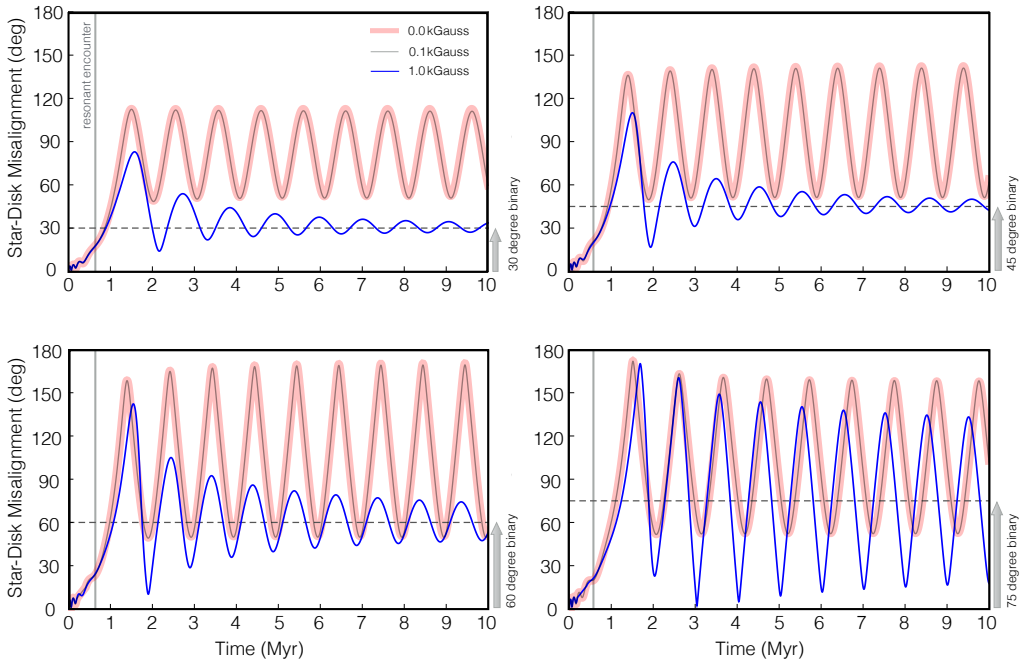

Figure 4.5: Star-disk misalignments as functions of time for a variety of disk-binary inclinations. This set of figures show similar information to that shown in Figure 4.4, except we now illustrate the evolution for a range of angles: 30 deg (top-left), 45 deg (top-right), 60 deg (bottom-left) and 75 deg (bottom-right). The thick, pink line is the field-free case, the thin, black line presents the weak-field (0.1 kGauss) case inherent to high-mass stars and the blue line denotes the strong-field (1 kGuass) case of low-mass stars. The over-all pattern is largely similar up to 60 deg, in that the star is drawn towards a binary-aligned state over the magnetic realignment timescale. Not even the strong fields can undo the extreme resonant acquisition of misalignments occurring as a result of a 75 deg binary inclination. These larger binary inclinations are less likely, but raise the possibility that we may find a rare population of retrograde planetary orbits around low-mass stars in future datasets.

Papaloizou, 2000; Uzdensky, Königl, and Litwin, 2002; Matt and Pudritz, 2004; Lai, Foucart, and Lin, 2011). A common limitation has been that torques are considered to arise solely as a result of magnetic induction associated with relative *azimuthal* motion between the stellar magnetosphere and the disk fluid. However, here we also considered magnetic induction arising from oblique rotation. To this end, we have found that the associated torques provide an important

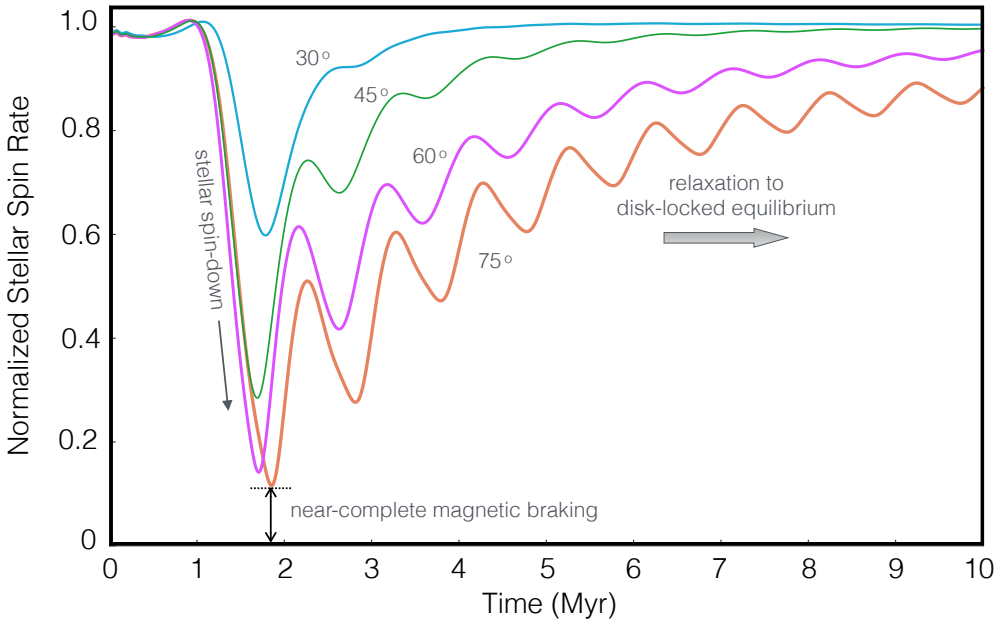

Figure 4.6: The time evolution of absolute stellar angular velocity in the case of a 1 kGauss dipole field, plotted in units of the equilibrium angular velocity (here corresponding to an 8 day period). We show the evolution for four values of disk-binary inclination, increasing from top to bottom: 30 deg (cyan line), 45 deg (green line), 60 deg (purple line), 75 deg (orange line). In each case, the star is prescribed to relax to a disk-locked equilibrium at an 8 day rotational period over a Kelvin-Helmholtz time. The relaxation is included in an *ad hoc* fashion and so the exact form of the rotation curves after $\sim$ 2 Myr is not to be taken too literally. However, as is most apparent for the higher inclinations, magnetic braking constitutes a significant mechanism for the removal of stellar angular momentum. Indeed, for large binary inclinations, the star can be almost entirely stopped and re-spun within a relatively brief time interval.

correction to the existing pictures. Accordingly, this effect constitutes an efficient source of braking upon the stellar spin.

The largest contribution to the torques affecting stellar orientation, as opposed to spin rate, arise from azimuthal induction. The influence of the disk material inside corotation is to spin the star up and align the stellar spin pole with the disk, with the opposite effect arising from the outer disk. This effect is amplified by stellar obliquity. In other words, when the star is tilted, a greater proportion of the disk is acting

to accelerate the stellar spin and align it with the disk. Inclusion of this aspect increases the stability of the disk-locked equilibrium proposed elsewhere (Koenigl, 1991; Mohanty and Shu, 2008).

The final addition to our picture of magnetic torques was to include (to leading order) the effect of finite disk thickness. Whilst simple and widely adopted, a short-coming of the razor-thin disk model is that a star inclined by 90 degrees to the disk is predicted to feel no magnetic torques arising from azimuthal field dragging alone (vertical induction still occurs). This is an artifact that comes about by supposing that there exists a negligible solid angle within which field lines penetrate radially the disk. However, though disk aspect ratios are small (~ 0.1), the inner edge of the disk is the closest point on the disk to the star and therefore can communicate a non-negligible torque to the central star (Equation 4.25).

We motivated the potential for magnetic torques to sculpt the mass-dependence of obliquities by showing that the calculated magnetic torquing timescale is $\sim$1 Myr for the 1 kG fields typical of low-mass stars whereas the analogous timescale applicable to high-mass stars was closer to 100 Myr. The fact that a typical protoplanetary disk lifetime sits right in the middle of these two timescales, at 3-10 Myr, indicates qualitatively different evolutionary scenarios during the disk-hosting stages of high and low-mass stars. In other words, star-disk magnetic torques constitute an influential factor in low-mass systems but may be neglected in high-mass systems.

The timescale analysis is compelling, and demonstrates that, were one to place a star and its disk in a misaligned configuration and leave them alone, a 1 kG dipole field would realign them before the disk dissipates. However, stars are likely to be aligned with their disks

in the absence of outside influences (Spalding, Batygin, and Adams, 2014). The excitation of misalignments must then come about by way of perturbations arising from a companion star (Batygin, 2012). Appropriately, next we coupled the updated magnetic torques derived here to the purely gravitational model presented in Spalding and Batygin (2014). Specifically, the star and the disk interacted through both gravitational and magnetic torques, with a massive companion causing the disk to precess with a period of 1 Myr.

As expected from the timescale analysis, the 0.1 kG fields characteristic of high-mass stars resulted in little deviation from a purely gravitational picture. However, the stronger 1 kG fields caused the star to align, not with the disk, but with the binary plane (except for extreme disk-binary inclinations of >75 degrees). Thus, the most important result of our paper emerges: *Dipole fields typical of lower-mass T Tauri stars realign the stellar spin axis with the plane of a perturbing companion on a timescale shorter than the disk lifetime. In this way, small misalignments occur naturally, but retrograde disks are prohibited in all but the more massive systems.*

Our results agree with the observational data presented in Figure 4.1. Retrograde circular orbits only exist among the higher-mass ($M \gtrsim 1.2\,\mathrm{M}_\odot$) population of stars. Despite the absence of retrograde orbits around the lower-mass stars, significant obliquities still persist in general. It is important to note, also, that the observations only reveal the *projected* obliquity of exoplanetary systems. A true inclination of 60 degrees, say, will on average appear sky-projected as a lower obliquity within our current observational dataset. On the other hand, distinguishing retrograde from prograde orbits is a much simpler task. The lack of retrograde systems, together with the degeneracy inherent to measuring sky-projections, means that the current observations are fully

consistent with our analysis here whereby small alignments persist while retrograde orbits are prohibited.

A more subtle point is that, although the low-mass inclinations approach binary-aligned equilibria, their time-evolution traces an oscillatory trajectory. Such oscillations in stellar orientation, especially for the 60 and 75 degree cases (Figure 4.5), take the star retrograde with respect to the disk for a small portion of the trajectory. If the disk were to rapidly dissipate before the amplitude of oscillations was sufficiently damped by magnetic interactions, and at a point in the oscillations where the star was in a retrograde position, such a system could conceivably produce retrograde planetary systems around low-mass stars. This scenario is much less likely than the alternative result of prograde systems, but does allow for the future detection of retrograde systems around low-mass stars, albeit at a significantly reduced frequency as compared to prograde systems.

Our analysis was largely based upon order-of-magnitude estimates. In accordance with this level of precision, we had to make several assumptions about the star-disk configuration. Perhaps most importantly, we chose the inner truncation radius of the disk such as to mimic a "disk-locked" scenario whereby the inner and outer disk torques cancelled at a specified equilibrium, aligned spin rate. In accordance with observations (Bouvier, 2013), we decided upon 8 days for this equilibrium spin period in our simulations. As can be seen in Figure (4.3), the chosen equilibrium period does indeed influence the characteristic magnetic torquing timescale. Had we chosen 3 days, for example, disk-locking would require a smaller truncation radius, resulting in stronger disk-star torques (both magnetic and gravitational). However, the relative variation in timescales between 3 and 10 day configurations is far smaller than the difference between high and

low-mass stars (owing to the B^2 dependence). Furthermore, because 8 days is in the middle of these extremes, the end result with respect to star-disk inclination is qualitatively similar across all realistic star-disk configurations.

One final omission that is worth a brief mention is the potential argument that, because our picture (disk-torquing) requires the presence of a companion, perhaps the mass-misalignment trend is merely a reflection of higher binarity in higher-mass stars. Whilst this particular aspect has not been examined in depth, Crida and Batygin (2014) analyzed the expected spin-orbit distribution arising out of the purely-gravitational disk-torquing picture presented in Batygin (2012). Whilst the expected distribution was consistent with that observed it was difficult to simultaneously fit the highest and lowest obliquities and little attention was paid to any mass dependence. It is difficult to see how such a sharp transition in obliquities may arise purely from such a smooth occurrence relation as mass vs binarity and so we feel the much sharper nature of the dipole field strength transition is a more likely cause.

Viability of the Disk-Torquing framework

Ultimately, our work here is a demonstration that the observed spin-orbit misalignments in exoplanetary systems can come about predominantly by way of mechanisms occurring during the early, disk-hosting phase. We do not expect the entirety of the observed misalignments to have originated through disk-torquing because dynamical interactions probably play a secondary role in the hot Jupiter delivery process (Ford and Rasio, 2006). It is important, therefore, to contrast the predictions of each model in order to determine which mechanism, if any, is dominant.

Dynamically-excited inclinations are likely to coincide with high eccentricities. Although controversy exists between analytic and numerical analyzes over the sense of eccentricity evolution during disk-driven migration (e.g., Goldreich and Sari 2003; Bitsch and Kley 2010; Kley and Nelson 2012), the general consensus is that eccentricity is limited to small values. As such, we predict that as datasets become more complete, the mass-misalignment trend will remain for circular systems, but not for eccentric systems ($e \gtrsim 0.1$). Such a pattern is already beginning to emerge (Figure 4.1) but will be fully tested when the upcoming *TESS* mission commences. Furthermore, a disk-torquing origin for misalignments is fully consistent with the existence of multi-transiting systems (Huber et al., 2013). Indeed, we expect future observations of such systems to reveal the same mass-misalignment trend as that currently measured for single planet systems, with the break between high and low obliquities occurring at a similar (although not necessarily identical) stellar mass.

Our work here has focused largely on close in systems. What can be said about more distant planets? An implicit assumption we have made is that throughout the dynamics, the disk acts like a rigid, planar body. Numerical simulations have demonstrated that in reality, the disk is likely to develop a mild warp in response to the perturbations of a companion (Larwood et al., 1996). Therefore, the possibility exists for the outer planets to occupy a different plane from the inner planets despite having undergone disk-torquing.

A more subtle difference between the outer and inner regions exists. One might imagine that close-in planets, having migrated through their natal disks, will be much more shielded from dynamical instabilities arising from perturbations later in the systems lifetime. This shielding arises both as a result of sitting in a deeper gravitational potential

well, but also through the stabilizing influence of general relativity[5]. Accordingly, we might expect there to exist a population of close-in systems which have obtained their orbits by way of coplanar disk migration, in addition to a separate population of planets around the same star that, for whatever reason, remained at larger radii within their disk, becoming subject to various dynamical instabilities later in their evolution.

In conclusion, the magnetically-facilitated realignment presented here provides a natural pathway for the generation, not only of high obliquities, but also their observed dependence upon mass. Such a "disk-torquing" model appeals to no assumptions beyond those within the bounds of what has been observed for T-Tauri systems, namely magnetic field strength, stellar spin rate, disk ionization state and disk mass. Out of such nominal parameters, the observed mass-misalignment trend arises naturally. Additionally, the conclusions presented here are fully consistent with the decades-old picture of smooth migration through a protoplanetary disk (Goldreich and Tremaine, 1980), leading to short-period orbits coplanar with the disk.

[5]Indeed, general relativity provides a considerable boost to stability of Mercury's orbit, despite being situated 10 times further from the Sun than some hot Jupiters are from their stars (Batygin, Morbidelli, and Holman, 2015).

Chapter 5

SPIN-ORBIT MISALIGNMENT AS A DRIVER OF THE *KEPLER* DICHOTOMY

ABSTRACT

During its 5 year mission, the *Kepler* spacecraft has uncovered a diverse population of planetary systems with orbital configurations ranging from single-transiting planets to systems of multiple planets co-transiting the parent star. By comparing the relative occurrences of multiple to single-transiting systems, recent analyses have revealed a significant over-abundance of singles. Dubbed the "*Kepler* Dichotomy," this feature has been interpreted as evidence for two separate populations of planetary systems: one where all orbits are confined to a single plane, and a second where the constituent planetary orbits possess significant mutual inclinations, allowing only a single member to be observed in transit at a given epoch. In this work, we demonstrate that stellar obliquity, excited within the disk-hosting stage, can explain this dichotomy. Young stars rotate rapidly, generating a significant quadrupole moment which torques the planetary orbits, with inner planets influenced more strongly. Given nominal parameters, this torque is sufficiently strong to excite significant mutual inclinations between planets, enhancing the number of single-transiting planets, sometimes through a dynamical instability. Furthermore, as hot stars appear to possess systematically higher obliquities, we predict that single-transiting systems should be relatively more prevalent around more massive stars. We analyze the *Kepler* data and confirm this signal to be present.

5.1 Introduction

In our solar system, the orbits of all 8 confirmed planets are confined to the same plane with an RMS inclination of ~1-2°, inspiring the notion that planets arise from protoplanetary disks (Kant, 1755; Laplace, 1796). By inference, one would expect extrasolar planetary systems to form with a similarly coplanar architecture. However, it is unknown whether such low mutual inclinations typically persist over billion-year timescales. Planetary systems are subject to many mechanisms capable of perturbing coplanar orbits out of alignment, including secular chaos (Laskar, 1996; Lithwick and Wu, 2012), planet-planet scattering (Ford and Rasio, 2008; Beaugé and Nesvorný, 2012) and Kozai interactions (Naoz, Farr, Lithwick, et al., 2011).

Despite numerous attempts, mutual inclinations between planets are notoriously difficult to measure directly (Winn and Fabrycky, 2015). In light of this, investigations have turned to indirect methods. For example, by comparing the transit durations of co-transiting planets, Fabrycky, Lissauer, et al. (2014) inferred generally low mutual inclinations ($\sim 1.0-2.2°$) within closely-packed *Kepler* systems. Additionally, within a subset of systems (e.g., 47 Uma and 55 Cnc) stability arguments have been used to limit mutual inclinations to $\lesssim 40°$ (Laughlin, Chambers, and Fischer, 2002; Veras and Armitage, 2004; Nelson, Ford, et al., 2014). On the other hand, Dawson and Chiang (2014) have presented indirect evidence of unseen, inclined companions based upon peculiar apsidal alignments within known planetary orbits. Obtaining a better handle on the distribution of planetary orbital inclinations would lend vital clues to planet formation and evolution.

Recent work has attempted to place better constraints upon planet-planet inclinations at a population level, by comparing the number of

single to multi-transiting systems within the *Kepler* dataset (Johansen et al., 2012; Ballard and Johnson, 2016). Owing to the nature of the transit technique, an intrinsically multiple planet system might be observed as a single if the planetary orbits are mutually inclined. An emerging picture is that although a distribution of small $\sim 5^\circ$ mutual inclinations can explain the relative numbers of double and triple-transiting systems, a striking feature of the planetary census is a significant over-abundance of single-transiting systems. Furthermore, the singles generally possess larger radii (more with $R_\mathrm{p} \gtrsim 4$ Earth radii), drawing further contrast.

The problem outlined above has been dubbed the "*Kepler* Dichotomy," and is interpreted as representing at least two separate populations; one with low mutual inclinations and another with large mutual inclinations that are observed as singles. The physical origin of this dichotomy remains unresolved (Morton and Winn, 2014; Becker and Adams, 2015). To this end, Johansen et al. (2012) proposed the explanation that planetary systems with higher masses undergo dynamical instability, leaving a separate population of larger, mutually inclined planets, detected as single transits. While qualitatively attractive, this model has two primary shortcomings. First, it cannot explain the excess of smaller single-transiting planets. Second, unreasonably high-mass planets are needed to induce instability within the required ~Gyr timescales. Accordingly, the dichotomy's full explanation requires a mechanism applicable to a more general planetary mass range. In this paper we propose such a mechanism – the torque arising from the quadrupole moment of a young, inclined star.

The past decade has seen a flurry of measurements of the obliquities, or spin-orbit misalignments, of planet-hosting stars (Winn, Fabrycky, et al., 2010; Albrecht et al., 2012; Huber et al., 2013; Morton and

Winn, 2014; Mazeh et al., 2015; Li and Winn, 2016). A trend has emerged whereby hot stars ($T_{\rm eff} \gtrsim 6200$ K) hosting hot Jupiters possess obliquities ranging from 0° to 180°, as opposed to their more modestly inclined, cooler (lower-mass) counterparts. Further investigation has revealed a similar trend among stars hosting lower-mass and multiple-transiting planets (Huber et al., 2013; Mazeh et al., 2015). Most relevant to the *Kepler* Dichotomy, Morton and Winn (2014) concluded at 95% confidence that single-transiting systems possess enhanced spin-orbit misalignment compared to multi-transiting systems.

Precisely when these spin-orbit misalignments arose in each system's evolution is still debated (Albrecht et al., 2012; Lai, 2012; Storch, Anderson, and Lai, 2014; Spalding and Batygin, 2015). However, the presence of stellar obliquities within currently coplanar, multi-planet systems hints at an origin during the disk-hosting stage (Huber et al., 2013; Mazeh et al., 2015). Indeed, many studies have demonstrated viable mechanisms for the production of disk-star misalignments, including turbulence within the protostellar core (Bate, Lodato, and Pringle, 2010; Spalding, Batygin, and Adams, 2014; Fielding et al., 2015) and torques arising from stellar companions (Batygin, 2012; Batygin and Adams, 2013; Spalding and Batygin, 2014; Lai, 2014; Spalding and Batygin, 2015). Furthermore, Spalding and Batygin (2015) proposed that differences in magnetospheric topology between high and low-mass T Tauri stars (Gregory, Donati, et al., 2012) may naturally account for the dependence of obliquities upon stellar (main sequence) $T_{\rm eff}$. Crucially, if the star is inclined relative to its planetary system whilst young, fast-rotating, and expanded (Shu, Adams, and Lizano, 1987; Bouvier, 2013), its quadrupole moment can be large enough to perturb a coplanar system of planets into a mutually-inclined configuration after disk dissipation.

In what follows, we analyze this process quantitatively. First, we calculate the mutual inclination induced between two planets as a function of stellar oblateness (J_2), demonstrating a proof-of-concept that stellar obliquity suffices as a mechanism for over-producing single transiting systems. Following this, we use N-body simulations to subject the famed, 6-transiting system *Kepler*-11 to the quadrupole moment of a tilted, oblate star. We show that not only are the planetary orbits mutually inclined, but for nominal parameters the system itself can undergo a dynamical instability, losing 3-5 of its planets, with larger mass planets preferentially retained. In this way, we naturally account for the slightly larger observed size of singles (Johansen et al., 2012).

5.2 Analytical Theory

In order to motivate the following discussion, consider two planets, orbiting in a shared plane around an inclined, oblate (high J_2) star. The effect of the stellar potential is to force a precession of each planetary orbit about the stellar spin pole, with the precession rate higher for the inner planet. If planet-planet coupling is negligible, the subsequent evolution would excite a mutual inclination between the planets of twice the stellar inclination (assuming fixed stellar orientation and negligible eccentricities). Alternatively, if planet-planet coupling is very strong, they will retain approximate coplanarity. Below, we analytically compute the system's evolution between these two extreme regimes (i.e., for general J_2).

Assumptions

We restrict our analytic calculation to small mutual inclinations between the planets and utilize Laplace-Lagrange secular theory (Murray and Dermott, 1999). This framework assumes the planets to be

far from mean motion resonances, allowing one to average over the orbital motion. Consequently, each planetary orbit becomes dynamically equivalent to a massive wire, a concept that is due to Gauss (Murray and Dermott, 1999; Morbidelli, 2002). Furthermore we set all eccentricities to zero[1].

The star's orientation will be held fixed. The validity of this assumption can be demonstrated by considering the ratio of stellar spin to planetary orbital angular momenta:

$$\frac{J_\star}{\Lambda_\mathrm{p}} \equiv \frac{I_\star M_\star R_\star^2 \Omega_\star}{m_p \sqrt{G M_\star a_p}}, \tag{5.1}$$

where $I_\star \approx 0.21$ is the dimensionless moment of inertia appropriate for a fully convective, polytropic star (Chandrasekhar, 1939), and the stellar rotation rate is $\Omega_\star = 2\pi/P_\star$. Consider a young, Sun-like star, possessing a rotation period of $P_\star = 10\,\mathrm{days}$ (on the slower end of observations; Bouvier 2013) and a radius of roughly $2R_\odot$ (Shu, Adams, and Lizano, 1987). A 10 Earth-mass object would need to orbit at over $\sim$100 AU in order to possess the angular momentum of the star. Thus, provided we deal with compact, relatively low-mass systems, the stellar orientation can be safely fixed to zero.

A further assumption is that the dynamical influence of stellar oblateness may be approximated using only the leading order quadrupole terms, neglecting those of order $O(J_2^2)$. Therefore, the disturbing part of the stellar potential (with $e = 0$) may be written as (Danby, 1992)

$$\begin{aligned} \mathcal{R} &= \frac{G m_\mathrm{p} M_\star}{2a_p} \left(\frac{R_\star}{a_p}\right)^2 J_2 \left(\frac{3}{2}\sin^2 i_p - 1\right) \\ &\approx \frac{G m_\mathrm{p} M_\star}{2a_p} J_2 \left(\frac{R_\star}{a_p}\right)^2 \left(6 s_p^2 - 1\right), \end{aligned} \tag{5.2}$$

[1] This approximation is simply for ease of analytics and will be lifted in the numerical analysis below.

where the second step has made the assumption of small planetary inclination i_p and defined a new variable $s_p \equiv \sin(i_p/2)$ (this definition is introduced to maintain coherence with traditional notation in celestial mechanics, e.g., Murray and Dermott (1999)).

Finally, it is essential to define an initial configuration for the planetary system. Both numerical and analytic modeling of planet-disk interactions suggest that embedded protoplanets have their inclinations and eccentricities damped to small values within the disk-hosting stage (Tanaka and Ward, 2004; Cresswell et al., 2007; Kley and Nelson, 2012). Furthermore, any warping of the disk in response to a stellar companion is expected to be small (Fragner and Nelson, 2010). Therefore, throughout this work we assume that the planets emerge from the disk with circular, coplanar orbits that are inclined by some angle $\beta_\star$ relative to the star. Note that we will always fix the stellar spin direction to be aligned with the z-axis, so $\beta_\star$, the stellar obliquity, constitutes the initial inclination of the planetary orbits in our chosen frame.

2-planet system

Incorporating the above assumptions, we may now write down the Hamiltonian ($\mathcal{H}$) that governs the dynamical evolution of the planetary orbits. To second order in inclinations (and dropping constant terms) we have (Murray and Dermott, 1999)

$$\mathcal{H} = \underbrace{\frac{Gm_1m_2}{a_2}\left[\left(s_1^2 + s_2^2\right) f_3 + s_1 s_2 f_{14} \cos(\Omega_1 - \Omega_2)\right]}_{\text{Planet-planet interaction}} \underbrace{-\frac{3Gm_1M_\star}{a_1} J_2 \left(\frac{R_\star}{a_1}\right)^2 s_1^2 - \frac{3Gm_2M_\star}{a_2} J_2 \left(\frac{R_\star}{a_2}\right)^2 s_2^2,}_{\text{Planet-stellar quadrupole interaction}} \tag{5.3}$$

where the prefactors are

$$f_3 = -\frac{1}{2} f_{14} = -\frac{1}{2}\left(\frac{a_1}{a_2}\right) b^{(1)}_{3/2}\left(\frac{a_1}{a_2}\right), \tag{5.4}$$

and $b^{(1)}_{3/2}$ is the Laplace coefficient

$$b^{(1)}_{3/2}(\alpha) \equiv \frac{1}{\pi}\int_0^{2\pi}\left[\frac{\cos\psi}{(1+\alpha^2-2\alpha\cos\psi)^{3/2}}\right] d\psi. \tag{5.5}$$

As we are using Hamiltonian mechanics, the dynamics must be described in terms of canonical variables. Traditional Keplerian orbital elements do not constitute a canonical set, so we transform to Poincaré (or, modified Delauney; Murray and Dermott 1999) variables, defined as

$$Z_\mathrm{p} \equiv m_\mathrm{p}\sqrt{G M_\star a_\mathrm{p}}\big(1-\cos(i_\mathrm{p})\big) \quad z_\mathrm{p} \equiv -\Omega_\mathrm{p}. \tag{5.6}$$

Physically, Z_p is the angular momentum of a circular orbit after subtracting its component in the z-direction. Notice that in the small angle limit,

$$Z_\mathrm{p} \approx \frac{1}{2} m_\mathrm{p}\sqrt{G M_\star a_\mathrm{p}} i_\mathrm{p}^2 \equiv \frac{1}{2}\Lambda_\mathrm{p} i_\mathrm{p}^2. \tag{5.7}$$

After substituting, we arrive at the governing Hamiltonian

$$\begin{aligned}\mathcal{H} = &-\mathcal{E}\left[\frac{Z_1}{\Lambda_1}+\frac{Z_2}{\Lambda_2}-2\sqrt{\frac{Z_1 Z_2}{\Lambda_1\Lambda_2}}\cos(z_1-z_2)\right] \\ &-\frac{3}{2}n_1 J_2\left(\frac{R_\star}{a_1}\right)^2 Z_1 - \frac{3}{2}n_2 J_2\left(\frac{R_\star}{a_2}\right)^2 Z_2,\end{aligned} \tag{5.8}$$

where for compactness we define

$$\mathcal{E} \equiv \frac{G m_1 m_2}{4 a_2}\left(\frac{a_1}{a_2}\right) b^{(1)}_{3/2}\left(\frac{a_1}{a_2}\right). \tag{5.9}$$

In order to complete the calculation, we define a complex variable for that represents the inclination of each planet

$$\begin{aligned}\eta_{\rm p} &\equiv \sqrt{\frac{Z_{\rm p}}{\Lambda_{\rm p}}}\big(\cos(z_{\rm p}) + \imath \sin(z_{\rm p})\big) \\ &\approx \frac{1}{\sqrt{2}} i_{\rm p}\big(\cos(\Omega_{\rm p}) - \imath \sin(\Omega_{\rm p})\big),\end{aligned} \tag{5.10}$$

where $\imath = \sqrt{-1}$. The purpose is to cast Hamilton's equations into an eigenvector/eigenvalue problem. Specifically, in terms of these new variables, we must solve

$$\dot{\eta}_{\rm p} = \imath \frac{\partial \mathcal{H}}{\partial \eta_{\rm p}^*} \frac{1}{\Lambda_{\rm p}}, \tag{5.11}$$

in which " * " denotes complex conjugation, yielding the matrix equation

$$\frac{d}{dt}\begin{pmatrix}\eta_1 \\ \eta_2\end{pmatrix} = -\imath \begin{pmatrix} B_1 + \nu_1 & -B_1 \\ -B_2 & B_2 + \nu_2 \end{pmatrix}\begin{pmatrix}\eta_1 \\ \eta_2\end{pmatrix},$$

where we have defined four frequencies as

$$\begin{aligned} B_1 &\equiv \frac{1}{4} n_1 \left(\frac{a_1}{a_2}\right)^2 b^{(1)}_{3/2}\left(\frac{a_1}{a_2}\right)\frac{m_2}{M_\star} \\ B_2 &\equiv \frac{1}{4} n_2 \left(\frac{a_1}{a_2}\right) b^{(1)}_{3/2}\left(\frac{a_1}{a_2}\right)\frac{m_1}{M_\star} \\ \nu_{\rm p} &= \frac{3}{2} n_{\rm p} J_2 \left(\frac{R_\star}{a_{\rm p}}\right)^2. \end{aligned} \tag{5.12}$$

The equation above may be solved using standard methods, whereby the solution is written as a sum of eigenmodes

$$\eta_{\rm p} = \sum_{j=1}^{2} \eta_{{\rm p},j} \exp(\imath \lambda_j t). \tag{5.13}$$

Indeed, the problem may be easily extended to N planets, though writing down all eigenvectors $\eta_{{\rm p},j}$ and eigenmodes λ_j rapidly becomes cumbersome.

Initial conditions and solution

A choice must be made for the initial conditions of the problem. As already mentioned above, here we choose the condition that both orbits are initially coplanar, having recently emerged from their natal disk, with the star inclined by some angle $\beta_\star$ relative to them. Accordingly, all four boundary conditions may be satisfied by requiring that

$$\eta_{\rm p}\big|_{t=0} = \frac{\beta_\star}{\sqrt{2}}. \tag{5.14}$$

What we seek is the mutual planet-planet inclination (denoted $\beta_{\rm rel}$). In the small angle approximation, we can compute this quantity using the relation

$$\begin{aligned}(1-\cos(\beta_{\rm rel})) &\approx \eta_1\eta_1^* + \eta_2\eta_2^* - (\eta_1\eta_2^* + \eta_2\eta_1^*) \\ &\approx \frac{1}{2}\beta_{\rm rel}^2.\end{aligned} \tag{5.15}$$

After solving for eigenvalues, eigenvectors and matching the initial conditions, we arrive at the solution for the mutual inclination of the two planets as a function of time, which takes the rather compact form

$$\boxed{\beta_{\rm rel}(t) = 2\beta_\star \mathcal{G}(J_2)\sin(\omega_0 t/2)}, \tag{5.16}$$

where we define the (semi-)amplitude of the oscillations between planets

$$\mathcal{G} = \mathcal{L}\left[1 + \mathcal{L}^2 + 2\left(\frac{\Lambda_2 - \Lambda_1}{\Lambda_2 + \Lambda_1}\right)\mathcal{L}\right]^{-1/2} \tag{5.17}$$

in terms of the ratio of frequencies

$$\begin{aligned}\mathcal{L} &\equiv \frac{\nu_1 - \nu_2}{B_1 + B_2} \\ &= 6J_2\left(\frac{R_\star}{a_1}\right)^2\left(\frac{a_2}{a_1}\right)^2 \frac{1}{b^{(1)}_{3/2}(\alpha)}\frac{M_\star}{m_2}\frac{1-\alpha^{7/2}}{1+\Lambda_1/\Lambda_2}.\end{aligned} \tag{5.18}$$

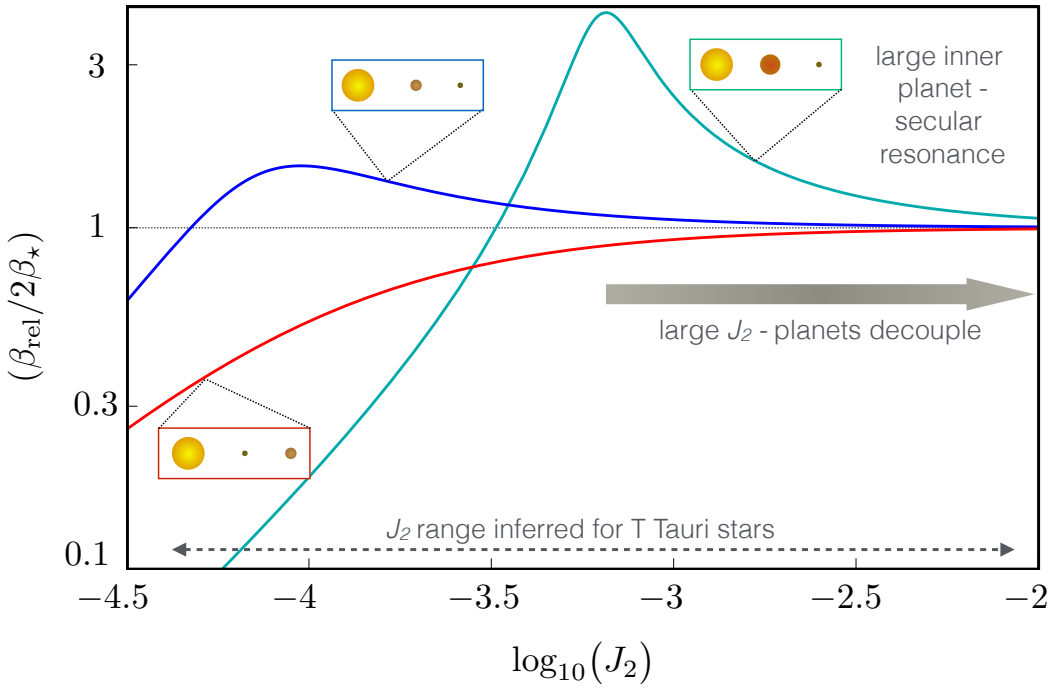

Figure 5.1: The amplitude of oscillations in mutual planet-planet inclinations excited between two initially coplanar, circular planetary orbits $\beta_{\rm rel}$, scaled by twice the stellar obliquity $\beta_\star$. The planets are situated at 0.05 AU and 0.1 AU for 3 different mass configurations: The red line has a 10 Earth mass planet outside a 1 Earth mass planet, where blue has the planets switched. The cyan line augments the inner planet to 100 Earth masses. Notice that any time the inner planet has more angular momentum, there exists a peak in the misalignments, representing resonance. In the limit of large J_2, the planets entirely decouple and reach mutual inclinations equal to twice the stellar obliquity.

A convenient consequence of the aligned initial conditions is that the oscillations are purely sinusoidal, evolving with half the frequency

$$\omega_0 \equiv \Big[(B_1 + B_2)^2 + (\nu_1 - \nu_2) \times \big(\nu_1 - \nu_2 + 2(B_1 - B_2)\big)\Big]^{1/2}. \tag{5.19}$$

One aspect to notice is that the amplitude is maximized when the equality

$$\nu_1 + \mathcal{K}^2 B_1 = \nu_2 + \mathcal{K}^2 B_2 \tag{5.20}$$

is satisfied, where $\mathcal{K} \equiv (\Lambda_1+\Lambda_2)/(\Lambda_1-\Lambda_2)$. The maximum amplitude, scaled by $\beta_\star$, can then be written as

$$2\mathcal{G}_{\max} = \frac{\Lambda_1 + \Lambda_2}{\sqrt{\Lambda_1\Lambda_2}}. \tag{5.21}$$

The significance of this result is best seen upon considering the outer planet to be a test particle, such that $B_1 = 0$ and $\Lambda_2 \to 0$. In such a scenario, the maximum of the amplitude $\mathcal{G}_{\max} \to \infty$. Such an unphysical result occurs as a consequence of a secular resonance (Murray and Dermott, 1999; Morbidelli, 2002; Spalding and Batygin, 2014; Batygin, Bodenheimer, and Laughlin, 2016), whereby the inner and outer bodies precess at similar rates. In reality, our earlier approximation that mutual inclinations are small breaks down in this regime and the inclusion of higher order terms is required.

In principle, one may also set $\Lambda_1 \to 0$ and conclude that the above resonance persists when the inner planet is a test particle. However, the resonant criterion in terms of stellar oblateness reads:

$$\begin{aligned} J_2\big|_{\rm res} \approx \frac{1}{6}&\left(\frac{a_1}{R_\star}\right)^2\left(\frac{a_1}{a_2}\right)^2\left(\frac{m_2}{M_\star}\right) \\ &\times\left(\frac{b^{(1)}_{3/2}(\alpha)}{\Lambda_2}\right)\frac{(\Lambda_1+\Lambda_2)^2}{(\Lambda_1-\Lambda_2)(1-\alpha^{7/2})}, \end{aligned} \tag{5.22}$$

which is negative when $\Lambda_1 < \Lambda_2$. Accordingly, the condition for secular resonance can only be satisfied when $\Lambda_1 > \Lambda_2$, i.e., when the inner planet possess more orbital angular momentum than the outer planet.

As an illustration, we plot the semi-amplitude $\mathcal{G}$ in Figure (5.1) appropriate for a configuration where the two planetary orbits are situated at 0.05 AU and 0.1 AU, both orbiting a solar-mass star with radius 0.01 AU (about twice the Sun's radius). Three cases are shown: the

red line depicts a 1 Earth mass planet interior to a 10 Earth mass planet while the blue line has the planets interchanged. The former configuration possesses a positive $J_2\big|_{\rm res}$, appearing as a maximum in the amplitude. The third situation (the cyan line) represents a 100 Earth mass planet interior to a 1 Earth mass body, illustrating that higher mass inner planets may more easily misalign their outer companion (equation 5.21), but $J_2\big|_{\rm res}$ is correspondingly higher.

Figure (5.1) demonstrates that misalignments of the order twice the stellar obliquity can be readily excited for reasonable values of J_2. By geometric arguments, the potential for such misalignments to take one of the planets out of transit depends upon the ratio $R_\star/a$. However, for the cases considered above, only $\sim 4^\circ$ of stellar obliquity are required to remove the two planets from a co-transiting configuration (less than the $\sim 7^\circ$ present in the solar system; Lissauer, Ragozzine, et al. 2011). Conversely, planets may remain co-transiting if the innermost planet is sufficiently distant, the planets are very massive and/or tightly packed, or the stellar quadrupole moment is particularly low.

5.3 Numerical Analysis

Several crucial aspects of real systems were neglected in order to obtain the analytic solution (5.16) above. Principally, we included only two planets whose orbits were assumed to be circular and only slightly mutually inclined. Additionally, in averaging over short-term motion, our adopted secular approach is unable to describe the full dynamics. A more subtle aspect was that we considered a constant J_2, when in reality, stars are expected to spin down and shrink over time until J_2 is essentially negligible (Irwin et al., 2008; McQuillan, Mazeh, and Aigrain, 2013; Bouvier, 2013).

In order to test our hypothesis within a more general framework, we

now turn to N-body simulations. To carry out the calculations, we employed the well-tested Mercury6 symplectic integration software package (Chambers 1999) [2]. In addition to standard planet-planet interactions, we modified the code to include the gravitational potential arising from a tilted star of given J_2, along with a term to produce general relativistic precession (following Nobili and Roxburgh (1986)).

For the sake of definiteness, the parameters of our modelled system were based off of *Kepler*-11, a star around which 6 transiting planets have been discovered (Lissauer, Fabrycky, et al., 2011). Detailed follow-up studies, using Transit Timing Variations, have constrained the masses of the innermost 5 planets and placed upper limits upon the mass of *Kepler*-11g, the outermost planet[3], making this system ideal for dynamical investigation. Though choosing one system is not exhaustive, our goal is to demonstrate the influence of a tilted star upon a general coplanar system of planets. We follow Lissauer, Jontof-Hutter, et al. (2013) and use their best-fit mass of 8 Earth Masses for *Kepler*-11g, with the stellar mass given by $0.961 M_\odot$ (see Table 5.1).

N-body simulation

For our numerical runs, we choose 10 values of stellar obliquity and 11 of initial stellar $J_2 = J_{2,0}$ (i.e., the oblateness immediately as the disk dissipates). Once again, we fix the stellar orientation aligned with the z-axis, but choose the initial planet-star misalignments:

$$\beta_\star \in \{5,\ 10,\ 20,\ 30,\ 40,\ 50,\ 60,\ 70,\ 80,\ 85\}. \tag{5.23}$$

The value of J_2 for a star deformed by its own rotation may be related to its spin rate $\omega_\star$ and Love number (twice the apsidal motion constant)

[2] http://www.arm.ac.uk/ jec/home.html

[3] The mass of *Kepler*-11g, is only loosely constrained, however for the purposes of this work, it is not particularly imperative to choose the "real" mass.

k_2 as follows (Sterne, 1939):

$$J_2 = \frac{1}{3}\left(\frac{\Omega}{\Omega_b}\right)^2 k_2, \tag{5.24}$$

where Ω_b is the break-up spin frequency at the relevant epoch. The Love number can be estimated by modeling the star as a polytope with index $\chi = 3/2$ (i.e., fully convective; Chandrasekhar 1939), which yields $k_2 \approx 0.28$. Observations constrain the spin-periods of T-Tauri stars to lie within the range $\sim 1 - 10$ days (Bouvier, 2013), while the break-up period is given by

$$T_{\rm b} = \frac{2\pi}{\Omega_b} \approx \frac{1}{3}\left(\frac{M_\star}{M_\odot}\right)^{-1/2}\left(\frac{R_\star}{2R_\odot}\right)^{3/2} \text{days}. \tag{5.25}$$

In our simulations below, we use the current mass of *Kepler*-11 for the star, but suppose its radius to be somewhat inflated relative to its current radius ($R_\star = 2R_\odot$), reflecting the T Tauri stage (Shu, Adams, and Lizano, 1987). With these parameters, we arrive at a reasonable range of $J_{2,0}$ of

$$10^{-4} \lesssim J_{2,0} \lesssim 10^{-2}, \tag{5.26}$$

within which we choose 11 values uniformly separated in log-space:

$$J_{2,0} \in \{10^{-4},\, 10^{-3.8} \ldots 10^{-2}\}. \tag{5.27}$$

In all runs, rather than allowing both $R_\star$ and J_2 to vary, we simply left $R_\star$ as a constant, letting J_2 decay exponentially over a timescale of $\tau = 1\,$Myr

$$J_2(t) = J_{2,0}\, \mathrm{e}^{(-t/\tau)}. \tag{5.28}$$

The choice for τ is essentially arbitrary, provided J_2 decays over many precessional timescales, owing to the adiabatic nature of the dynamics

(Lichtenberg and Lieberman, 1992; Morbidelli, 2002). Our choice of 1 Myr roughly coincides with a Kelvin-Helmholtz timescale (Batygin and Adams, 2013) but is chosen also to save computational time.

For each case, our integrations span 22 million years, beginning with the initial condition of a coplanar system possessing the current semi-major axes of the *Kepler*-11 system, but with eccentricities set to zero (Lissauer, Jontof-Hutter, et al., 2013). In order to analyze the results, we sample the system 6 times between 19 and 22 Myr, and at each step calculate the maximum number of transiting planets that could be observed from a single direction. The results at all six times were then averaged.

The determination of the maximum number of transits was accomplished as follows. We begin by checking whether all possible pairs within the 6 planets mutually transit, where the criterion for concluding a pair of planets to be non-transiting is

$$\left|\sin(\beta_{\rm rel})\right| > \sin(\beta_{\rm crit}) \approx \frac{R_\star}{a_1} + \frac{R_\star}{a_2}, \tag{5.29}$$

where in the above formula we used the current radius of *Kepler*-11 ($R_\star = 1.065 R_\odot$, as opposed to the inflated value relevant to the T Tauri stage). If any single pair of planets was non-transiting, we proceeded to choose each possible combination of 5 out of the 6 and performed a similar pairwise test to identify potentially observable 5-transiting systems. If no set of 5 passed the test we chose all sets of 4, etc, until potentially finding that only one planet could be seen transiting. We note that the criterion above neglects the possibility of fortunate orbital configurations allowing two mutually inclined orbits to intersect along the line of sight. This complication, however, does not affect our qualitative picture.

5.4 Results

The numerical results are presented in Figure (5.2), where the x-axis depicts the initial stellar $J_2 = J_{2,0}$. The y-axis refers to the misalignment $\beta_\star$ between the stellar spin axis and the initial plane of the 6 planets. Each run has been given its own rectangular box, within which the color represents the maximum number of co-transiting planets that may be observed around the star (as discussed above). The numerics verify our analytic result, in that the observable multiplicity may be significantly reduced solely as a consequence of stellar obliquity.

As expected, higher values of $J_{2,0}$ result in fewer transiting planets, provided the star is tilted relative to the planetary orbits. As with our analytic results, even small stellar obliquities are sufficient to reduce the transit count, with 5° of obliquity reducing the transit number to as little as 3 (Figure (5.2)). However, planet-planet mutual inclination was not the only source of the reduction in transit number. A crucial finding was that for large enough $J_{2,0}$ and $\beta_\star$, the stellar quadrupole potential caused the system to go unstable, casting 3-5 planets out of the system or into the central body, with planet-planet collisions existing as an additional possibility not captured in our simulations (Boley, Contreras, and Gladman, 2016).

The region of instability (i.e., where at least one planet was lost) is outlined by a dotted line in Figure (5.2). Interestingly, the areas of instability map closely onto the regions where only a single transit remains. In other words, almost every single-transiting system coming out of the integration had lost planets through dynamical instability. Furthermore, each time instability occurred, the 2 lowest mass members were lost: *Kepler*-11b and f, with the next lowest mass body, *Kepler*-11c often joining them. Such a preference for retaining more massive planets is indeed reflected in the data as a slightly larger typ-

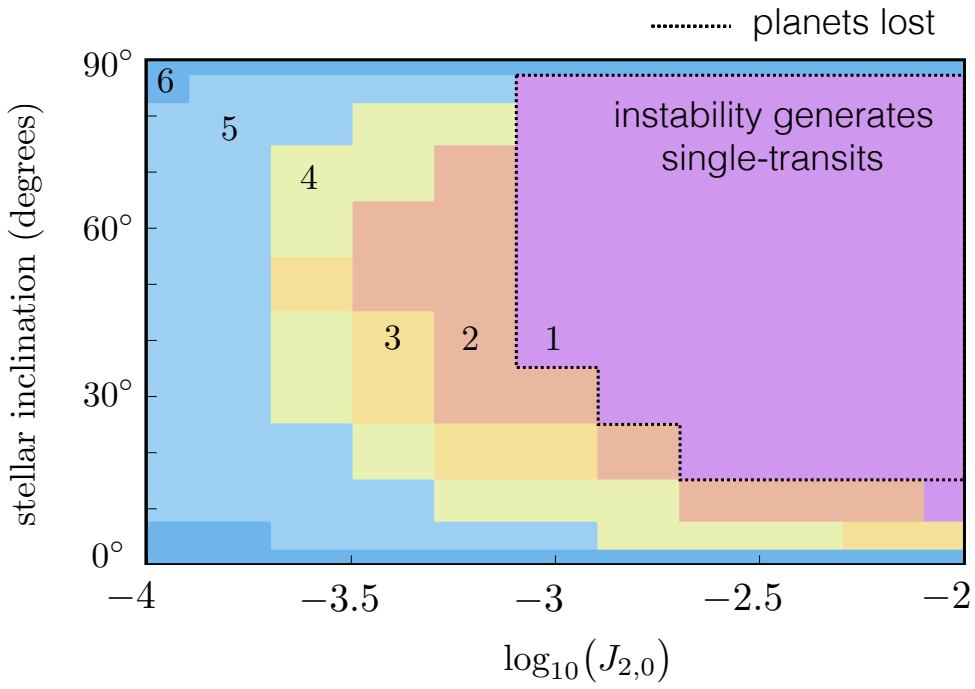

Figure 5.2: The maximum number of transits detectable after 22 million years of integrating *Kepler*-11 with a tilted, oblate star. The x-axis denotes the value of J_2 immediately after disk dispersal ($J_{2,0}$) and the y-axis represents the stellar inclination. The runs where planets were lost through instability are outlined by a dotted line, which corresponds closely to the region where only single transits can be observed (the purple region).

ical radius for single-transiting systems (Johansen et al., 2012). More testing is required to determine whether this a generic feature of our model, however.

We showed that for any given two-planet system, there exists a resonant J_2 if the inner planet has more angular momentum than the outer. However, the picture becomes much more complicated in a multi-planet system, where each planet introduces two additional secular modes (one for eccentricity one for inclination; Murray and Dermott 1999), increasing the density of resonances in Fourier space. As the stellar J_2 decays, its influence sweeps across each resonance, providing ample opportunity to excite mutual inclinations. If the two planets, *Kepler*-11d and f, were alone, they could become resonant at $J_2\big|_{\text{res}} \sim$

$10^{-2.4}$, which coincides approximately with the onset of instability in the low-inclination runs (Figure 5.2) but not exactly, for the reasons mentioned above.

5.5 Discussion

In recent years, the *Kepler* dataset has grown sufficiently comprehensive to facilitate statistically robust investigations at a population level. Out of this data has emerged a so-called "*Kepler* Dichotomy"; the notion that single-transiting systems are too common to be explained as resulting from a simple distribution of mutual inclinations within systems of higher multiplicity (Johansen et al., 2012; Ballard and Johnson, 2016).

In separate studies, significant misalignments have been detected between the stellar spin axes and the planetary orbits they host, particularly around stars with main sequence $T_{\rm eff} \gtrsim 6200\,{\rm K}$ (Winn, Fabrycky, et al., 2010; Albrecht et al., 2012; Mazeh et al., 2015; Li and Winn, 2016). This trend initially became apparent within the hot Jupiter dataset and was consequently often interpreted as evidence for a post-disk, high-eccentricity migration pathway for hot Jupiter formation[4]. However, a similar trend has now emerged within *Kepler* systems, including the multi-transiting sub-population (Huber et al., 2013; Mazeh et al., 2015), with little evidence supporting a tidal origin (Li and Winn, 2016). These observations cumulatively suggest that many of the misalignments originated from directly tilting the protoplanetary disk, thereby inclining all planets in the system at once (Batygin, 2012; Spalding and Batygin, 2014; Lai, 2014; Spalding and Batygin, 2015; Fielding et al., 2015).

[4]The dependence on host star temperature (and therefore mass) was attributed to tidal dissipation within the convective regions of lower-mass stars (Winn, Fabrycky, et al., 2010; Lai, 2012).

A consequence of primordially-generated spin-orbit misalignments is that stellar obliquity would be present at the end of the natal disk's life, leaving the planetary orbital architecture subject to the quadrupole moment of their young, rapidly-spinning and expanded host star. This paper has demonstrated that such a configuration naturally misaligns close-in systems and, furthermore, provides a mechanism for dynamical instability that by-passes the problem encountered in earlier work that unreasonably large planets were required to induce instability (Johansen et al., 2012).

The observable multiplicity of transiting systems can be reduced either by inclining planetary orbits relative to each other, or by intrinsically reducing the number of planets. Here, we have shown that both can be at play, with modest J_2 and stellar obliquity causing misalignments, whereas sufficiently large values thereof lead to dynamical instability, shedding planets. The origin of the instability is likely secular in nature, and significant planet-planet inclinations have been shown to reduce the inherent stability of planetary systems in numerous previous works (Laughlin, Chambers, and Fischer, 2002; Veras and Armitage, 2004; Nelson, Ford, et al., 2014). In support of this interpretation, our simulations resulted in planetary instability at much smaller J_2 when obliquity was high $\gtrsim 40^\circ$. Accordingly, we would expect multiplicity (both transiting and intrinsic) to be lower around hot stars, which tend to possess higher obliquities (Winn, Fabrycky, et al. 2010; see below).

Predictions

Imposing stellar obliquity as a source of the *Kepler* Dichotomy leads to several predictions. Naturally, stars leaving the disk-hosting stage with larger J_2 and obliquity are more likely to end up observed as exhibiting single-transits, either as a result of dynamical instability

or the excitation of mutual planet-planet inclinations. As mentioned above, there is an observed trend whereby stars with $T_{\rm eff} \gtrsim 6200\,{\rm K}$ exhibit higher obliquity (Winn, Fabrycky, et al., 2010; Albrecht et al., 2012; Mazeh et al., 2015) and so, on the face of it, one would expect a higher relative incidence of singles around higher mass stars. The picture is, however, complicated by the universal feature of stellar evolution models that more massive stars contract along their Hayashi tracks faster (Siess, Dufour, and Forestini, 2000). Accordingly, the influence of J_2 in more massive stars may have decayed to a greater extent than in lower-mass stars by the time their natal disk dissipates, partly offsetting the impact of their larger typical obliquities.

The above complications notwithstanding, both our analytical and numerical analyses suggest a greater sensitivity of the degree of misalignment to stellar obliquity than to stellar J_2. Consequently, we make the prediction that *hot stars possess more abundant single-transiting systems relative to cool stars*.

Previous work has already suggested the existence of our predicted trend. Specifically, both hotter stars and, independently, single-transiting systems appear to exhibit higher obliquities (Morton and Winn, 2014; Mazeh et al., 2015). The overlapping of these two findings implies at least a weak trend toward more singles around hotter stars. In order to further test this prediction, we carried out a simple statistical analysis of confirmed *Kepler* planets, as we now describe.

Kepler data

To obtain data on confirmed, *Kepler* systems, we downloaded the data from the "Confirmed Planets" list (as of July 2016) on the NASA Exoplanet Archive website[5]. The systems were filtered to include

[5] http://exoplanetarchive.ipac.caltech.edu

only those in the *Kepler* field, though the conclusions that follow do not change qualitatively if non-*Kepler* detections are included.

In Figure (5.3), we split the data into "hot" stars with $T_{\rm eff} > 6200\,{\rm K}$ (132 in total) and "cool" stars, with $T_{\rm eff} < 6200\,{\rm K}$ (1504 in total). For each sub-population, we illustrate the fraction of systems as a function of the number of planets observed in transit. The hot stars clearly demonstrate a larger fraction of singles and a smaller fraction of multiples for each value of multiplicity, in agreement with the predictions of our model. In order to quantify the significance of this agreement, we carry out a statistical test that quantitatively compares the two populations.

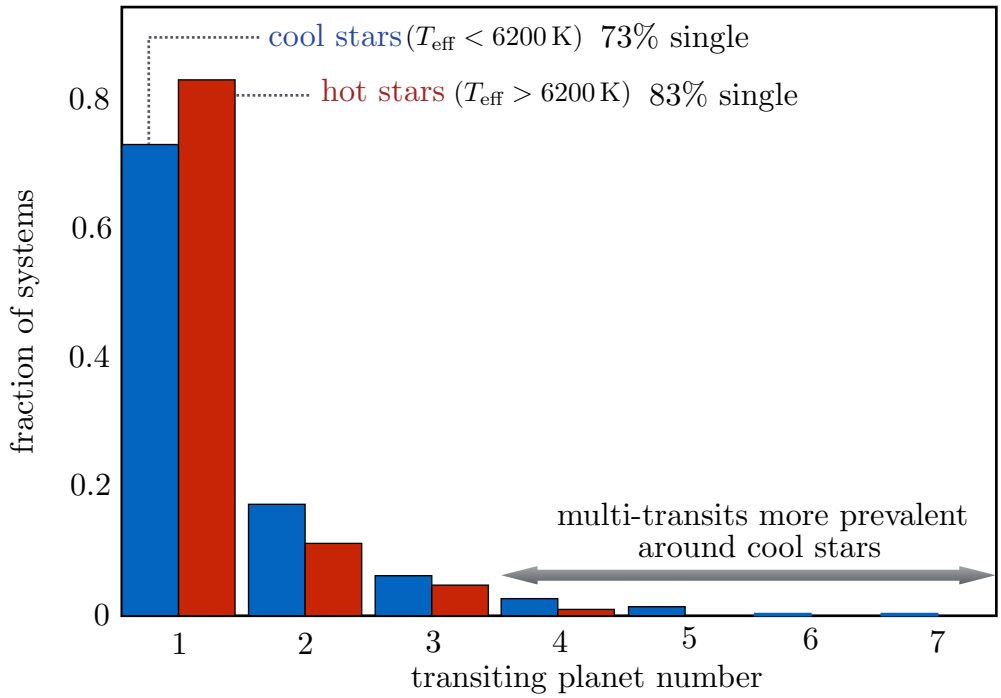

Figure 5.3: Fraction of systems exhibiting each number of transiting planets from 1 to 7 within the hot ($T_{\rm eff} > 6200\,{\rm K}$, red bars) and cool ($T_{\rm eff} < 6200\,{\rm K}$, blue bars) sub-samples of planet-hosting Kepler stars. There were 132 hot stars and 1504 cool stars in the data used, of which 83% and 73% respectively exhibited single transits. Accordingly, transiting systems around hot stars show a stronger tendency toward being single, in agreement with the predictions of our presented model (see text).

Using Bayes' theorem, with a uniform prior, we generated a binomial distribution for hot stars and cool stars separately that illustrates the probability of the data, given an assumption about what fraction of systems are single. Such an argument is similar to determining the fairness of a coin flip, where heads equates to a single system and tails a multi system. Specifically, we plot

$$\mathcal{P}(\{\text{data}\}|S) = AS^{N_\text{s}}(1-S)^{N_\text{t}-N_\text{s}}, \tag{5.30}$$

where N_s is the number of single systems within a population of N_t total stars and A is a normalization coefficient (Sivia, 1996). The variable S is the single bias weighting; the probabilistic tendency for a population of planet-hosting stars to display single transits as opposed to multiples. The quantity $\mathcal{P}(\{\text{data}\}|S)$ gives the probability of reproducing the data if the underlying tendency is S. In the hot population, $N_\text{t} = 132$ and $N_\text{s} = 110$, whereas the cool population had $N_\text{t} = 1504$ and $N_\text{s} = 1098$.

As can be seen from Figure (5.4), the two distributions are visually distinct, with hotter stars possessing a stronger bias towards singles, with a significance of 2.9σ [6]. More data are needed to tease out this relationship further and to isolate the influence of a tilted star versus other confounding factors, such as the dependence upon stellar mass of the occurrence rate of giant planets. For now, we conclude that the data supports our general prediction that hotter, more oblique stars possess a relatively greater abundance of single-transiting planets.

A separate prediction relates to the distance of the planets from the host star. Specifically, the quadrupole moment falls off as $R_\star^2/a^2$, whereas the coplanarity required for transit grows as $a/R_\star$, and so

[6] Where σ^2 here is defined as the sum of the squares of the standard deviations of each individual distribution.

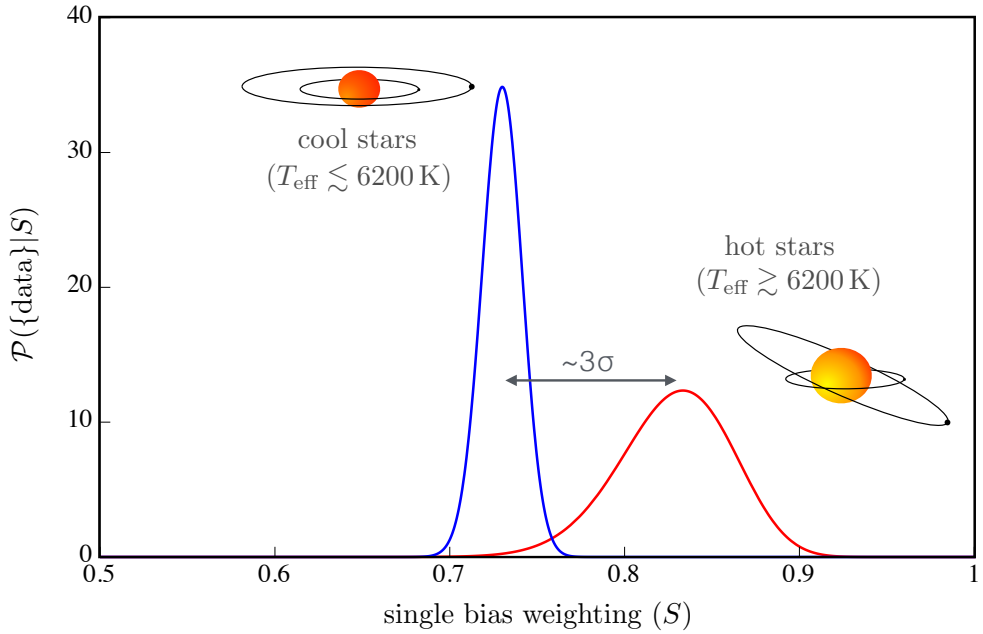

Figure 5.4: Probability of the data, given an intrinsic fraction S of singles out of systems with hot (red line) and cool (blue line) stars. The separation of the peaks is roughly $2.9\,\sigma$ (as defined in the text). Therefore, to a very high confidence, hot stars possess relatively more singles, as our hypothesis predicts.

the overall magnitude of our proposed mechanism should become negligible within more distant systems. In consequence, we predict that the "*Kepler* Dichotomy" signal will weaken for systems at larger orbital distances. As future missions, such as *TESS* collect more data, this unique aspect of our model will become amenable to observational tests.

A caveat to the above analysis is that the dichotomy appears to persist within the population of planets around M-dwarfs (Ballard and Johnson, 2016). This is problematic, as these stars are expected to exhibit lower inclinations, being cooler on the main sequence. We interpret this as stellar oblateness being effective across all stellar masses, but being relatively more important within the hotter, more inclined population. This is supported by our numerical simulations, where even small obliquities reduced the transit number if oblateness was large

enough (Figure (5.2)).

The origin of spin-orbit misalignments

Our work here essentially relies upon the assumption that stellar obliquity is excited early on, in the disk-hosting stage. This is not the only potential origin for spin-orbit misalignments, with alternative pathways including secular chaos (Lithwick and Wu, 2012), planet-planet scattering (Ford and Rasio, 2008) and Kozai interactions (Naoz, Farr, Lithwick, et al., 2011; Petrovich, 2015b). These mechanisms are traditionally inseparable from the idea that hot Jupiters migrate through a post-disk, high-eccentricity pathway (Wu and Murray, 2003; Petrovich, 2015a). Whereas it is likely that some hot Jupiters formed in this way, it is unlikely to constitute the dominant pathway (Dawson, Murray-Clay, and Johnson, 2014) and, furthermore, cannot explain the spin-orbit misalignment distribution in *Kepler* systems (Mazeh et al., 2015; Li and Winn, 2016). Rather, disk-driven migration constitutes a favourable mechanism that may retain multiple planet systems within the same plane, and can account for the observed spin-orbit misalignments if the disk itself becomes misaligned with respect to the host star.

To that end, multiple studies have shown that a stellar companion is dynamically capable of exciting star-disk misalignments across the entire observed range of spin-orbit misalignments (Batygin, 2012; Spalding and Batygin, 2014; Lai, 2014). Specifically, the tidal potential of a companion star, or even that of the star cluster itself, induces a precession of the disk orientation, leading to significant star-disk misalignments, usually by way of a secular resonance (Spalding and Batygin, 2014). Although observations of disk orientation in young binary systems are elusive, there exists at least one known example of

a binary where each star has a disk with its plane misaligned to that of the binary (Jensen and Akeson, 2014), just as in the aforementioned theoretical picture. Furthermore, stellar multiplicity appears to be a nearly universal outcome of star formation (Duchêne and Kraus, 2013; Beuther et al., 2014).

Within the framework of primordial excitation of spin-orbit misalignments, the dependence upon stellar mass (or $T_{\rm eff}$) has been linked to the observed multipolar field topology of higher mass T Tauri stars compared with the more dipolar configuration seen in lower-mass T Tauri stars (Gregory, Donati, et al., 2012). The weaker dipoles of higher mass stars increase their magnetic realignment timescales above that of their lower-mass counterparts, naturally explaining the observed trend in spin-orbit misalignments with stellar $T_{\rm eff}$, and therefore mass (Spalding and Batygin, 2015). Our work here has demonstrated an additional consistency between observations and primordially excitied spin-orbit misalignments, namely that the *Kepler* Dichotomy naturally arises from the dynamical response of multi-planet systems to the potential of an oblate, tilted star.

5.6 Conclusions

This paper investigates the origin of the "*Kepler* Dichotomy," within the context of primordially-generated spin-orbit misalignments. We have shown that the quadrupole moment of such misaligned, young, fast-rotating stars is typically capable of exciting significant mutual inclinations between the hosted planetary orbits. In turn, the number of planets available for observation through transit around such a star is reduced, either through dynamical instability or directly as a result of the mutual inclinations, leaving behind an abundance of single-transiting systems (Johansen et al., 2012). The outcome is an apparent

Kepler-11						
Property	b	c	d	e	f	g
Mass (Earth masses)	1.9	2.9	7.3	8.0	2.0	8.0
Radius (Earth radii)	1.80	2.87	3.12	4.19	2.49	3.33
a (AU)	0.091	0.107	0.155	0.195	0.250	0.466
Period (days)	10.3	13.0	22.7	32.0	46.7	118.4

Table 5.1: The parameters of the *Kepler*-11 system. The mass of *Kepler*-11g only has upper limits set upon it, but we follow Lissauer, Jontof-Hutter, et al. (2013) and choose a best fit mass of 8 Earth masses here.

reduction in multiplicity of tilted, hot stars, with their observed singles being slightly larger, as a consequence of many having undergone dynamical instabilities, in accordance with observations.

Through the conclusions of this work, the origins of hot Jupiters and of compact *Kepler* systems, the *Kepler* Dichotomy, and spin-orbit misalignments, are all placed within a common context.

Chapter 6

THE UBIQUITY OF STELLAR OBLATENESS AS A DRIVER OF DYNAMICAL INSTABILITY

ABSTRACT

The *Kepler* mission and its successor *K2* have brought forth a cascade of transiting planets. Many of these planetary systems exhibit multiple transiting members, but a large fraction possess only a single transiting example. This overabundance of singles has lead to the suggestion that up to half of *Kepler* systems might possess significant mutual inclinations between orbits, reducing the transiting number (the so-called "*Kepler* Dichotomy"). In a recent paper, Spalding et al. (2016) demonstrated that the quadrupole moment arising from a young, oblate star is capable of misaligning the contitue orbits of a close-in planetary system enough to reduce their transit number. Moreover, the 6-transiting system *Kepler*-11 was shown to become destabilized during the process. Here, we investigate the ubiquity of the stellar obliquity-driven instability within systems of lower multiplicity. We find that the instability occurs in most planetary systems analysed, including those possessing only 2 planets. Given the known parameters of T Tauri stars, we predict that between 1/4 and 1/2 of super-Earth mass systems may encounter the instability, in general agreement with the fraction required to explain the *Kepler* Dichotomy.

6.1 Introduction

The ever-growing yield of exoplanetary detections continues to reveal peculiarities between the properties of our own solar system and the galactic norm (Batalha et al., 2013; Fabrycky, Lissauer, et al., 2014). Among these, we highlight two features in particular. The first is that planetary orbits hosted by other stars frequently occupy a region interior to about 0.4 AU (where AU = Astronomical Unit), i.e., Mercury's approximate position in our solar system. In contrast, extrasolar planetary systems are awash with examples of planets orbiting significantly closer than Mercury (Batalha et al., 2013).

A second key aspect of the solar system is that the angular momentum vectors of the eight confirmed planets are mutually inclined by only $\sim 1 - 2\,^\circ$. In the 18th century, this coplanarity inspired the so-called "Nebular Hypothesis," wherein planetary systems originate from flat disks of gas and dust (Kant 1755, Laplace 1796).[1] Given the ubiquity with which planets form within disks, the expectation is that other planetary systems emerge from their protoplanetary nebula possessing a coplanar architecture. However, the frequency with which this coplanarity is retained over Gyr timescales is not fully understood.

Observational determination of mutual inclinations between extrasolar planetary orbits has proved exceedingly difficult (Winn and Fabrycky, 2015). Inclined planetary companions are frequently hypothesized as explanations for peculiar signals among transiting planets (Dawson and Chiang, 2014; Lai and Pu, 2017), and under special circumstances stability arguments have been used to place limits upon mutual inclinations (Laughlin, Chambers, and Fischer, 2002; Veras and Armitage, 2004; Nelson, Ford, et al., 2014). In addition, among systems with

[1] In contrast, the absence of material inside of Mercury's orbit remains mysterious (Batygin, Morbidelli, and Holman, 2015).

multiple transiting planets, the relative transit durations reveal mutual inclinations, but are generally limited to small values owing to the requirement that the planets simultaneously transit.

A separate method of ascertaining mutual inclinations has been to compare the relative numbers of multi-transiting systems to single-transiting systems (Lissauer, Ragozzine, et al., 2011; Johansen et al., 2012; Tremaine and Dong, 2012; Ballard and Johnson, 2016). If planetary systems are typically as coplanar as the solar system, one would expect to observe a larger abundance of multi-transiting systems than from a hypothetical population with larger mutual inclinations. Though conclusions differ in the literature (Tremaine and Dong, 2012), it is generally difficult to fit the observed multiplicity distribution using a single population of mutually coplanar planetary systems; there are too many single-transiting systems. Rather, some fraction (up to 50%; Johansen et al. 2012; Ballard and Johnson 2016) of systems either possess large mutual inclinations and therefore reveal only one planet at a time in transit, or alternatively this fraction of stars host only one planet.

The aforementioned over-abundance of single systems has been dubbed the "*Kepler* Dichotomy." Planet-planet interactions alone are generally unable to excite sufficient mutual inclinations (Becker and Adams, 2015), unless a massive exterior companion exists (Lai and Pu, 2017). Others have proposed a dichotomy in disk properties (Moriarty and Ballard, 2016). However, there still exists no widely-accepted explanation for the dichotomy. Furthermore, it remains unclear whether the singles are truly single, or rather members of mutually inclined multi systems.

The earliest attempt to explain the dichotomy proposed dynamical

instability within the single systems (Johansen et al., 2012), consistent with the larger sizes of single-transiting planets. This idea was disfavoured, largely owing to the unrealistically large masses required in order to trigger instability within Gyr timescales. To that end, Spalding and Batygin (2016) demonstrated that the quadrupole moment arising from a tilted, oblate central star is sufficient to misalign the orbits of planets enough to reduce their transit number. Upon simulating the 6-transiting *Kepler*-11 system, the stellar quadrupole was found to drive dynamical instability over a multi-Myr timescale, partly resolving the timescale issue in Johansen et al. (2012).

The primary goal of this paper is to deduce the ubiquity of the aforementioned instability mechanism across different planetary systems. Specifically, Spalding and Batygin (2016) were unable to say whether the instability is likely to occur in planetary systems with lower multiplicities than *Kepler*-11. Within a simplified, analytical framework, 2-planet systems were shown susceptible to becoming misaligned with one-another, but a more sophisticated treatment is required to investigate the potential for dynamical instabilities. Accordingly, in this work, we simulate systems with multiplicities ranging from 2 to 4 planets.

We find that the instability occurs in most systems simulated, including even 2-planet systems. Therefore, our second goal is to develop insight into the mechanism of instability. In brief, we show that the stellar quadrupole tilts the planetary orbits to a point where the precession rates of their longitudes of pericenter become approximately commensurate. This commensurability drives the eccentricities upward until the orbits cross, triggering instability. We provide a qualitative outline of the dynamics in this work, leaving a focused, quantitative description of the instability for a future paper.

6.2 Methods

In order to determine the influence of a tilted, oblate star upon *Kepler* systems in general, we simulated the first 20 million years of a selection of 11 planetary systems. For each system, we performed a suite of 110 N-body simulations, where each simulation corresponds to a different combination of stellar obliquity and stellar oblateness. Throughout each simulation, the stellar oblateness is allowed to decay, reflecting contraction onto the main sequence, though many systems undergo instability before the 20 million year simulation is concluded. For those that remain stable, we compute the mutual inclinations between the remaining planets in order to determine how many of the planets could be observed in transit.

Choice of systems

Our goal was to determine whether the obliquity-driven instability mechanism proposed in Spalding and Batygin (2016) is generic across planetary systems with lower multiplicities than $Kepler$-11. Accordingly, we modelled 6 examples of 2-planet systems, 3 examples of 3-planet systems, and 2 examples of 4-planet systems. We drew the system parameters from real, detected systems where measurements are available of the planetary masses Jontof-Hutter et al. (2016). The properties of these systems are outlined in Table 6.1.

Choosing real rather than fabricated systems has 2 advantages. First, we can be sure that the masses and semi-major axes in our simulations are representative of planetary system architectures known to exist. Second, given that these systems are observed to exhibit multiple transits, we may place constraints upon the obliquities of the host stars in order that their coplanarity has been retained. Such constraints upon stellar obliquity are particularly valuable in systems of low-mass

Modelled system parameters									
Name	$M_\star$ ($M_\odot$)	a_1 (AU)	m_1 (Earth masses)	a_2 (AU)	m_2 (Earth masses)	a_3 (AU)	m_3 (Earth masses)	a_4 (AU)	m_4 (Earth masses)
K2-38	1.07	0.0505	12	0.0965	9.9	-	-	-	-
Kepler-10	0.913	0.0169	3.33	0.241	17.2	-	-	-	-
Kepler-29	0.979	0.0922	4.5	0.1090	4.0	-	-	-	-
Kepler-36	1.071	0.1153	4.45	0.1283	8.08	-	-	-	-
Kepler-131	1.02	0.1256	16.13	0.1708	8.25	-	-	-	-
Kepler-307	0.907	0.0904	7.4	0.105	3.6	-	-	-	-
Kepler-18	0.972	0.0446	6.9	0.0751	17.3	0.117	16.4	-	-
Kepler-51	1.04	0.253	2.1	0.384	4.0	0.509	7.6	-	-
Kepler-60	1.041	0.0734	4.2	0.0852	3.9	0.103	4.2	-	-
Kepler-79	1.17	0.117	10.9	0.187	5.9	0.287	6.0	0.386	4.1
Kepler-223	1.13	0.0771	7.4	0.0934	5.1	0.123	8.0	0.148	4.8

Table 6.1: The parameters of the simulated *Kepler* systems. Initially, we set all eccentricities to zero. Date are obtained from (Jontof-Hutter et al., 2016) and exoplanetarchive.

planets, where alternative techniques for spin-orbit misalignment measurements are notoriously difficult to accomplish (Winn, Fabrycky, et al., 2010; Wang et al., 2017).

Numerical Set-up

We begin by performing numerical simulations of planetary systems orbiting stars with varying degrees of obliquities and quadrupole moments. Throughout, we utilize the mercury6 N-body symplectic integrator (Chambers, 1999). The planets move under the action of their own mutual gravity, along with that of the host star. Expanded to quadrupole order, the stellar potential may be written as

$$V_\star = -\frac{GM_\star}{r}\left[1 - \left(\frac{R_\star}{r}\right)^2 J_2\left(\frac{3}{2}\cos^2\theta - \frac{1}{2}\right)\right], \tag{6.1}$$

where θ is the angle between the planet's position and the spin axis of the star. The stellar mass and radius are denoted $M_\star$ and $R_\star$, the distance from the center of the star is written r, and G is Newton's

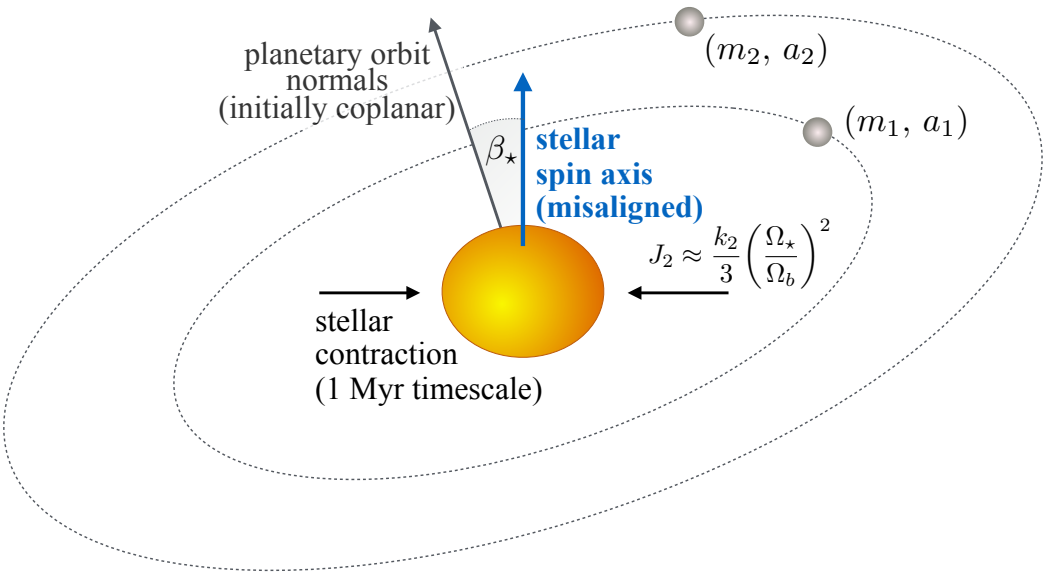

Figure 6.1: A schematic of our numerical simulations. The planetary system is initialized with coplanar orbits, all sharing a mutual inclination of $\beta_\star$ with the stellar spin axis. The star begins with an oblateness parameter $J_2 = J_{2,0}$ which decays exponentially on a 1 million year timescale. The simulations are carried out using the symplectic N-body integrator mercury6 (Chambers, 1999).

gravitational constant. The quantity J_2 is known as the second gravitational moment and encodes the star's oblateness, to quadrupole order.

A measurement of J_2 in distant stars is well beyond observational capabilities. However, it can be shown (Sterne, 1939; Ward, Colombo, and Franklin, 1976) that J_2 relates to the stellar spin rate $\Omega_\star$ through the expression

$$J_2 \approx \frac{k_2}{3}\left(\frac{\Omega_\star}{\Omega_b}\right)^2, \tag{6.2}$$

where k_2 is the Love number and $\Omega_b = \sqrt{GM_\star/R_\star^3}$ is the stellar break-up angular velocity. This approximation holds when $\Omega_\star \ll \Omega_b$, which is the case for most T Tauri stars (Bouvier, 2013). The benefit of parameterizing J_2 as above is the ability to directly measure $\Omega_\star$, and to obtain k_2 and Ω_b from stellar models. Specifically, the Love

number k_2 may be computed from polytropic models of polytropic index $\chi = 3/2$, yielding $k_2 \approx 0.28$ (Chandrasekhar, 1939; Batygin and Adams, 2013).

Owing primarily to Kelvin-Helmholtz contraction, the product $J_2 R_\star^2$ will decay with time, and with it the quadrupole moment. We choose to parameterize this contraction by supposing that the radius of the star is fixed at $R_\star = 2R_\odot$, reflecting the inflated radius typical of young stars (Shu, Adams, and Lizano, 1987). However, we allow J_2 to undergo exponential decay such that

$$J_2(t) = J_{2,0} \exp(-t/\tau_c), \tag{6.3}$$

where $J_{2,0}$ is the initial value of J_2 and the Kelvin-Helmholtz timescale $\tau_c = 1\,\mathrm{Myr}$ (Batygin and Adams, 2013).

In our prescription 6.2 for J_2, we prescribe $M_\star$ and $R_\star$, yielding Ω_b, along with a value $k_2 = 0.28$. The final component is the stellar spin rate. Here, we must draw from observations of young stars (Bouvier, 2013) which suggest a distribution of rotation periods ranging from $\sim 1 - 10\,\mathrm{days}$. Using the parameters above, we arrive at a range of $J_{2,0}$ given by

$$10^{-4} \lesssim J_{2,0} \lesssim 10^{-2}. \tag{6.4}$$

Accordingly, in our simulations we choose 11 values of $J_{2,0}$, equally separated in log-space:[2]

$$\log_{10}(J_{2,0}) \in \{-4,\ -3.8,\ \ldots,\ -2\}. \tag{6.5}$$

[2]It should be noted that our simulations will begin subsequent to disk-dispersal, meaning that the stellar radius is likely to be somewhat reduced from $2R_\odot$ and so our strongest quadrupole is a slight over-estimate.

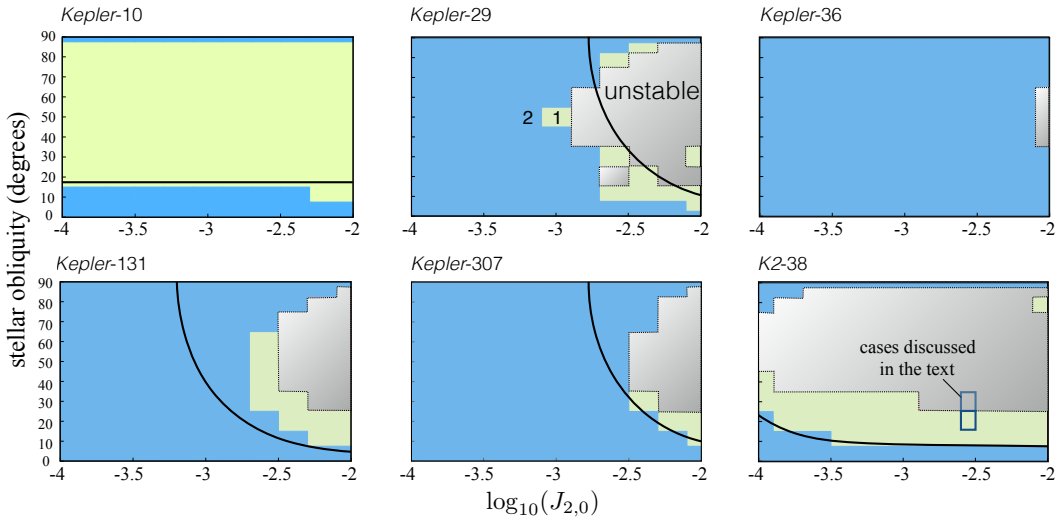

Figure 6.2: The number of planets detectable in transit after 20 million years of simulation from an initially 2-planet configuration. Solid black lines denote the critical obliquity as a function of $J_{2,0}$ predicted to reduce the transit number from 2 to 1 according the the formula Spalding and Batygin (2016). The dotted line outlines the region where one of the two planets was lost owing to dynamical instability. We explore the mechanism of instability in more detail by examining the cases outlined in blue on the plot for $K2$-38.

In all simulations, we fix the spin axis of the star to be parallel to the z-axis. This approximation holds provided the angular momentum of the star is significantly larger than that of the planetary orbits. A planet of mass m_p following a circular orbit at semi-major axis a_p, possesses angular momentum $m_p\sqrt{GM_\star a_p}$, which, when divided by that of a star of dimensionless moment of inertia $I \approx 0.21$, yields an angular momentum ratio between the two of

$$\begin{aligned} j &\equiv \frac{m_p\sqrt{GM_\star a_p}}{IM_\star R_\star^2\omega_\star} \\ &\approx 0.05\left(\frac{m_p}{10M_{earth}}\right)\left(\frac{M_\star}{M_\odot}\right)^{-1/2} \\ &\left(\frac{P_\star}{10\,\text{days}}\right)\left(\frac{R_\star}{R_\odot}\right)^{-2}\left(\frac{a_p}{0.1\,\text{AU}}\right)^{1/2}. \end{aligned} \tag{6.6}$$

The smallness of j validates our assumption that the stellar spin axis

does not change significantly with time.

We note that our modelled systems take their masses and semi-major axes from observed systems, but we are not necessarily attempting to reconstruct the history of these systems in detail. Rather, we are using their orbital parameters as general guidelines for "typical" planetary system parameters. As initial conditions, we set all eccentricities to zero. For each value of $J_{2,0}$, we run simulations with 10 different initial stellar obliquities ($\beta_\star$), spread between 0 and 90 degrees, including:

$$\beta_\star \in \{5,\ 10,\ 20,\ 30,\ 40,\ 50,\ 60,\ 70,\ 80,\ 85\}. \tag{6.7}$$

Determination of transit number

At each time step in our model runs, we determine the maximum number of planets that can be seen transiting by computing the mutual inclination between all of the planetary orbital pairs. Considering a pair of planets i and j, the mutual inclination I_{ij} will remove them from transit if the following criterion is satisfied

$$\left|\sin(I_{ij})\right| \gtrsim \frac{R_\star}{a_i} + \frac{R_\star}{a_j}. \tag{6.8}$$

For example, given three planets we compute I_{12}, I_{13}, and I_{23}. If all satisfy the above criterion, the transit number is unity. If I_{12} and/or I_{23} do not satisfy the criterion but I_{13} does, the transit number is 2, etc. Given that the mutual inclination will change with time, potentially bringing the planet pairs into and out of mutual transit, we average the transit number over the final 10 time-steps of the integration (spanning $\sim 10^5$ years).

Caveat: Disk Potential

It is important to point out one confounding factor in our results. We began with an initial condition whereby the planetary system

possessed a non-zero inclination with respect to the stellar spin axis. However, in any physical situation like this, it is important to ask how the system was set up in that configuration, especially if that configuration is not a steady-state. Here, the key assumption was that the disk dispersed on a short enough timescale such that the planets inherited the disk's plane exactly.

To examine this problem, we cannot simply add a disk potential to the numerical simulations, because in that case fixing the stellar precession axis is no longer valid (Spalding and Batygin, 2014). The disk will induce a nodal regression upon the planetary orbits of (Hahn, 2003)

$$\nu_{\rm crit} \approx n_p \frac{\pi \sigma a_p^2}{M_\star} \frac{a_p}{h}, \tag{6.9}$$

where σ is the disk's surface density and h is the disk's scale height. We may define the time of disk dispersal as the point at which ν_d is approximately equal to the nodal regression induced by the stellar quadrupole moment ($\nu_\star = (3/2)J_2(R_\star/a_p)^2$). This criterion corresponds to a disk surface density of

$$\begin{aligned} \sigma_{\rm d} &\approx \left(\frac{3M_\star h J_2}{2\pi a^3}\right)\left(\frac{R_\star}{a}\right)^2 \\ &\approx 200 {\rm g\,cm^{-2}}, \end{aligned} \tag{6.10}$$

where we used $J_2 = 10^{-3}$, $h/a = 0.05$ and $R_\star = 2R_\odot$. The surface density of the MMSN at 0.1 AU is approximately 50,000 $\rm gcm^{-2}$, meaning that disk dispersal for our purposes happens at the point when the disk possesses roughly 1% of its original mass (Armitage, 2010). The final stages of disk dispersal in the inner regions are thought to progress through viscous accretion, subsequent to photoevaporative starvation from gas accreting inwards from the outer disk. The viscous

time at 0.1 AU is given by

$$\begin{aligned}\tau_\nu &\approx \frac{a_p^2}{\nu} \\ &\approx \frac{a_p^2}{\alpha h^2 \Omega} \\ &\approx 2000 \text{ years}, \end{aligned} \tag{6.11}$$

whereas the precession timescale from the stellar quadrupole is roughly 300 years. Given that the disk dissipates on a longer timescale than the precession timescale, the system might reduce its spin-orbit misalignment during disk dissipation as the stellar quadrupole begins to dominate over the disk's quadrupole. More work is required in order to investigate this possibility. The timescales and physics governing disk dispersal are poorly understood, and so we leave this aspect of the problem as a caveat, to be returned to once better constraints become available.

6.3 Results & Discussion

For each planetary system, we construct a grid of colors representing the 110 chosen combinations of stellar obliquity and initial $J_{2,0}$. Systems of 2 planets are illustrated in Figure 6.2 and those with 3 or 4 planets are depicted in Figures 6.3 & 6.4. The number of co-transiting planets associated with each color is labeled on the figures. Crucially, we outline the cases where instability occurred with a dotted line and grey shading. Here, instability is defined as the loss of at least one planet from the system. In reality, the escape velocities of the planets considered are too low to typically remove other planets from the system entirely. Rather, the end result is that planets that are lost will end up either colliding with the star, or colliding with the remaining planets. We do not take account of the collisions themselves in this work.

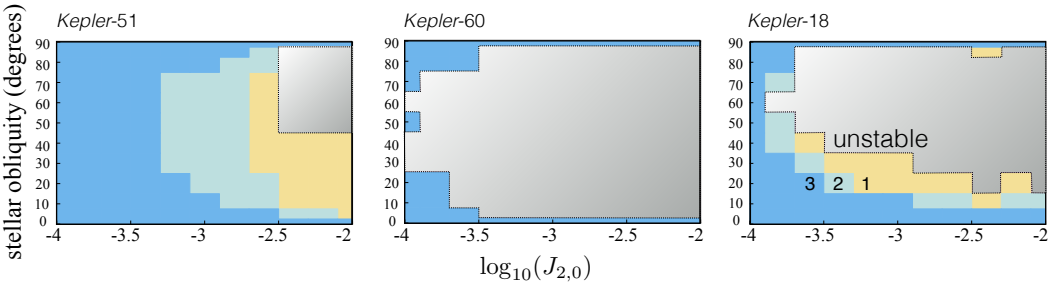

Figure 6.3: The number of planets detectable in transit after 20 million years of simulation from an initially 3-planet configuration. The dotted line outlines the region where one or more planets were lost owing to dynamical instability.

An analytic formula was derived in Spalding and Batygin (2016), relating the mutual inclination excited owing to the stellar quadrupole, under the assumptions of circular orbits and low inclinations. For the 2-planet systems, we draw a solid black line that denotes this predicted boundary between coplanar and misaligned orbits.

As stated above, our primary goal was to delineate the ubiquity of stellar oblateness as an instability mechanism. To that end, we note that only *Kepler*-10 was immune to instability for all chosen parameters, with *Kepler*-36 remaining stable all but two times. All other systems were susceptible, at least for the upper range of $J_{2,0}$. Accordingly, we conclude that the instability mechanism uncovered in Spalding and Batygin (2016) constitutes a viable pathway toward instability for low and high-multiplicity systems alike. In general terms, the range of $J_{2,0}$ leading to instability is slightly smaller for the 3 and 4 planet systems than 2-planet systems; however, given our small sample size such a pattern is by no means statistically significant.

Eccentricities

If a single-transiting system is observed, it is difficult to infer whether there exist any non-transiting companions. Within the frame of our present investigation, a key signature of dynamical instability is the

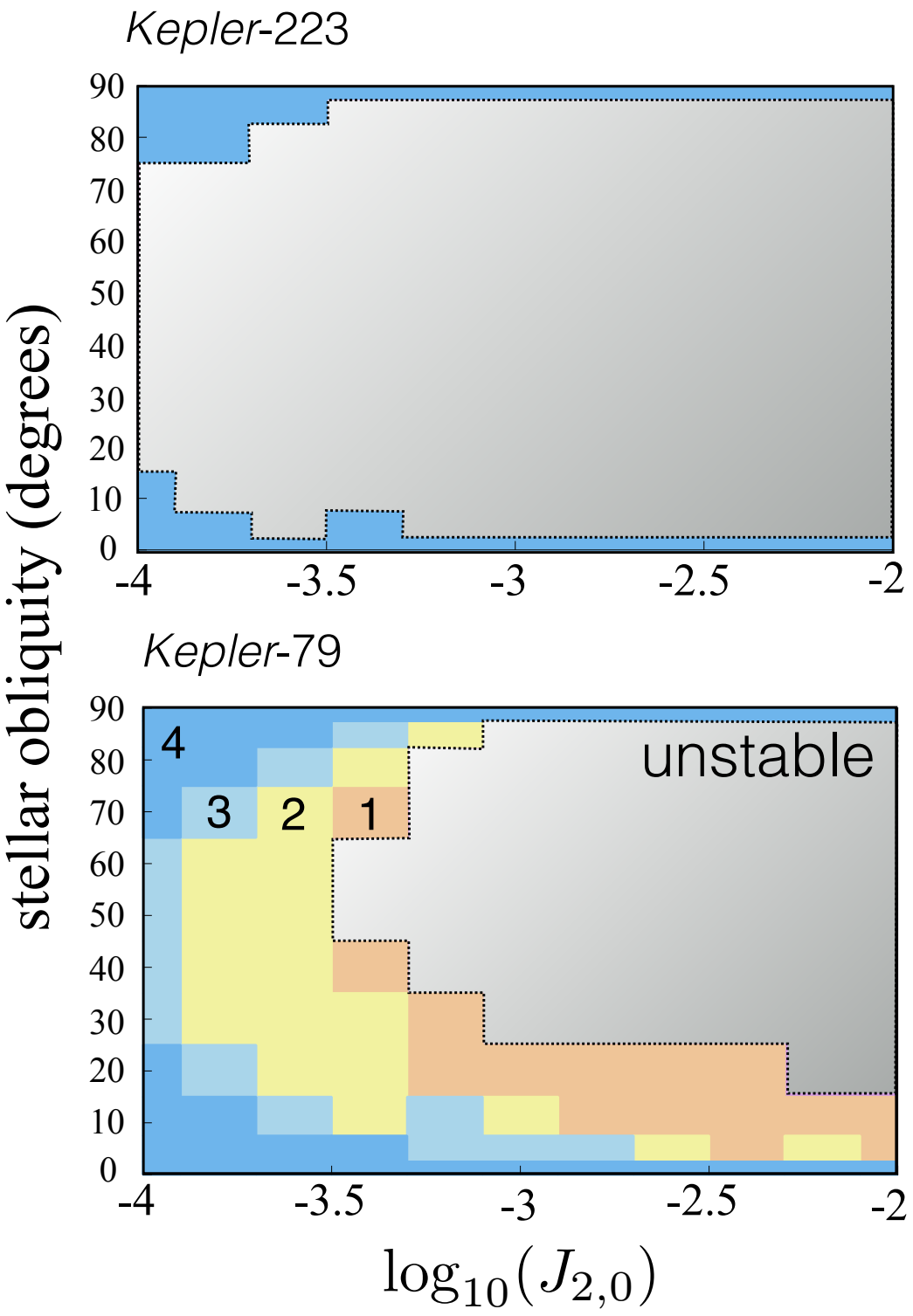

Figure 6.4: The number of planets detectable in transit after 20 million years of simulation from an initially 4-planet configuration. The dotted line outlines the region where one or more planets were lost owing to dynamical instability.

presence of significant eccentricity within the planetary orbits that remain subsequent to instability. Eccentricity therefore constitutes an observable signature of instability, however, for the shortest-period systems tidal effects are likely to have damped out any traces of primordial eccentricity. The tidal circularization timescale is given by (Murray and Dermott, 1999)

$$\begin{aligned}\tau_e \equiv \left|\frac{e}{\dot{e}}\right| &\approx \frac{2}{21}\frac{Q}{k_{2,p}n_p}\frac{m_p}{M_\star}\left(\frac{a_p}{R_p}\right)^5 \\ &\approx 40\left(\frac{a_p}{0.1\mathrm{AU}}\right)^{\frac{13}{2}}\left(\frac{Q/k_{2,p}}{1000}\right)\left(\frac{2R_{\mathrm{Earth}}}{R_p}\right)^5 \mathrm{Gyr}, \end{aligned} \tag{6.12}$$

where $k_{2,p}$ is the planetary Love number and Q_p is its tidal quality factor. Put another way, planets possessing 10 Earth masses and 2 Earth radii will circularize within a Gyr for semi-major axes below $a_p \sim 0.05$ AU. Those with semi-major axes exceeding $a_p \sim 0.1$ AU ought to possess eccentricities that are relatively unaffected by tides, though numerous other dynamical interactions are capable of exciting, or indeed damping, their eccentricities.

With the caveat regarding tidal circularization in mind, it is interesting to tabulate the orbital parameters of the planet that remains after dynamical instability within the four most unstable 2-planet examples – *K*2-38, *Kepler*-27, *Kepler*-131, and *Kepler*-307. As can be seen from Table 6.2, the mean eccentricity of the remaining planet is roughly $\bar{e}_i \approx 0.3 - 0.4$.

Cumulatively, we may propose the following observational signature. First, consider a sample of single-transiting systems beyond 0.1 AU. Suppose that they are composed of two populations: a fraction f_{in} that have undergone dynamical instability and a fraction f_{in} that have not. The latter fraction did not pass a dynamical instability, and appear single owing to exhibiting mutual inclinations with unseen companions,

or alternatively were born single. According to our proposed mechanism, the population that experienced instability should possess a mean eccentricity of $\bar{e}_{\rm inst} \approx \bar{e}_i$. If the mean across both populations is $\bar{e}$ and the mean of the stable population is $\bar{e}_{\rm st} \ll \bar{e}_{\rm inst}$, one can show that

$$\begin{aligned} f_{\rm in} &= \frac{\bar{e} - \bar{e}_{\rm st}}{\bar{e}_{\rm inst} - \bar{e}_{\rm st}} \\ &\approx \frac{\bar{e}}{\bar{e}_{\rm inst}}, \end{aligned} \tag{6.13}$$

where the second equality assumes the stable population will exhibit eccentricities much lower than the unstable population.

Typically, the *Kepler* Dichotomy is quoted as reflecting a roughly equal split between the large and small inclination systems, i.e., $f_{in} = 1/2$ (Johansen et al., 2012; Ballard and Johnson, 2016). In order to reproduce this fraction with $\bar{e}_{u,o} \approx 0.4$, we would predict $\bar{e}_o \approx 0.2$. Of course, this is a very simplified picture, but outlines the feasibility of learning about the true underlying abundance of planets despite only observing the proportion that transit.

During the planets' close encounters at high eccentricity, the semi-major axes of both planets are altered. The remaining planet generally experiences an increase in semi-major axis, indicating a gain in energy at the cost of the second planet, which usually ends up colliding with the central body. Related to this point, recall that the stellar radius was held fixed in the code, and J_2 was forced to decay, leaving the star modestly larger than it would be in reality during the later stages of the simulation. Accordingly, there exists the possibility that in real systems, more energy would need to be transferred to collide with a smaller star, and larger semi-major axes and/or eccentricity influences might occur. In addition, depending upon the exact mechanism of instability, tides may "save" the inner planet by damping its eccentricity

before it enters a star-crossing trajectory. These details of the problem do not alter the general picture.

Our discussion in this section uses eccentricities and semi-major axes obtained from the mercury6 N-body code. However, we did not model collisions between planets, which is likely to influence the final eccentricity distribution. Accordingly, the eccentricities in reality may be smaller than we predict here owing to dissipative processes associated with the physics of merging. Though the quantitative nature of our predictions are subject to numerous uncertainties, the qualitative prediction is that a population of single-transiting systems ought to exhibit larger eccentricities than those possessing unseen companion planets.

6.4 Mechanism of instability

If the stellar quadrupole only induced instability in systems with 3 or more planets, it would have been difficult to understand in simple terms the physical mechanism of instability. However, the onset of instability in 2-planet systems leaves the process amenable to analytic investigation.

In Spalding and Batygin (2016), 2-planet systems were studied analytically by expanding the planet-planet interaction disturbing potential to lowest (second) order in inclinations, and assuming zero eccentricities (Lagrange-Laplace secular theory; Murray and Dermott 1999). This approach yielded a closed-form solution for the relative inclination excited between the two planetary orbits. The locus of stellar J_2 and $\beta_\star$ taking the two transits out of the same plane is drawn onto Figure 6.2, and agrees relatively well with the transition between coplanar and misaligned systems. However, the framework was ill-equipped to explain why greater inclinations or oblateness give rise to instability.

2-planet systems							
System	$a_{1,i}\,(AU)$	$\bar{a}_{1,f}$ (AU)	$a_{2,i}\,(AU)$	$\bar{a}_{2,f}$ (AU)	$\bar{e}_{1,f}$	$\bar{e}_{2,f}$	$\bar{e}_f$
K2-38	0.0505	0.0732	0.0965	0.1815	0.4507	0.4091	0.4242
Kepler-29	0.0922	0.1502	0.1090	0.1418	0.4028	0.3351	0.3701
Kepler-131	0.1256	0.1488	0.1708	0.2541**	0.3572	0.3840**	0.3603
Kepler-307	0.0904	0.0952	0.105	0.1378*	0.3195	0.3665*	0.3224

Table 6.2: The semi major axes and eccentricities of the 4 most unstable 2-planet systems resulting from our simulations. For each case where instability occurred, we recorded the eccentricity and semi-major axis of the remaining planet, then took the mean of all the results (denoted by an overbar, with the subscript 'f' meaning 'final,' 'i' representing 'initial" and the number corresponding to the particular planet). The mean is only a very general guideline as to what to expect, but the results suggest that a population of single-transiting systems that had undergone our proposed instability mechanism would be expected to yield an average eccentricity of roughly 0.3-0.4.

In order to do so, we lift the assumptions of circular orbits and low inclination by utilising a different expansion of the disturbing potential, one that uses semi-major axis ratio as a small parameter (Kaula, 1962):

$$\mathcal{H} = \frac{Gm_1m_2}{a_2}\sum_{l=2}^{l=\infty}\left(\frac{a_1}{a_2}\right)^l A_l(e_1, e_2, I_1, I_2) \times \cos(j_1\lambda_1 + j_2\lambda_2 + j_3\varpi_1 + j_4\varpi_2 + j_5\Omega_1 + j_6\Omega_2), \tag{6.14}$$

where the above form is written succinctly, with significant information encoded in the value of A_l. The constants j_i are constructed such that $\sum_{i=1}^{6} j_i = 0$ (Murray and Dermott, 1999), and the angles λ_i, ϖ_i and Ω_i are respectively the mean longitude, longitude of pericenter, and argument of ascending nodes of the planetary orbits.

The above Hamiltonian contains infinite "harmonics" – the cosine terms – each associated with its own specific resonance. Here, a resonance may be thought of as a restoring torque that tends to force libration about some constant value of the argument. If we can assume

that the system is close to one of these resonances, and no other resonances overlap significantly, it is possible to ignore the other harmonics and consider the dynamics associated with one harmonic alone (Lichtenberg and Lieberman, 1992; Morbidelli, 2002). In order to determine which harmonic(s) must be retained, we turn to our numerical simulations.

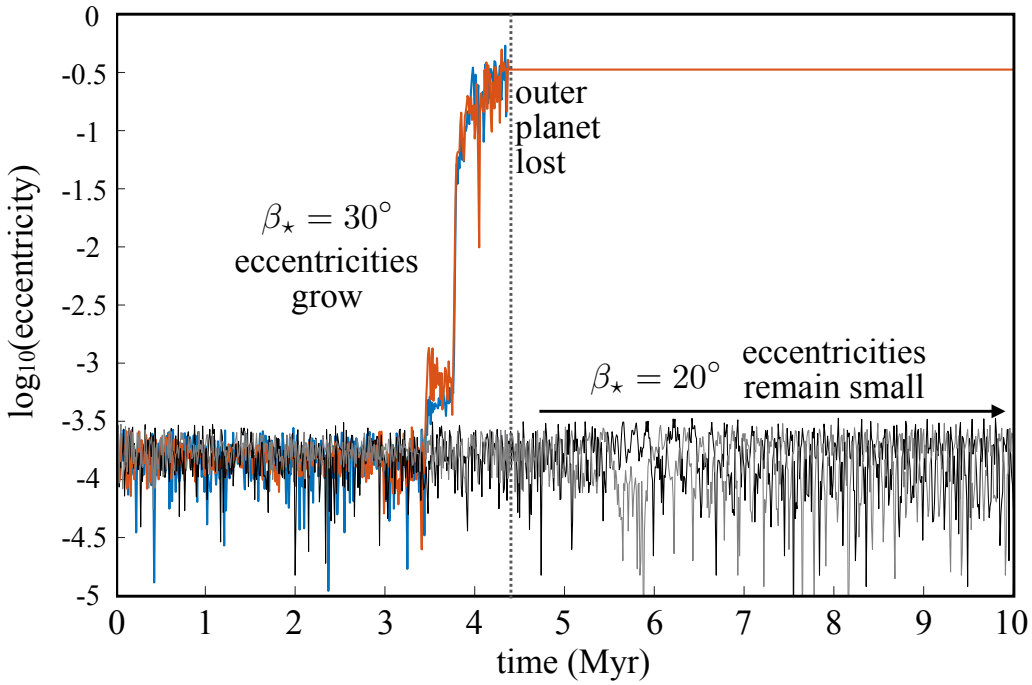

Figure 6.5: The evolution of eccentricity of both planets in the K2-38 system when the stellar obliquity is set at 30° (blue, inner planet and red, outer planet) and 20° (grey, inner planet and black, outer planet). For both cases, oblateness decays from $J_{2,0} = 10^{-2.6}$. The difference in dynamics between the two cases is profound. Whereas at 20° both planets remain circular, at 30° both eccentricities begin to grow in unison at 3.75 Myr. After reaching eccentricities of roughly 1/2, instability sends the outer planet into the central star. We discuss this process in the text.

Beginning with *K*2-38, we consider two cases: one that undergoes instability and another that does not, annotated in Figure 6.2. The same value of $J_{2,0} = 10^{-2.6}$ is chosen, with the stable case having $\beta_\star = 20°$ and the unstable case corresponding to $\beta_\star = 30°$. In Figure 6.5 we plot the eccentricities of both planets as a function of time at each value

of stellar obliquity. Notably, in the stable 20° case, both eccentricities remain low, but the dynamics change qualitatively at 30°. In the unstable case, both eccentricities begin to grow simultaneously at ~ 3.75 Myr until roughly 0.6 Myr later, when the system undergoes instability and the outer planet is lost through collision with the central star.

Eccentricity growth of the kind described above is a common outcome of capture into a secular resonance (Ward, Colombo, and Franklin, 1976; Batygin, Bodenheimer, and Laughlin, 2016), whereby two frequencies become roughly commensurate, causing them to "lock" as system parameters evolve. In order to deduce which resonance the system enters we illustrate the evolution of the argument $\varpi_1 - \varpi_2$ in Figure 6.6. Concurrent with the initiation of eccentricity-growth, the system enters a libration of $\varpi_1 - \varpi_2$ around π, i.e., the orbits are roughly anti-aligned. Accordingly, the resonance corresponds to a commensurability between the frequencies $\dot{\varpi}_1$ and $\dot{\varpi}_2$.

Interestingly, $\varpi_1 - \varpi_2$ appears to librate around $\varpi_1 - \varpi_2 = 0$ with a large amplitude for a brief period before the resonant growth of eccentricity begins. Furthermore, this brief period of apparent libration corresponds to an order of magnitude increase in eccentricity, from $e_i \sim 10^{-4}$ to $e_i \sim 10^{-3}$. This libration does not imply resonant locking. A circulating trajectory in phase-space will appear to librate if the center of libration is offset from the origin and the libration amplitude is small enough (Lichtenberg and Lieberman, 1992; Morbidelli, 2002). Furthermore, the impulsive nature of the eccentricity rise is not characteristic of resonant locking.

With the understanding that eccentricity growth commences at $\dot{\varpi}_1 \approx \dot{\varpi}_2$, we can begin to develop a criterion for the onset of instability

within a given planetary system. We expand Hamiltonian 6.14, but remove all harmonics except for $\cos(\varpi_1 - \varpi_2)$. For illustration, we expand the potential to fourth (hexadecapolar) order, but in order to adequately treat the resonant dynamics, higher order expansions are likely required (e.g., Boué, Laskar, and Farago 2012). The disturbing function acting between the two planets may then be written

$$\begin{aligned}
\mathcal{R}_{12} &= \mathcal{R}_{\rm quad} + \mathcal{R}_{\rm oct} + \mathcal{R}_{\rm hexa} \\
\mathcal{R}_{\rm quad} &= \frac{Gm_1m_2}{a_2}\left(\frac{a_1}{a_2}\right)^2 \frac{2+3e_1^2}{128(1-e_2^2)^{3/2}} \\
&\quad \times \Big[1+3\cos(2I_1)\Big]\Big[1+3\cos(2I_2)\Big] \\
\mathcal{R}_{\rm oct} &= -\frac{Gm_1m_2}{a_2}\left(\frac{a_1}{a_2}\right)^3 \frac{15e_1e_2(4+3e_1^2)}{4096(1-e_2^2)^{5/2}}\cos(\varpi_1-\varpi_2) \\
&\quad \times \Big[5\cos(I_1)\big(3\cos(I_1)-2\big)-1\Big]\Big[(1+\cos[I_1])\Big] \\
&\quad \times \Big[5\cos(I_2)\big(3\cos(I_2)-2\big)-1\Big]\Big[(1+\cos[I_2])\Big] \\
\mathcal{R}_{\rm hexa} &= \frac{Gm_1m_2}{a_2}\left(\frac{a_1}{a_2}\right)^4 \left[\frac{9(15e_1^4+40e_1^2+8)(3e_2^2+2)}{4194304(1-e_2^2)^{7/2}}\right] \\
&\quad \times \big(20\cos(2I_1)+35\cos(4I_1)+9\big) \\
&\quad \times \big(20\cos(2I_2)+35\cos(4I_2)+9\big).
\end{aligned} \tag{6.15}$$

In addition to the planet-planet disturbing potential, the stellar disturbing potential may be written (Danby, 1992)

$$\mathcal{R}_{J_2,p} = -\frac{Gm_pM_\star}{2a_p}J_2\left(\frac{R_\star}{a_p}\right)^2\left[\frac{3}{2}\sin^2(I_p)-1\right](1-e_p^2)^{-3/2}. \tag{6.16}$$

In order to solve for the inclinations at which $\dot{\varpi}_1 \approx \dot{\varpi}_2$, we use

Lagrange's planetary equations (Murray and Dermott, 1999)

$$m_p\sqrt{GMa_p}\frac{d\varpi_p}{dt} = \frac{\sqrt{1-e_p^2}}{e_p}\frac{\partial\mathcal{R}}{\partial e_p} + \frac{\tan(I_p/2)}{\sqrt{1-e_p^2}}\frac{\partial\mathcal{R}}{\partial I_p} - m_p\sqrt{GMa_p}\frac{3GM_\star}{c^2a(1-e_p)}n_p, \tag{6.17}$$

where the full disturbing function is given by

$$\mathcal{R} = \mathcal{R}_{J_2,1} + \mathcal{R}_{J_2,2} + \mathcal{R}_{12}, \tag{6.18}$$

and we have introduced the speed of light c through the inclusion of general relativistic precession (Wald, 2010).

The precession frequencies $\dot{\varpi}_i$ depend upon the orbital inclinations I_1 and I_2. In Figure 6.7 we plot the evolution of both planetary inclinations for 4 different cases corresponding to $\beta_\star = \{30°, 40°, 50°, 60°\}$ and $J_{2,0} = 10^{-2.6}$. Initially, both inclinations are equal to $\beta_\star$. As time proceeds, the location in I_1-I_2 space follows an arc (the blue points), with the location oscillating about $I_1 = I_2 = \beta_\star$ with gradually increasing amplitude. Eventually, this trajectory takes the system into a configuration where $\dot{\varpi}_1 - \dot{\varpi}_2 \approx 0$. We plot the locus of $\dot{\varpi}_1 - \dot{\varpi}_2 = 0$, after setting $\varpi_1 - \varpi_2 = \pi$ and $e_1 = e_2 = 0.01$ (i.e., small).

The red points in Figure 6.7 correspond to eccentricities above 0.01, corresponding to trajectories that begun their secular resonant growth of eccentricity. If our above argument, that eccentricity growth begins at exact resonance, we would expect the blue points to turn to red points as soon as the blue arc intersects the contours of $\dot{\varpi}_1 - \dot{\varpi}_2 \approx 0$. However, these contours do not match exactly to the transition between low and high eccentricity evolution. This fact is likely a consequence of our assumption in the above calculation that the planetary inclinations are stationary in time. In reality, they are oscillating on a similar

timescale to the eccentricities, meaning it is not strictly appropriate to treat the set-up as a 1-degree of freedom system (i.e., e and ϖ), but rather it is necessary to include a second degree of freedom (I and Ω). Despite the resonant criterion failing quantitatively, the qualitative picture remains unchanged.

We emphasise that the above expressions do not make any assumptions regarding inclinations. This aspect is key, because at small inclinations no configuration exists that brings the two precession frequencies close to one another (see dashed contour int Figure 6.7). However Figure 6.7 indicates that when the inner planet is inclined by more than $\sim 40\,^{\circ}$, the two frequencies can be brought close to one another.

The requirement of planetary inclinations may be understood by noting that the inner planet's greater proximity to the star contributes to a faster J_2-induced precession rate in the coplanar case. However, as the inner planet is tilted, the stellar quadrupole's influence weakens such that there exists a critical inclination at which the two planets are precessing at equal rates. Though different in important aspects, the effect whereby higher inclinations open up a system to resonant behaviour is reminiscent of the Kozai-Lidov resonance which has found wide-spread usage within celestial mechanics (Kozai, 1962; Fabrycky and Tremaine, 2007; Nagasawa, Ida, and Bessho, 2008; Naoz, Farr, Lithwick, et al., 2011). The resonance we outline may likewise have had wide-spread importance in the evolution of systems around oblate central bodies.

Resonances do not exist at low inclinations in $K2$-38 owing to the low angular momentum of the inner body relative to the outer body. The planet-planet induced precession cannot overcome the greater influence of the stellar quadrupole at shorter orbital periods. It was

found in Spalding and Batygin (2016) that resonance in the argument of ascending node only existed if the inner planet possessed more angular momentum than the outer planet. A similar scenario is found here. It is possible to find low-inclination resonant values of J_2 in the systems, such as $Kepler$-131 that possess an inner planet with more angular momentum than the outer planet. However, the resonant value of J_2 is an order of magnitude larger than the largest value we considered and so plays no role in these dynamics. High inclinations must be excited if the system is to enter resonance.

To close our discussion of the instability itself, we illustrate why the aforementioned eccentricity growth leads to instability. We plot in the bottom panel of Figure 6.6 the pericenters, apocenters, and semi-major axes of both planets in the unstable case. Instability corresponds roughly to the time when the pericenter of the outer planet coincides with the apocenter of the inner planet. If the orbits were perfectly anti-aligned and in the same plane this configuration corresponds to orbit-crossing. Whereas they are not in the same plane in general, their libration around $\varpi_1 - \varpi_2 = \pi$ suggests the orbits come close to crossing.

6.5 Conclusions

Ubiquity of instability

The primary motivation for this work was to determine whether the gravitational perturbation arising from a tilted, oblate star is sufficient to destabilize systems of planets possessing low multiplicity. We studied 11 systems, 6 of which possess 2 planets, 3 possess 3 planets, and 2 possess 4 planets. We find that instability occurred in all but one system for nominal values of stellar oblateness and obliquity. However, instability only occurred in general for $J_2 \gtrsim 10^{-3}$ and stellar

obliquities $\beta_\star \gtrsim 30°$, with the range varying widely.

If we suppose that $J_2 \gtrsim 10^{-3}$ leads to instability in most systems, then this equate to periods

$$P_\star \lesssim 20\pi \left(\frac{R_\star^3}{GM_\star}\right)^{1/2}$$
$$P_\star \lesssim 3\,\text{days}, \tag{6.19}$$

though the critical value can vary for different assumptions on the appropriate stellar radius. T Tauri stars spin with periods ranging between about 1-10 days, with the median of the distribution lying close to 3-5 days (Bouvier, 2013). Furthermore, there is evidence that stars spin up slightly, to periods below 3 days, immediately following disk dissipation (Bouvier et al., 2014; Karim et al., 2016). These observations suggest that a relatively large fraction, perhaps as many as 1/2 of systems, are subject to this instability.

In addition to the proportion of systems exhibiting large enough quadrupole moments, we must also consider the distribution of stellar obliquities. The stellar obliquity of hot stars (surface temperature above 6200 K) hosting hot Jupiters appears to be close to isotropic (Winn, Fabrycky, et al., 2010; Albrecht et al., 2012). However, the picture changes for cool stars and smaller planets (Li and Winn, 2016; Winn, Petigura, et al., 2017), where the obliquities appear substantially reduced. If stellar obliquity was distributed isotropically, and $150° > \beta_\star > 30°$ triggered instability, we would expect an unstable fraction given by

$$f_{30} = \frac{\int_{30}^{150} \sin(\theta) d\theta}{\int_0^{180} \sin(\theta) d\theta}$$
$$= 0.87. \tag{6.20}$$

We consider this value as an extreme case; however, it illustrates that a modestly enhanced stellar obliquity distribution can bring a significant fraction of systems into the realms of instability.

Depending upon the true values of many currently uncertainty parameters, the instability mechanism might turn out to be almost ubiquitous, or extremely rare. The estimates are limited by the so-far small sample size of 11 modelled systems, poor knowledge of young star radii and rotational evolution, along with the present dearth of spin-orbit misalignment measurements in systems of lower-mass planets (Wang et al., 2017). With those caveats in mind, the approximate, yet slightly optimistic discussion above suggests that somewhere between 1/2 to 1/4 of super-Earth systems might pass through a phase where their host star's quadrupole moment triggers instability.

Observational tests

An addition goal of this work was to progress toward a method of distinguishing single-transiting systems with unseen transiting companions from those systems possessing a single planet intrinsically. One way to accomplish this directly is through the measurement of transit timing variations arising both from direct perturbations upon the transiting planet (Agol et al., 2005; Nesvorný et al., 2012), and from astrometric variations of the stellar light curve induced from the perturbations upon the star itself (Millholland, Wang, and Laughlin, 2016). However, here we propose that if the stellar oblateness drives instability in a significant fraction of systems, one may distinguish single transiting from single planet systems at a population level by measuring the eccentricities of the transiting planets. We find that typical eccentricities excited lie between 0.3 and 0.4 (Table 6.2), and that tidal circularization is ineffective at erasing these eccentricities

provided the planet resides outside of roughly 0.1 AU.

Given that the stellar quadrupole falls of as the square of semi-major axis, we would expect that the mechanism is less effective for more distant systems. Indeed, in a general sense, we would predict that the closest single-transiting planets exhibit low eccentricities, owing to tides. A little further away we would expect the eccentricities to grow, before decaying again as the instability mechanism becomes less effective. Uncertainties on tidal dissipation, together with the influence of semi-major axis upon stellar obliquities (Li and Winn, 2016; Dai and Winn, 2017) make a preition fo the value of the proposed peak highly speculative.

Finally, our analysis of planetary system stability allows us to place loose constraints upon stellar obliquity in order for specific multi planet systems to have remained coplanar. For example, we predict that the stellar obliquity of $K2$-38 is under 10°, otherwise the two planetary orbits ought to have been misaligned with one another. Likewise $Kepler$-10 is probably no more misaligned with its planetary orbits than $\sim 20^{\circ}$. We are hesitant to make similar predictions regarding $Kepler$-223, as although it appeared highly unstable in our integrations, we did not take care to reproduce the multi-resonant configuration as is currently observed (Mills et al., 2016), which might help retain the planets within the same plane.

Future directions

This work considered an initial condition whereby the planetary orbits were coplanar, assuming the disk to have dissipated more rapidly that the orbits can reconfigure into their equilibrium potential. Future treatments should consider this aspect. In particular, the disk itself leads to a precession of longitudes of periapse for embedded planets.

Given our finding that the instability is driven by a resonance between $\dot{\varpi}$ of planetary pairs, it would be a fruitful investigation to consider how the disk's gradual dissipation alters the secular phase space (Ward, 1981).

We obtained a qualitative understanding of the instability mechanism, namely, that the values of $\dot{\varpi}$ of both planets can be brought close to together by way of quadrupole-driven inclinations. The resulting resonance leads to eccentricity growth and orbit-crossing. However, we did not treat this problem in a full, 2-degree of freedom framework. To do so would better elucidate the quantitive criteria governing the instability. Furthermore, within this framework the disk potential may be added as an additional term, and the stellar orientation may be allowed to evolve with time, providing an analytic framework for following the system all the way from formation within a massive disk, to the onset of instability subsequent to disk dispersal.

Cumulatively, we have shown that the contraction of the host star, an evolutionary phase common to all planetary systems, can play a key role in sculpting the resulting planetary systems. Our own solar system was likely not sensitive to the Sun's quadrupole moment owing to the relatively large semi-major axis of Mercury. Its enhanced stability is in part responsible for Earth's low eccentricity and stable conditions over billions of years. By turning toward exoplanetary systems, we see that the host star is not always the giver of life that is in our system, but rather its gravity may disrupt and destroy the tranquility of the systems it hosts.

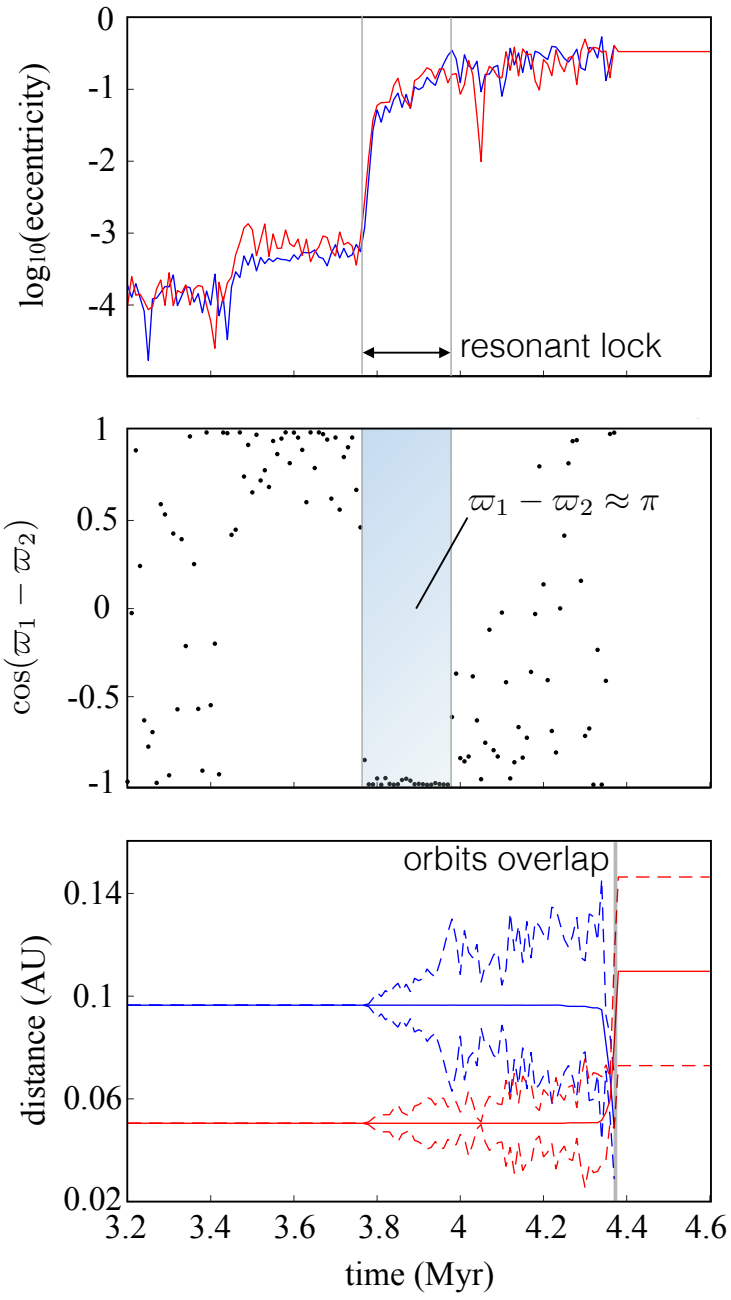

Figure 6.6: A closer look at the dynamics close to the time of instability of $K2$-38 with parmeters $\beta_\star = 30°$, $J_{2,0} = 10^{-2.6}$. Top panel: The evolution of eccentricity as a function of time for the outer planet (blue) and the inner planet (red). Middle panel: Time evolution of the resonant argument $\cos(\varpi_1 - \varpi_2)$ through instability. Notice that the argument librates close to π during the main phase of eccentricity growth (the shaded, blue region), which is indicative of secular resonant capture. During these dynamics, $\dot{\varpi}_1 \approx \dot{\varpi}_2$. Bottom panel: Illustration of ultimate cause of instability. The solid lines illustrate semi-major axis of the inner (red) and outer (blue) planets, whilst the dotted lines denote the apocenter (upper) and pericenter (lower) of the orbits. Secular resonance is broken as the orbits begin to cross (time ≈ 3.98 Myr), and instability ensues soon after (time ≈ 4.36 Myr).

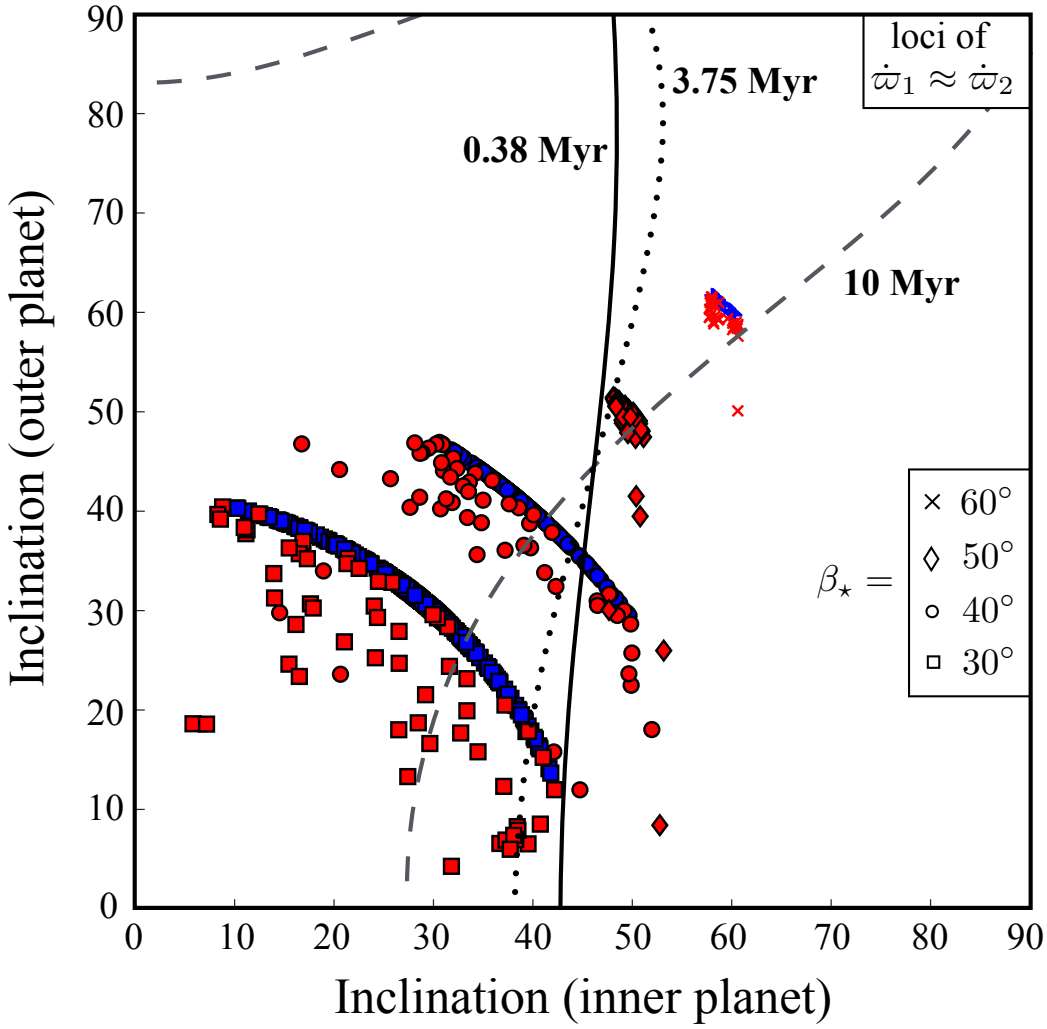

Figure 6.7: Evolution of the orbital inclinations of both planets compared to the locus of $\dot{\varpi}_1 - \dot{\varpi}_2 = 0$ as computed from equation 6.18. We plot 4 different cases corresponding to $\beta_\star = \{30°, 40°, 50°, 60°\}$ and $J_{2,0} = 10^{-2.6}$. In each case, blue corresponds to the evolution before instability, and red after wards (defined as having $e_1 > 0.01$). The solid, dotted and dashed lines denote $\dot{\varpi}_1 - \dot{\varpi}_2 = 0$ at times 0.38 Myr (the time of instability for $\beta_\star = 60°$), 3.75 Myr (instability time for $\beta_\star = 40°$) and a long-time example of 10 Myr included to illustrate that when the stellar quadrupole is removed, resonance may still be encountered if the planetary inclinations are excited sufficiently.

ACKNOWLEDGMENTS

This research is based in part upon work supported by NSF grant AST 1517936 and the NESSF Graduate Fellowship in Earth and Planetary Sciences (C.S). We thank Erik Petigura, Josh Winn, and Greg Laughlin for insightful conversations.

Chapter 7

A SECULAR RESONANT ORIGIN FOR THE LONELINESS OF HOT JUPITERS

ABSTRACT

Despite decades of inquiry, the origin of giant planets residing within a few tenths of an astronomical unit from their host stars remains unclear. Traditionally, these objects are thought to have formed further out before subsequently migrating inwards. However, the necessity of migration has been recently called into question with the emergence of in-situ formation models of close-in giant planets. Observational characterization of the transiting sub-sample of close-in giants has revealed that "warm" Jupiters, possessing orbital periods longer than roughly 10 days more often possess close-in, co-transiting planetary companions than shorter period "hot" Jupiters, that are usually lonely. This finding has previously been interpreted as evidence that smooth, early migration or in situ formation gave rise to warm Jupiter-hosting systems, whereas more violent, post-disk migration pathways sculpted hot Jupiter-hosting systems. In this work, we demonstrate that both classes of planet may arise via early migration or in-situ conglomeration, but that the enhanced loneliness of hot Jupiters arises due to a secular resonant interaction with the stellar quadrupole moment. Such an interaction tilts the orbits of exterior, lower mass planets, removing them from transit surveys where the hot Jupiter is detected. Warm Jupiter-hosting systems, in contrast, retain their coplanarity due to the weaker influence of the host star's quadrupolar potential relative to planet-disk interactions. In this way, hot Jupiters and warm Jupiters are placed within a unified theoretical framework that may be readily validated or falsified using data from upcoming missions such as *TESS*.

7.1 Introduction

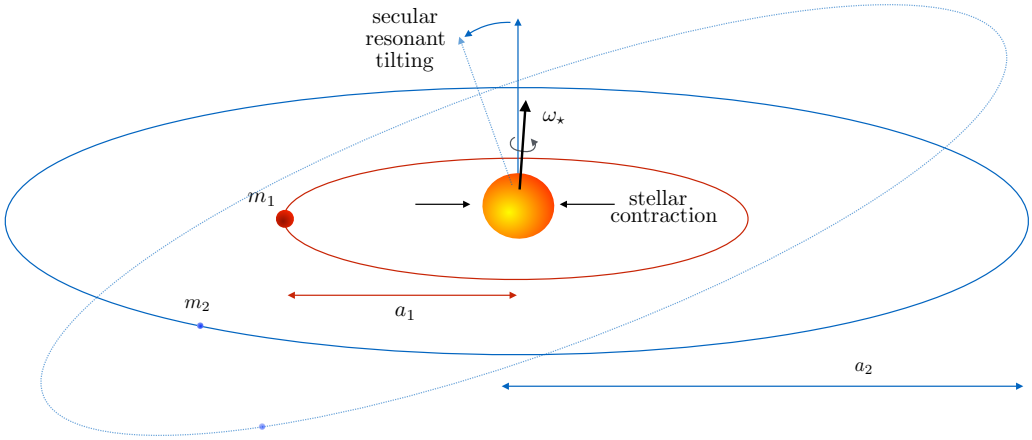

Figure 7.1: A schematic of the set up considered in the text. A giant planet with mass m_2 follows a circular orbit with semi-major axis a_1. Exterior, lies a lower-mass planet m_2 on circular orbit with semi-major axis a_2. The exterior orbit is forced to undergo nodal regression due to a combination of stellar quadrupolar potential and secular perturbations from the inner giant planet's orbit. The giant's orbit, in turn, is regressing mostly owing to secular perturbations form the stellar oblateness. Initially, the inner planet regresses faster but as the stellar quadrupole decays (as a result of physical contraction), a commensurability is encountered in the two frequencies, leading to the secular resonant excitation of mutual inclinations between the planets.

Arguably the longest-standing problem in exoplanetary science concerns the origin and evolution of so-called "hot Jupiters" (Mayor and Queloz, 1995). Planets in this category are loosely defined as possessing masses comparable to Jupiter, but residing on orbits with periods shorter than about 10 days. Similarly to the giant planets in our solar system, these objects are thought to have formed through the "core-accretion" pathway (Stevenson, 1982; Pollack et al., 1996). Within this framework, a $\sim 10-15$ Earth mass solid core conglomerates whilst still embedded within the natal protoplanetary disk, accretes a comparable-mass envelope and subsequently initiates a period of runaway gas accretion, yielding a Jupiter-mass planet.

Traditionally, the in situ formation of hot Jupiters has been considered

impossible, owing to the difficulty in constructing sufficiently large cores within the hot inner regions of the protoplanetary nebula, where solid grains are relatively scarce (Lin, Bodenheimer, and Richardson, 1996; Rafikov, 2006). Consequently, the prevailing notion is that hot Jupiters formed further out, beyond the snow line, before subsequently migrating inwards. This migration can occur either during the disk-hosting stage (through so-called type II migration; Lin, Bodenheimer, and Richardson 1996; Kley and Nelson 2012) or later, via the excitation of large eccentricity followed by tidal circularization (Wu and Murray, 2003; Beaugé and Nesvorný, 2012). For brevity, we will group these migration mechanisms into two categories: "early" for when the hot Jupiters reach their close-in orbits before the disk disperses, and "late," referring to migration proceeding subsequent to disk-dispersal.

A separate sub-population of giant planets that is progressively becoming better characterized is the "warm Jupiter" class of close-in bodies (Steffen et al., 2012; Huang, Wu, and Triaud, 2016), which are defined, again loosely, as residing on orbits of period $\sim 10 - 30$ days. Like the hot Jupiters, these objects lie interior to the ice line, and therefore suffer from many of the same arguments against in situ formation as their hotter counterparts. However, a crucial difference is that warm Jupiters exhibit tidal circularization timescales that are typically too long to have migrated via a late pathway, particularly when no exterior giant companion is detected (Dong, Katz, and Socrates, 2013; Petrovich and Tremaine, 2016). Accordingly these giants appear to have attained their close-in orbits prior to disk dispersal.

Within published literature, the distinction between "warm" and "hot" has been somewhat arbitrary. However, the recent study of Huang, Wu, and Triaud (2016), along with some earlier investigations (Steffen

et al., 2012), have pointed out an empirical distinction between the transiting subsample of the two populations. Specifically, the fraction of warm Jupiters possessing close-in (i.e., periods < 50 days), co-transiting companions is roughly 50%, in contrast to the hot Jupiters, where the analogous fraction is close to 0%, with only one counter-example, WASP-47b currently known (Becker, Vanderburg, et al., 2015; Weiss et al., 2017). This pattern has been interpreted as evidence in support of a high-eccentricity origin for hot Jupiters, with close-in companions being cast out during the migration. In contrast, warm Jupiters were interpreted to arise from smooth migration within a natal disk, where WASP-47b constitutes the innermost tail of this population.

Recent work has begun to question the necessity of migration for the formation of close-in giant planets (Boley, Contreras, and Gladman, 2016; Batygin, Bodenheimer, and Laughlin, 2016). In particular, Batygin, Bodenheimer, and Laughlin (2016) considered the long-term dynamical evolution of a close-in giant planet forming in situ, with a super Earth residing on an exterior orbit. As the host star contracts, and as the giant planet grows, the outer planet transitions from a regime where its nodal regression rate is smaller than that of the giant's, to a regime where the two frequencies are approximately commensurate. This results in a convergent encounter with a secular resonance that tilts the orbit of the outer companion, potentially all the way to 90°. Moreover, if the giant planet's orbit is sufficiently eccentric ($e \gtrsim 0.05$) the outer orbit may instead have its eccentricity raised, by a similar secular resonance in terms of the precession of perihelia, leading to dynamical instability within the system. From the point of view of transit surveys, both outcomes will lead to a lonely close-in giant, except for fortunate viewing geometries.

A key limitation of the above picture, mentioned in Batygin, Bodenheimer, and Laughlin (2016), is that tidal interactions with the disk gas itself may induce nodal regression upon the outer planet's orbit that quenches the resonant tilting that would otherwise occur in the absence of a disk (Hahn, 2003). In other words, if the physical mechanism responsible for the onset of the secular resonance occurs whilst the disk is still around, the system may retain coplanarity, and the giant planet will co-transit with its close-in companions. For the purposes of this work, "in situ" formation is dynamically equivalent to "early" migration, because both processes lead to systems that are already close-in at the time of disk dissipation, and so we make no statements regarding which of the two scenarios is more likely.

The key finding of this paper is that the resonance is encountered later for closer-in systems. That is, hot Jupiter-hosting systems encounter the resonance later than warm Jupiter systems. Given fiducial disk lifetimes and stellar rotation periods (Haisch Jr, Lada, and Lada, 2001; Bouvier, 2013), we expect giant planets to become lonely when orbiting interior to ~ 0.1 AU (or, ≈ 11.6 days for a solar mass star, i.e., suggestively close to the warm Jupiter - hot Jupiter divide). At larger orbital radii, systems may still encounter the resonance, but will do so whilst embedded in the disk gas, which can therefore prevent inclination excitation.

In brief, we show that hot Jupiters will become lonely in transit surveys, not because they formed differently from warm Jupiters, but because they encountered the aforementioned resonance after their disk dissipated, when nothing prevented their outer companions from being driven to high inclinations.

7.2 Analytical Theory

To set up the problem, suppose a giant planet, of mass m_1 orbits at a semi-major axis a_1 interior to a less massive planet, say, a super Earth of mass m_2 at semi-major axis a_2 (Figure 7.1). Young stars possess large radii $R_\star$ and rotate rapidly (Shu, Adams, and Lizano, 1987; Bouvier, 2013), leading to significant oblateness. This oblateness, parameterized via the second gravitational moment J_2, leads to precession of the argument of perihelion ϖ and regression of the longitudes of ascending node Ω of the planetary orbits.

The protoplanetary disk is expected to damp inclinations and eccentricities to small values (Kley and Nelson, 2012), allowing the gravitational disturbing potential influencing the planets to be expanded to second order in eccentricities and inclinations (or 4th order near secular resonances (Batygin, Bodenheimer, and Laughlin, 2016)). At such an order, the inclination and eccentricity degrees of freedom are decoupled and therefore may be treated in isolation. In this work, we assume the orbits to be circular, such that Ω and inclination i together constitute the only degree of freedom. Alternatively one may assume the orbits are coplanar, but instead consider the eccentricity degree of freedom in isolation. The logic and numerical coefficients are very similar in both cases, so we do not work through both, but include a brief discussion of eccentricity dynamics in Section 3.1.

Stellar Evolution

For a circular orbit with semi-major axis a_p and mean motion n_p, the stellar-induced nodal regression rate is given by (Murray and Dermott, 1999)

$$\dot{\Omega}_\mathrm{p} \equiv \nu_{\star,\mathrm{p}} = \frac{3}{2} n_\mathrm{p} J_2 \left(\frac{R_\star}{a_\mathrm{p}} \right)^2, \tag{7.1}$$

where $p = \{1, 2\}$; see Figure 7.1. The aforementioned second gravitational moment, J_2 is related to the stellar spin angular velocity $\omega_\star$ and Love number (twice the apsidal motion constant) k_2 through the relation (Sterne, 1939):

$$J_2 = \frac{1}{3}\left(\frac{\omega_\star}{\omega_b}\right)^2 k_2, \tag{7.2}$$

where ω_b is the break-up angular velocity of the star. The Love number can be extracted from polytropic stellar models with index $\chi = 3/2$ (i.e., fully convective; Chandrasekhar 1939), leading to $k_2 \approx 0.28$ (Batygin and Adams, 2013), which is the numerical value we adopt throughout. The spin periods of T Tauri stars may be constrained through observation (Bouvier, 2013) and in general lie within the range of $\sim 1 - 10$ days. Substituting expression (7.2) into Equation (7.1) yields,

$$\nu_{\star,\mathrm{p}} = n_\mathrm{p}\frac{k_2}{2}\left(\frac{\omega_\star}{n_\mathrm{p}}\right)^2\left(\frac{R_\star}{a_\mathrm{p}}\right)^5, \tag{7.3}$$

thereby casting the nodal regression rate in terms of quantities that are either directly observable or may be inferred from simple models.

With time, the central star will contract ($\dot{R}_\star < 0$) and so $\nu_{\star,\mathrm{p}}$ will decrease. Additional time-dependence may arise owing to stellar spin-down; however, owing to the high order of $R_\star$ in equation 7.3 we ignore any changes in $\omega_\star$ (as discussed below, the dynamics do not depend sensitively on the details, only that $\nu_{\star,\mathrm{p}}$ decreases).

To a good approximation, the contraction of a protostar may be modelled as Kelvin-Helmholtz contraction of a polytropic body (Batygin and Adams, 2013):

$$R_\star(t) = R_{\star,0}\left(1 + \frac{t}{\tau_\mathrm{c}}\right)^{-\frac{1}{3}}, \tag{7.4}$$

where we define the contraction timescale (1/3 of the Kelvin-Helmholtz timescale):

$$\tau_c \equiv \frac{GM_\star^2}{28\pi\sigma T_{\rm eff}^4 R_{\star,0}^3}. \tag{7.5}$$

In this expression, G is the gravitational constant, σ is the Steffan-Boltzmann constant and the stellar mass $M_\star$ is taken equal to 1 solar mass ($M_\odot$) throughout. The above analytic form agrees well with the numerical pre-main sequence evolution models of Siess, Dufour, and Forestini (2000) provided a value of $R_{\star,0} \gtrsim 6R_\odot$ is chosen[1] for a solar mass star with surface temperature $T_{\rm eff} = 4270\,{\rm K}$.

Capture into secular resonance

Planet-planet interactions will induce modal regression in addition to that arising from the stellar quadrupole. It can be shown through linear secular perturbation theory (Murray and Dermott, 1999; Morbidelli, 2002) that the time-averaged regression rate of the inner planet $< \nu_1 >$ takes the form

$$< \nu_1(t) > \approx \nu_{\star,1}(t) + \frac{1}{4}\frac{m_2}{M_\star}\left(\frac{a_1}{a_2}\right)^2 b_{3/2}^{(1)}\left(\frac{a_1}{a_2}\right) n_1, \tag{7.6}$$

where the first term results from the oblateness of the host star, which decays with time, and the second term arises owing to planet-planet interactions. Furthermore, we have introduced the function $b_{3/2}^{(1)}(a_1/a_2)$, known as a Laplace coefficient (Murray and Dermott, 1999), defined as

$$b_{3/2}^{(1)}(\alpha) \equiv \frac{1}{\pi}\int_0^{2\pi}\left[\frac{\cos(\psi)}{(1+\alpha^2-2\alpha\cos\psi)^{3/2}}\right]d\psi. \tag{7.7}$$

[1]The initial radius simply has to be large, rather than an exact value, because the star essentially loses information about initial conditions within the disk's lifetime.

Analogously, the time-averaged nodal regression rate of the outer planet is given by

$$< \nu_2(t) > \approx \nu_{\star,2}(t) + \frac{1}{4}\frac{m_1}{M_\star}\left(\frac{a_1}{a_2}\right) b^{(1)}_{3/2}\left(\frac{a_1}{a_2}\right) n_2. \tag{7.8}$$

We will assume that the semi-major axes and masses are fixed, reflecting the fact that most planet-building and migration occurs before the disk dissipates. Then, the ratio between stellar and planetary orbital angular momenta is given by

$$j \equiv \frac{I_\star M_\star R_\star^2 \omega_\star}{m_p \sqrt{G M_\star a_p}}, \tag{7.9}$$

where $I_\star \approx 0.21$ is the dimensionless moment of inertia, as calculated for a fully convective, polytropic star (Chandrasekhar, 1939). For nominal hot Jupiter parameters; a Jupiter-mass planet at 0.05 AU, orbiting a star with $R_\star \sim 2R_\odot$, spinning with a period of 3 days, we find that $j \gg 1$. As a result, we will consider the stellar spin axis to be fixed, a statement that the planetary orbits possess significantly less angular momentum than the star (Batygin, Bodenheimer, and Laughlin, 2016). We note that this approximation begins to break down as the star contracts, the stellar rotation period is long, or if the planet is situated further out, i.e., in the warm Jupiter regime. Whereas a full account of the star spin dynamics is not expected to affect our arguments with respect to planet-planet inclinations, numerous recent observational investigations (Li and Winn, 2016; Dai and Winn, 2017) are beginning to detect a trend whereby more distant transiting planets exhibit larger spin-orbit misalignments. While suggestive, we shall not explore this aspect of the problem further here.

The stellar quadrupole's influence upon the inner planet will be significantly larger than its effect upon the outer planet ($(\nu_{\star,1}/\nu_{\star,2}) =$

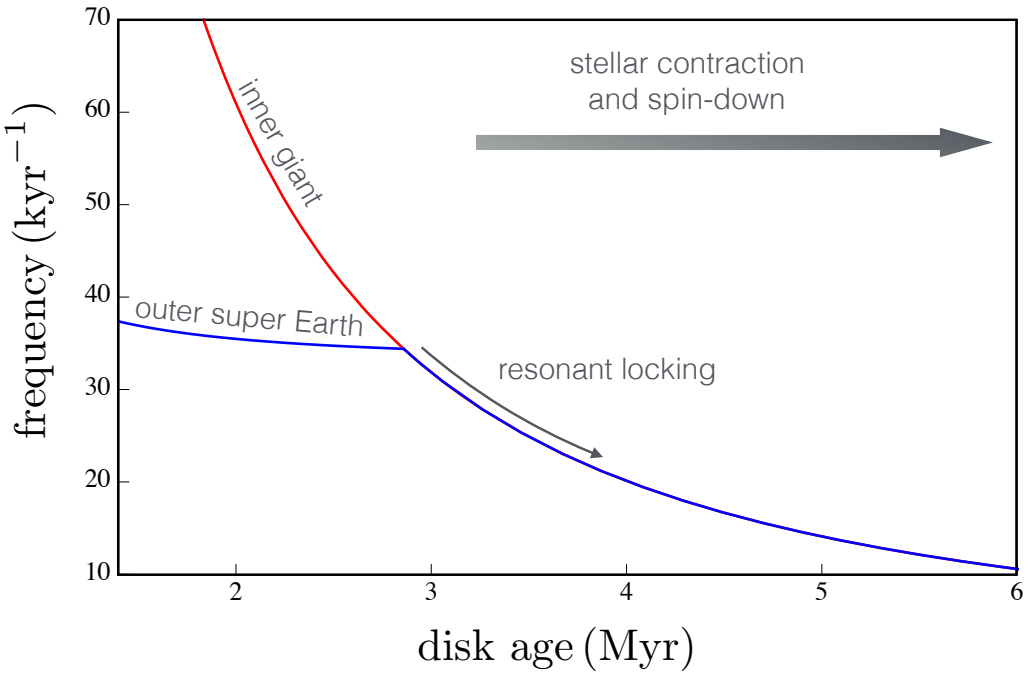

Figure 7.2: The time evolution of the nodal regression frequencies for both planets as the host star contracts. The requirement to turn a giant planet-super Earth system into an apparently lonely giant is that $\nu_2 < \nu_1$ (i.e., the red line is above the blue line) at the point when the disk dissipates, such that a point is crossed where the two frequencies are roughly commensurate. As argued in the text, this will always happen as the giant grows, but can be bypassed due to planet-disk interactions. If this is the picture dominating the hot Jupiter-warm Jupiter distribution, we would expect to see more hot Jupiters with companions around faster-rotating, massive stars and a gradual drop in companion fraction toward smaller semi-major axes. Parameters used in this illustrative figure are $m_1/M_\star = 10^{-3}$, $m_2/M_\star = 10^{-5}$, $a_1 = 0.04$ AU, $a_2 = 0.1$ AU, $P_\star = 3$ days around a solar mass star. Resonance is encountered at $t = 2.86$ Myr.

$(a_2/a_1)^{7/2} \gg 1$). Consequently, as the star contracts, the inner planet's nodal regression frequency will decrease more rapidly than that of the outer planet's. For nominal parameters, the initial state has $\nu_1 > \nu_2$, but at a later stage the star has contracted to the point where the two frequencies become similar (Figure 7.2). As discussed in more detail in Batygin, Bodenheimer, and Laughlin (2016), the result of such a commensurability in frequencies is capture into a secular resonance and excitation of inclination within the outer companion's orbit. Ac-

cordingly, if the giant was detected through transit it would appear "lonely" except under a fortuitous viewing geometry.

Influence of the disk

The above discussion showed how close-in giants may become lonely, but made little distinction between "hot" and "warm" Jupiter-hosting systems. In this section, we show that considering gravitational interactions between the planets and their natal disk naturally leads to closer-in systems experiencing resonant excitation of inclinations more often than more distant systems, thereby accounting for the increased loneliness of hot vs warm Jupiters.

Determining the detailed dynamics of planets embedded within gaseous disks constitutes an active field of research on its own (Kley and Nelson, 2012). Here we will concern ourselves with a simplified yet instructive description of the dynamics, involving two qualitatively separate processes. Specifically, planet-disk interactions tend to damp the eccentricities and inclinations of embedded planets (Tanaka and Ward, 2004), together with inducing precession in the planetary arguments of perihelion and regression of the longitudes of ascending node (Hahn, 2003).

We will show below that the most important effect for our purposes is the disk-induced regression of the node. Tidal disk-planet interactions are expected to damp the outer planet's orbital inclination over a timescale given approximately by (Tanaka and Ward, 2004)

$$\tau_{\rm inc} \equiv \left| \frac{di_2}{dt} \frac{1}{i_2} \right|^{-1} \approx \zeta \frac{P_2}{2\pi} \left(\frac{M_\star}{m_2} \right) \left(\frac{M_\star}{\Sigma_2 a_2^2} \right) \beta^4, \tag{7.10}$$

where $\beta \equiv h/a_2 \approx 0.05$ is the disk's aspect ratio, Σ_2 is the disk's surface density at a_2, the numerical constant $\zeta \approx 2$, and P_2 is the outer planet's orbital period.

In order to determine whether the disk's inclination damping will inhibit the adiabatic growth of inclination described above, we intro-

duce the libration timescale for the resonant argument $\Omega_1 - \Omega_2$ within resonance (Morbidelli, 2002; Batygin, Bodenheimer, and Laughlin, 2016)

$$P_{\rm lib} \approx \frac{P_2}{2\pi}\frac{2}{3s_1}\left(\frac{M_\star}{m_1}\right)\left(\frac{a_2}{a_1}\right)^2, \tag{7.11}$$

where $s_1 \equiv \sin(i_1/2)$, with i_1 being the inclination of the inner planet's orbit with respect to the stellar spin axis. The secular resonant inclination excitation will be prevented if the adiabatic limit is broken (Henrard, 1993), i.e.,

$$\tau_{\rm inc} \lesssim P_{\rm lib}. \tag{7.12}$$

If we suppose the disk to follow a minimum mass solar nebula profile (Hayashi, 1981) of $\Sigma(a) \approx 2000(a/1{\rm au})^{-3/2}{\rm g\,cm^{-2}}$, $a_2 \approx 0.2\,{\rm AU}$, $a_1 = 0.1\,{\rm AU}$, $m_2 = 10^{-5}\,M_\odot$ and $m_1 = 10^{-3}\,M_\odot$ the disk will damp inclination growth provided $s_1 \lesssim 0.2$, or $i_1 \lesssim 20°$. Accordingly, disk-induced inclination damping may prevent the secular resonance from driving inclination growth for systems aligned with their natal disk. However, owing to the uncertainties in both the calculation of damping timescales and the order-of-magnitude nature of inequality 7.12, it is difficult to determine whether resonant growth is prevented in all cases.

Given the uncertainties in computing the importance of direct disk-driven inclination-damping, let us now consider an additional mechanism by which the disk may prevent resonant growth of inclination; the regression of nodes induced by the disk's gravitational potential. It may be shown that the disk's quadrupole induces a regression rate of (Hahn, 2003)

$$\nu_{pd} \approx n_p \frac{\pi\Sigma_p a_p^2}{M_\star \beta}, \tag{7.13}$$

and the modal regression occurs in the same direction as that induced by the stellar quadrupole and planet-planet interactions. If one assumes a surface density profile of the MMSN, $\Sigma_p \propto a_p^{-3/2}$ (Hayashi, 1981) the disk-induced modal regression frequency $\nu_{pd} \propto a_p^{-1}$, such that more distant planets experience a slower rate arising from the disk's quadrupole.

In the interest of simplicity, and for illustrative purposes, we only include the disk's effect upon the outer, smaller planet. Ultimately our arguments are not particularly sensitive to this decision. However, giant planets are expected to open gaps in the disk (Crida, Morbidelli, and Masset, 2006), and the MRI-active inner region of the nebula is expected to possess a lower gas density (Armitage, 2011). Both of these effects are likely to significantly diminish the disk's secular influence upon the inner giant's orbit. Including the disk-induced nodal regression to $< \nu_2(t) >$ given above yields

$$\left\langle \left(\nu_2(t)/n_2 \right\rangle \right) \approx \frac{3}{2} J_2 \left(\frac{R_\star}{a_2} \right)^2 + \frac{1}{4} \frac{m_1}{M_\star} \left(\frac{a_1}{a_2} \right) b_{3/2}^{(1)} \left(\frac{a_1}{a_2} \right) + \frac{\pi \Sigma_2 a_2^2}{\beta M_\star}. \tag{7.14}$$

In order to determine the importance of disk-induced nodal regression, we must formulate the evolution of the disk's mass and surface density. Observational constraints upon disk masses remain challenging, and intrinsic variation between the evolution of individual disks makes a single, generalized parameterisation impossible. For our purposes, it suffices to use an average disk mass evolution. The observed decay of disk accretion rates with time (Calvet et al., 2005) is well approximated by the following parameterization

$$M_{\rm disk}(t) = \frac{M_{\rm disk,0}}{1 + t/\tau_v}, \tag{7.15}$$

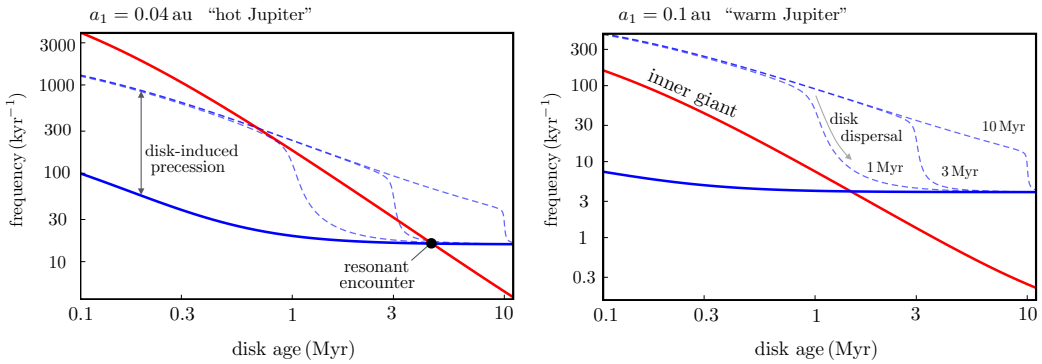

Figure 7.3: An illustration of the influence of the disk's quadrupole. The solid blue line represents the outer planet's nodal regression in the case with no disk, whereas the three dashed lines represent the case where the disk's quadrupole moment is included. When the outer planet is forced to regress faster than the giant (red line) throughout the entire disk lifetime, the secular resonant encounter described in the text is prevented. The left panel considers a hot Jupiter, at 0.04 AU interior to a test particle at 0.12 au. The right panel depicts the case for a Warm Jupiter at 0.1 AU with an exterior test particle at 0.3 au. The closer, hot Jupiter system encounters the secular resonance later (black circle) and so the disk is more likely to have dispersed, whereas the warm Jupiter system entirely bypasses the secular resonance even for very short disk lifetimes (e.g., 1 Myr).

where the viscous decay time $\tau_\nu = 0.5\,\mathrm{Myr}$ and the initial disk mass $M_{\mathrm{disk},0} = 0.05\mathrm{M}_\odot$. We may sanity-check this result by writing the surface density profile as

$$\Sigma(a,t) = \Sigma_0(t)\left(\frac{a}{a_0}\right)^{-3/2} \tag{7.16}$$

yielding the disk mass

$$M_{\mathrm{disk}}(t) = 4\pi\Sigma_0(t=0)a_{\mathrm{out}}^{1/2}a_0^{3/2}. \tag{7.17}$$

In order to achieve $M_{\mathrm{disk},0} = 0.05\,M_\odot$ the disk must begin with a surface density at 1 AU of $\Sigma_0(t=0) \approx 6500\,\mathrm{g\,cm^{-2}}$, which is similar to the "minimum-mass extrasolar nebula" inferred by requiring the observed populations of close-in super Earths formed close to their current locations (Chiang and Laughlin, 2013). Accordingly, prescription (7.15) constitutes a reasonable approximation to the disk's global evolution.

Viscous evolution alone is notoriously unable to match observational deductions regarding disk dispersal timescales. Rather, the current consensus is that, after $\sim 1 - 10$ Myr of viscous evolution, the disk disperses over a short ($\Delta t \lesssim 10^5$ years) timescale (Alexander et al., 2014), beginning with the inner few au. To account for the two-timescale nature of disk evolution we parameterize the surface density as

$$\Sigma_0(t) = \frac{\Sigma_0|_{t=0}}{1 + t/\tau_v}\left[\frac{1}{2} - \frac{1}{\pi}\arctan\left(\frac{t - \tau_d}{\Delta t}\right)\right], \tag{7.18}$$

where τ_d is the time of disk dispersal, ranging from $\sim 1 - 10$ Myr.

In the disk-free case (Figure 7.2) $< \nu_2 >$ is always greater than $< \nu_1 >$ initially. However, the influence of the disk upon the outer planet increases its regression frequency above that of the inner giant when the system is relatively far from the central star. To illustrate this effect, we present the evolution of $< \nu_1 >$ and $< \nu_2 >$ for two systems (Figure 7.3). The first is a hot Jupiter, orbiting at $a_1 = 0.04$ AU interior to a companion at $a_2 = 0.12$ au. In this scenario, the disk quadrupole is not sufficient to take the outer planet's regression rate above the giant's and so the resonant criterion is met at a disk age under 1 Myr.

If the the giant planet has already formed at this early stage, secular resonant excitation will proceed. However, if the giant is not yet formed, the system has a second chance to encounter resonance, after the disk disperses. When the disk dispersal time is $\tau_d = 1$ Myr or $\tau_d = 3$ Myr, the system encounters secular resonance as it would have in the absence of a disk (Figure 7.2). Owing to the strong influence of the central star's quadrupole, only very long-lived disks will disperse after the system can subsequently encounter secular resonance (e.g., 10 Myr in this case) and so in most cases, this hot Jupiter will end up appearing lonely in transit surveys.

The second case presented would generally be described as possessing a "warm Jupiter" at 0.1 AU and an exterior companion at 0.3 au. In this case, the influence of the disk overcomes the nodal regression induced by the more distant central star's oblateness. Accordingly, the resonance is quenched and inclination excitation does not occur. If, for example, the disk had dissipated already by $\sim$ 1 Myr, this system would undergo resonant capture and become a lonely warm Jupiter system. More typical disk lifetimes (Haisch Jr, Lada, and Lada, 2001) tend to prevent secular resonant tilting when the giant planet lies beyond $\sim$ 0.1 AU - which is close to the oft-quoted dividing line between what is considered a "warm" or a "hot" Jupiter.

Criterion for Loneliness

The above discussion shows that when the disk is still present, it is likely to quench the secular resonant dynamics, especially in more distant systems. Consequently, the criterion for whether a giant planet will resonantly excite the inclination of its outer companion is simply that *the inner planet is regressing faster than the outer planet at the time of disk dissipation*:

$$\boxed{\nu_1\big|_{t=\tau_{\rm d}} > \nu_2\big|_{t=\tau_{\rm d}}}. \tag{7.19}$$

By substituting expressions (7.3, 7.4, 7.6 and 7.8) into the above inequality, we may reformulate the criterion in terms of a critical stellar spin period at the time of disk dissipation $P_\star\big|_{t=\tau_{\rm d}}$ below which inclination is excited. After some algebra, we arrive at the criterion

for tilting to occur and the generation of a lonely giant planet:

$$P_\star\big|_{t=\tau_\mathrm{d}} \lesssim P_1\sqrt{2k_2}\left(\frac{M_\star}{m_1}\right)^{1/2}\left(\frac{R_\star(\tau_\mathrm{d})}{a_1}\right)^{5/2} \times\left[\frac{1-\alpha^{7/2}}{\alpha^{5/2}b^{(1)}_{3/2}(\alpha)}\right]^{1/2}\left(1-\frac{\Lambda_2}{\Lambda_1}\right)^{-1/2}, \tag{7.20}$$

where P_1 is the inner planet's orbital period, $\alpha \equiv a_1/a_2$ and $\Lambda_\mathrm{p} \equiv m_\mathrm{p}\sqrt{GM_\star a_\mathrm{p}}$.

It is worth noting that the above criterion was derived within the secular regime, and so assumes that the two planets are not caught in first or second order mean-motion resonances. Terms associated with these resonances enter the disturbing potential at first and second order respectively in eccentricity, potentially swamping the second order secular dynamics considered here (Murray and Dermott, 1999). Accordingly, if our criterion is to be applied to close-in giant planet systems with observed exterior companions, care must be taken to check whether the resonant arguments appropriate to first or second order mean motion resonances are librating or circulating. In general, for nearly circular orbits, this is equivalent to requiring that the period ratios lay more than a few per cent from exact commensurability, though precise libration widths depend upon the resonance considered and the eccentricity.

7.3 Results & Discussion

The criterion (7.20) is represented in Figure 7.4 by way of 3 plots, corresponding to 3 nominal times of disk dissipation, $\tau_\mathrm{d} = \{1\,\mathrm{Myr},\ 3\,\mathrm{Myr},\ 10\,\mathrm{Myr}\}$. Using the above prescription for stellar contraction (equation 7.4), these times correspond to stellar radii $R_\star(\tau_\mathrm{d}) = \{2.4\,R_\odot,\ 1.7\,R_\odot,\ 1.1\,R_\odot\}$. Within each plot, we display lines representing 3 stellar spin periods $P\big|_{t=\tau_\mathrm{d}} = \{10\,\mathrm{days},\ 3\,\mathrm{days},\ 1\,\mathrm{day}\}$, spanning the observed range of T

Tauri spin periods (Bouvier, 2013), with $m_1 = 10^{-3} M_\odot$, $m_2 = 10^{-5} M_\odot$ and $M_\star = M_\odot$. For the relevant spin period and τ_d, an outer planet with a_2 above the line is expected to encounter resonance and become misaligned. The region where coplanarity is expected to be maintained even for a relatively fast 1 day stellar rotation period is shaded.

The key message of Figure 7.4 is that there is significantly more semi-major axis space available for close, outer companions to Jupiters residing beyond ~ 0.1 AU than hotter Jupiters. Therefore, the loneliness of closer-in giants may naturally arise owing to the greater tendency for their outer companions to become resonantly inclined and taken out of transit surveys.

Superimposed on Figure 7.4, we have placed points representing the four cases in Huang, Wu, and Triaud (2016) where a giant planet lies interior to a close companion. All four lie within the shaded region, consistent with our hypothesis. The hot Jupiter system WASP-47 might have misaligned WASP-47d if its disk dissipated early (~ 1 Myr) and the star was particularly rapidly-rotating (~ 1 day; see top panel). As more examples are detected, we expect the shaded region to become filled in to a significantly greater extent than the regions between the 1 and 10 day lines.

The Hot Jupiter - Warm Jupiter Distinction

Despite the somewhat arbitrary distinction between a "hot" versus a "warm" Jupiter, the dearth of close-in companions to hot Jupiters has been taken as evidence that there is a physical distinction between the formation pathway of each planetary regime (Steffen et al., 2012; Huang, Wu, and Triaud, 2016). In this paper, we have shown that separate formation pathways are not required to explain the loneliness of hot Jupiters. Simply by forming closer to their host stars, these

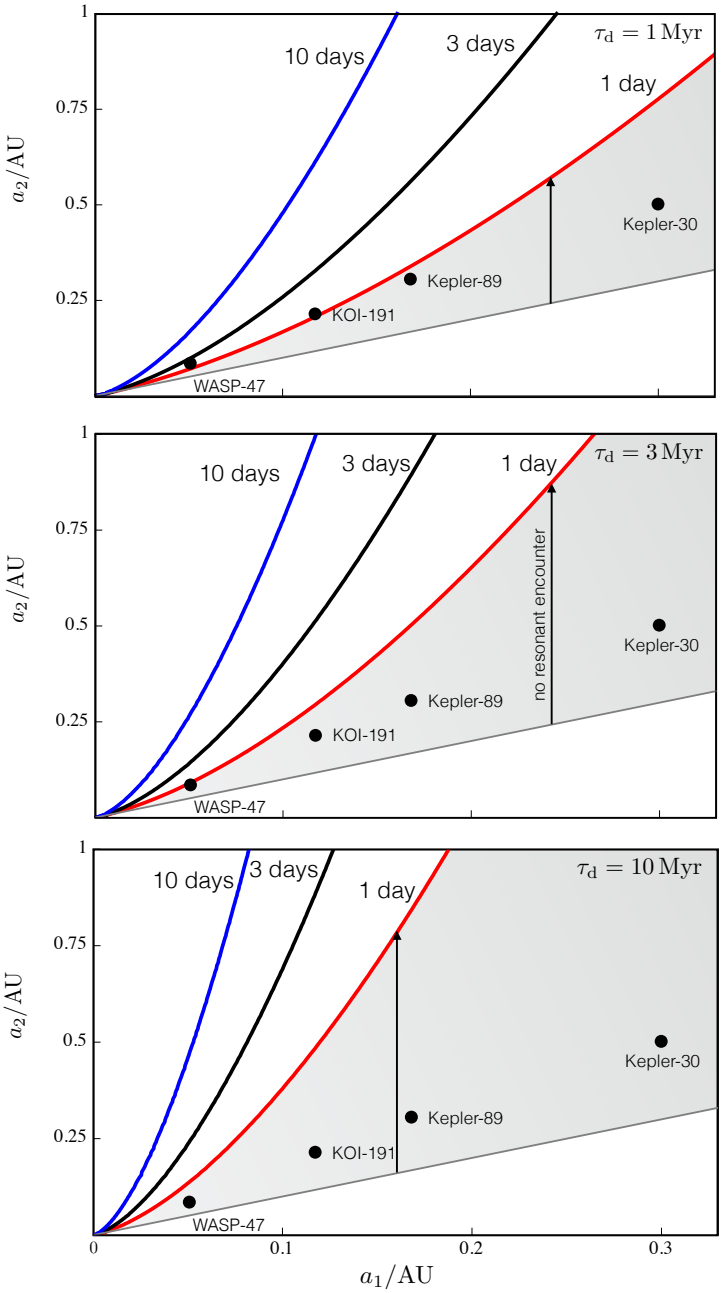

Figure 7.4: Loci of systems expected to undergo resonant excitation of inclination before disk dissipation at 1 Myr (top panel), 3 Myr (middle panel) and 10 Myr (bottom panel). Outer companions within the shaded region will not encounter the resonance and will remain coplanar with the inner giant. We have plotted the configuration of the four systems known where a giant lies interior to a lower-mass planet. All four lie within the region where coplanarity is expected to persist around a well-aligned star. Interestingly, the innermost example, WASP-47, lies almost exactly on the boundary, consistent with it being the closest-in known example and only hot Jupiter with a close outer companion.

systems were more susceptible to perturbations from the host star's quadrupole moment, facilitating a secular resonance that tilted their outer companions.

Our proposed mechanism is directly falsifiable in that we would not expect to find transiting outer companions above the upper-most line in Figure (7.4), though too large of an a_2 will eventually break our assumption that the star possesses most of the system's angular momentum, altering the criteria derived above somewhat. Additionally, owing to uncertainties in disk lifetime and T Tauri spin rates, finding a transiting outer companion between the 3 day and 10 day lines is not necessarily a falsification – one can simply suppose the young star was rotating rapidly, or the disk was late to dissipate. Consequently, predictions may be falsified most readily in a statistical sense.

In the framework of our model, fewer outer companions should be found to transit outside the shaded region in Figure (7.4) than in the shaded region, even after correcting for observational biases. The semi-major axis distribution within the shaded region is expected to resemble those of lower-mass *Kepler* systems (Tremaine and Dong, 2012; Morton, Bryson, et al., 2016). Having only four examples makes it difficult to rigorously evaluate these hypothesis currently.

We should note that it is possible to view mutually inclined orbits via transit if their lines of nodes are fortunately commensurate with the line of sight. Consequently, if all hot Jupiters possess inclined companions, we would expect to see a small fraction of those companions in transit surveys (Steffen et al., 2012). The lack of such detections suggests that any close companions to hot Jupiters are not simply misaligned, but lost from the system entirely.

We propose two potential mechanisms whereby the dynamics de-

scribed here will not simply misalign, but remove close companions to hot Jupiters. First, lower-mass *Kepler* systems often exhibit high multiplicity (Fabrycky, Lissauer, et al., 2014), as opposed to the simple 2-planet system described here. It has been previously demonstrated (Spalding and Batygin, 2016) that misaligning one or more components of such closely-packed systems has the potential to destabilize the entire architecture. Furthermore, any additional planets within the system introduce extra secular modes and potential resonances that the system sequentially encounters as the central star contracts.

A second mechanism for complete loss of companions arises if the giant planet's orbit possesses an eccentricity higher than $e_1 \sim 0.05$. Here, an additional secular resonance becomes applicable whereby the outer orbit has its eccentricity, as opposed to its inclination, raised. This process will eject the outer planet from the system by way of a lowering of its pericenter until the orbits cross (Batygin, Bodenheimer, and Laughlin, 2016). As alluded to in Section 2, the quantitative criteria for encountering this eccentricity resonance are similar to those of the inclination resonance (Murray and Dermott, 1999), but disks are generally expected to damp planetary eccentricities to a point where the inclination resonance should dominate (Kley and Nelson, 2012; Batygin, Bodenheimer, and Laughlin, 2016). However, many warm Jupiters are known to be eccentric (Dong, Katz, and Socrates, 2013), potentially forced by exterior giant companions (Bryan et al., 2016), hinting that super Earths may occasionally be lost through the eccentricity resonance. Cumulatively, more work is needed to elucidate how often companions are expected to be tilted versus lost entirely.

Inner Companions

This work has focused on the tilting of outer companions to giant planets, and has talked little of inner companions. By inspection of equation (7.20), one can see that the secular resonance cannot be encountered if the inner planet has less angular momentum then the outer planet ($\Lambda_1 < \Lambda_2$). Accordingly, the resonant misalignment mechanism proposed here is not capable of explaining the absence of inner companions to hot Jupiters versus warm Jupiters (Huang, Wu, and Triaud, 2016). However, the only known inner companion to a hot Jupiter, WASP-47e, resides at the particularly close-in distance of 0.017 au, not much larger than the radius of the young star itself ($0.017\,\text{au} \approx 3.6 R_\odot$). Whereas we have not identified a specific mechanism that removes inner companions, their rarity may simply arising owing to limited physical space within a hot Jupiter's orbit. We expect that more interior companions will be found by the *TESS* mission (Ricker et al., 2015), however, they are likely to be rare.

7.4 Summary

The existence of giant planets inside the snowline has traditionally favoured an explanation whereby the planet itself, or at least its multiple Earth mass core, forms at large radii before subsequently migrating inwards. This migration can occur early, during the disk-hosting stage (Kley and Nelson, 2012), or long after, through a high-eccentricity pathway (Wu and Murray, 2003; Beaugé and Nesvorný, 2012). Between the two formation channels, the high-eccentricity pathway encounters more theoretical challenges in forming warm Jupiters (Dong, Katz, and Socrates, 2013), and empirical challenges in forming hot Jupiters (Dawson, Murray-Clay, and Johnson, 2014).

With a single exception, hot Jupiters are found to possess no close-in

transiting companions, in contrast to their slightly cooler counterparts, the warm Jupiters, roughly half of which are found with co-transiting close companions (Steffen et al., 2012; Becker, Vanderburg, et al., 2015; Huang, Wu, and Triaud, 2016). This evidence appears consistent with a high-eccentricity origin for hot Jupiters and an early, possibly in situ, origin for warm Jupiters. Interestingly, around 50% of Super Earth systems are thought to be significantly inclined (Johansen et al., 2012), possibly also owing to mutual inclinations induced by the host star (Spalding and Batygin, 2016).

Systems of super Earths are generally thought to form through early migration or in situ (Lee and Chiang, 2016), much like warm Jupiter systems. Thus, in the picture of high-eccentricity migration, hot Jupiters are exceptional – the lone class of planets who swung in from the outer regions of the planetary system long after the dispersal of the protoplanetary disk. In this paper, we have demonstrated that by taking account of the stellar quadrupole moment, hot Jupiters and warm Jupiters may have formed through identical pathways. However, the hot Jupiters, precisely because of their close-in configuration, encounter a secular resonance after the dispersal of their natal disk, and tilt their outer companions' orbits beyond the reach of transit surveys.

The relative unimportance of the Sun to the solar system planets' orbits has caused many to ignore stellar non-sphericity in exoplanetary systems. In contrast, the results of this paper, and of related works (Batygin, Bodenheimer, and Laughlin 2016; Spalding and Batygin 2016), illustrate the key role of the stellar oblateness to the long-term dynamical evolution, and eventual architecture, of compact exoplanetary systems.

BIBLIOGRAPHY

Adams, Fred C (2010). "The birth environment of the Solar System". In: *Annual Review of Astronomy and Astrophysics* 48, pp. 47–85.

Adams, Fred C and Marco Fatuzzo (1996). "A Theory of the Initial Mass Function for Star Formation in Molecular Clouds". In: *The Astrophysical Journal* 464, p. 256.

Affer, Laura et al. (2013). "Rotation in NGC 2264: a study based on CoRoT? photometric observations". In: *Monthly Notices of the Royal Astronomical Society* 430.2, pp. 1433–1446.

Agapitou, Vasso and John CB Papaloizou (2000). "Accretion disc-stellar magnetosphere interaction: field line inflation and the effect on the spin-down torque". In: *Monthly Notices of the Royal Astronomical Society* 317.2, pp. 273–288.

Agol, Eric et al. (2005). "On detecting terrestrial planets with timing of giant planet transits". In: *Monthly Notices of the Royal Astronomical Society* 359.2, pp. 567–579.

Albrecht, Simon et al. (2012). "Obliquities of hot Jupiter host stars: Evidence for tidal interactions and primordial misalignments". In: *The Astrophysical Journal* 757.1, p. 18.

Alecian, E et al. (2012). "A high-resolution spectropolarimetric survey of Herbig Ae/Be stars–I. Observations and measurements?" In: *Monthly Notices of the Royal Astronomical Society* 429.2, pp. 1001–1026.

Alexander, R et al. (2014). "Protostars and Planets VI ed H". In: *Beuther et al*.

Anderson, Kassandra R, Fred C Adams, and Nuria Calvet (2013). "Viscous Evolution and Photoevaporation of Circumstellar Disks Due to External Far Ultraviolet Radiation Fields". In: *The Astrophysical Journal* 774.1, p. 9.

Andrews, Sean M, David J Wilner, Catherine Espaillat, et al. (2011). "Resolved images of large cavities in protoplanetary transition disks". In: *The Astrophysical Journal* 732.1, p. 42.

Andrews, Sean M, DJ Wilner, AM Hughes, et al. (2009). "Protoplanetary disk structures in Ophiuchus". In: *The Astrophysical Journal* 700.2, p. 1502.

Armitage, Philip J (2010). *Astrophysics of planet formation*. Cambridge University Press.

– (2011). "Dynamics of protoplanetary disks". In: *Annual Review of Astronomy and Astrophysics* 49, pp. 195–236.

Armitage, PJ and CJ Clarke (1996). "Magnetic braking of T Tauri stars". In: *Monthly Notices of the Royal Astronomical Society* 280.2, pp. 458–468.

Ballard, Sarah and John Asher Johnson (2016). "The Kepler dichotomy among the M dwarfs: half of systems contain five or more coplanar planets". In: *The Astrophysical Journal* 816.2, p. 66.

Batalha, Natalie M et al. (2013). "Planetary candidates observed by Kepler. III. Analysis of the first 16 months of data". In: *The Astrophysical Journal Supplement Series* 204.2, p. 24.

Bate, MR, G Lodato, and JE Pringle (2010). "Chaotic star formation and the alignment of stellar rotation with disc and planetary orbital axes". In: *Monthly Notices of the Royal Astronomical Society* 401.3, pp. 1505–1513.

Batygin, Konstantin (2012). "A primordial origin for misalignments between stellar spin axes and planetary orbits". In: *Nature* 491.7424, pp. 418–420.

Batygin, Konstantin and Fred C Adams (2013). "Magnetic and gravitational disk-star interactions: An interdependence of PMS stellar rotation rates and spin-orbit misalignments". In: *The Astrophysical Journal* 778.2, p. 169.

Batygin, Konstantin, Peter H Bodenheimer, and Gregory P Laughlin (2016). "In Situ Formation and Dynamical Evolution of Hot Jupiter Systems". In: *The Astrophysical Journal* 829.2, p. 114.

Batygin, Konstantin and Alessandro Morbidelli (2011). "Onset of secular chaos in planetary systems: period doubling and strange attractors". In: *Celestial Mechanics and Dynamical Astronomy* 111.1, pp. 219–233.

– (2013). "Analytical treatment of planetary resonances". In: *Astronomy & Astrophysics* 556, A28.

Batygin, Konstantin, Alessandro Morbidelli, and Matthew J Holman (2015). "Chaotic disintegration of the inner solar system". In: *The Astrophysical Journal* 799.2, p. 120.

Batygin, Konstantin, Alessandro Morbidelli, and Kleomenis Tsiganis (2011). "Formation and evolution of planetary systems in presence of highly inclined stellar perturbers". In: *Astronomy & Astrophysics* 533, A7.

Beaugé, C and D Nesvorný (2012). "Multiple-planet scattering and the origin of hot Jupiters". In: *The Astrophysical Journal* 751.2, p. 119.

Beck, JG and P Giles (2005). "Helioseismic determination of the solar rotation axis". In: *The Astrophysical Journal Letters* 621.2, p. L153.

Becker, Juliette C and Fred C Adams (2015). "Oscillations of relative inclination angles in compact extrasolar planetary systems". In: *Monthly Notices of the Royal Astronomical Society* 455.3, pp. 2980–2993.

Becker, Juliette C, Andrew Vanderburg, et al. (2015). "WASP-47: A hot Jupiter system with two additional planets discovered by K2". In: *The Astrophysical Journal Letters* 812.2, p. L18.

Bell, Cameron PM et al. (2013). “Pre-main-sequence isochrones–II. Revising star and planet formation time-scales”. In: *Monthly Notices of the Royal Astronomical Society* 434.1, pp. 806–831.

Belyaev, Mikhail A, Roman R Rafikov, and James M Stone (2013). “Angular Momentum Transport by Acoustic Modes Generated in the Boundary Layer. I. Hydrodynamical Theory and Simulations”. In: *The Astrophysical Journal* 770.1, p. 67.

Beuther, Henrik et al. (2014). *Protostars and planets VI*. University of Arizona Press.

Bitsch, Bertram and Wilhelm Kley (2010). “Orbital evolution of eccentric planets in radiative discs”. In: *Astronomy & Astrophysics* 523, A30.

Boley, Aaron C, AP Granados Contreras, and B Gladman (2016). “The in situ formation of giant planets at short orbital periods”. In: *The Astrophysical Journal Letters* 817.2, p. L17.

Borderies, Nicole and Peter Goldreich (1984). “A simple derivation of capture probabilities for the J+ 1: J and J+ 2: J orbit-orbit resonance problems”. In: *Celestial Mechanics and Dynamical Astronomy* 32.2, pp. 127–136.

Boué, Gwenaël, Jacques Laskar, and François Farago (2012). “A simple model of the chaotic eccentricity of Mercury”. In: *Astronomy & Astrophysics* 548, A43.

Bouvier, J (2013). “Observational studies of stellar rotation”. In: *European Astronomical Society Publications Series* 62, pp. 143–168.

Bouvier, Jérôme et al. (2014). “Angular momentum evolution of young low-mass stars and brown dwarfs: observations and theory”. In: *Protostars and Planets VI*, pp. 433–450.

Bryan, Marta L et al. (2016). “Statistics of Long Period Gas Giant Planets in Known Planetary Systems”. In: *The Astrophysical Journal* 821.2, p. 89.

Calvet, Nuria et al. (2005). “Disk evolution in the Orion OB1 association”. In: *The Astronomical Journal* 129.2, p. 935.

Caselli, Paola et al. (2002). “Dense Cores in Dark Clouds. XIV. N2H+ (1-0) maps of dense cloud cores”. In: *The Astrophysical Journal* 572.1, p. 238.

Cesaroni, R et al. (2005). “A study of the Keplerian accretion disk and precessing outflow in the massive protostar IRAS 20126+ 4104”. In: *Astronomy & Astrophysics* 434.3, pp. 1039–1054.

Chambers, John E (1999). “A hybrid symplectic integrator that permits close encounters between massive bodies”. In: *Monthly Notices of the Royal Astronomical Society* 304.4, pp. 793–799.

Chandrasekhar, S. (1939). *An introduction to the study of stellar structure*.

Chiang, EI and P Goldreich (1997). "Spectral energy distributions of T Tauri stars with passive circumstellar disks". In: *The Astrophysical Journal* 490.1, p. 368.

Chiang, Eugene and Gregory Laughlin (2013). "The minimum-mass extrasolar nebula: In situ formation of close-in super-Earths". In: *Monthly Notices of the Royal Astronomical Society* 431.4, pp. 3444–3455.

Cresswell, Paul et al. (2007). "On the evolution of eccentric and inclined protoplanets embedded in protoplanetary disks". In: *Astronomy & Astrophysics* 473.1, pp. 329–342.

Crida, A, A Morbidelli, and F Masset (2006). "On the width and shape of gaps in protoplanetary disks". In: *Icarus* 181.2, pp. 587–604.

Crida, Aurélien and Konstantin Batygin (2014). "Spin-orbit angle distribution and the origin of (mis) aligned hot Jupiters". In: *Astronomy & Astrophysics* 567, A42.

Dai, Fei and Joshua N Winn (2017). "The Oblique Orbit of WASP-107b from K2 Photometry". In: *The Astronomical Journal* 153.5, p. 205.

Danby, John (1992). "Fundamentals of celestial mechanics". In: *Richmond: Willman-Bell,| c1992, 2nd ed.*

Dawson, Rebekah I (2014). "On the tidal origin of hot Jupiter stellar obliquity trends". In: *The Astrophysical Journal Letters* 790.2, p. L31.

Dawson, Rebekah I and Eugene Chiang (2014). "A class of warm Jupiters with mutually inclined, apsidally misaligned close friends". In: *Science* 346.6206, pp. 212–216.

Dawson, Rebekah I, Ruth A Murray-Clay, and John Asher Johnson (2014). "The Photoeccentric Effect and Proto-hot Jupiters. III. A Paucity of Proto-hot Jupiters on Super-eccentric Orbits". In: *The Astrophysical Journal* 798.2, p. 66.

Donati, J-F et al. (2010). "Magnetospheric accretion and spin-down of the prototypical classical T Tauri star AA Tau". In: *Monthly Notices of the Royal Astronomical Society* 409.4, pp. 1347–1361.

Dong, Subo, Boaz Katz, and Aristotle Socrates (2013). "Warm Jupiters need close "friends" for high-eccentricity migration: a stringent upper limit on the perturber's separation". In: *The Astrophysical Journal Letters* 781.1, p. L5.

Draine, BT, WG Roberge, and Ao Dalgarno (1983). "Magnetohydrodynamic shock waves in molecular clouds". In: *The Astrophysical Journal* 264, pp. 485–507.

Duchêne, Gaspard and Adam Kraus (2013). "Stellar multiplicity". In: *Annual Review of Astronomy and Astrophysics* 51, pp. 269–310.

Eisloffel, Jochen et al. (1996). "Molecular hydrogen in the outflow from Cep E". In: *The Astronomical Journal* 112, p. 2086.

Fabrycky, Daniel C, Jack J Lissauer, et al. (2014). "Architecture of Kepler's multi-transiting systems. II. New investigations with twice as many candidates". In: *The Astrophysical Journal* 790.2, p. 146.

Fabrycky, Daniel C and Joshua N Winn (2009). "Exoplanetary spin-orbit alignment: results from the ensemble of Rossiter-McLaughlin observations". In: *The Astrophysical Journal* 696.2, p. 1230.

Fabrycky, Daniel and Scott Tremaine (2007). "Shrinking binary and planetary orbits by Kozai cycles with tidal friction". In: *The Astrophysical Journal* 669.2, p. 1298.

Fatuzzo, Marco, Fred C Adams, and Philip C Myers (2004). "Generalized collapse solutions with nonzero initial velocities for star formation in molecular cloud cores". In: *The Astrophysical Journal* 615.2, p. 813.

Fielding, Drummond B et al. (2015). "The turbulent origin of spin–orbit misalignment in planetary systems". In: *Monthly Notices of the Royal Astronomical Society* 450.3, pp. 3306–3318.

Ford, Eric B and Frederic A Rasio (2006). "On the relation between hot Jupiters and the Roche limit". In: *The Astrophysical Journal Letters* 638.1, p. L45.

– (2008). "Origins of eccentric extrasolar planets: testing the planet-planet scattering model". In: *The Astrophysical Journal* 686.1, p. 621.

Foucart, Francois and Dong Lai (2011). "Evolution of spin direction of accreting magnetic protostars and spin–orbit misalignment in exoplanetary systems–II. Warped discs". In: *Monthly Notices of the Royal Astronomical Society* 412.4, pp. 2799–2815.

Fragner, Moritz M and Richard P Nelson (2010). "Evolution of warped and twisted accretion discs in close binary systems". In: *Astronomy & Astrophysics* 511, A77.

Fulton, Benjamin J et al. (2017). "The California-Kepler Survey. III. A Gap in the Radius Distribution of Small Planets". In: *arXiv preprint arXiv:1703.10375*.

Gallet, Florian and Jérôme Bouvier (2013). "Improved angular momentum evolution model for solar-like stars". In: *Astronomy & Astrophysics* 556, A36.

Ghez, AM, G Neugebauer, and K Matthews (1993). "The multiplicity of T Tauri stars in the star forming regions Taurus-Auriga and Ophiuchus-Scorpius: A 2.2 micron speckle imaging survey". In: *The Astronomical Journal* 106, pp. 2005–2023.

Ghosh, P. and F. K. Lamb (1979). "Accretion by rotating magnetic neutron stars. III - Accretion torques and period changes in pulsating X-ray sources". In: *The Astrophysical Journal* 234, pp. 296–316. DOI: 10.1086/157498.

Ghosh, P and FK Lamb (1978). "Disk accretion by magnetic neutron stars". In: *The Astrophysical Journal* 223, pp. L83–L87.

Goldreich, Peter and Re?em Sari (2003). "Eccentricity evolution for planets in gaseous disks". In: *The Astrophysical Journal* 585.2, p. 1024.

Goldreich, Peter and Scott Tremaine (1979). "The excitation of density waves at the Lindblad and corotation resonances by an external potential". In: *The Astrophysical Journal* 233, pp. 857–871.

Goldreich, Peter and Scott Tremaine (1980). “Disk-satellite interactions”. In: *The Astrophysical Journal* 241, pp. 425–441.

Goldstein, H (1950). *Addison-Wesley World Student Series*.

Goodman, AA et al. (1993). “Dense cores in dark clouds. VIII-Velocity gradients”. In: *The Astrophysical Journal* 406, pp. 528–547.

Gregory, SG, J-F Donati, et al. (2012). “Can We Predict the Global Magnetic Topology of a Pre-main-sequence Star from Its Position in the Hertzsprung–Russell Diagram?” In: *The Astrophysical Journal* 755.2, p. 97.

Gregory, SG, M Jardine, et al. (2010). “The magnetic fields of forming solar-like stars”. In: *Reports on Progress in Physics* 73.12, p. 126901.

Gu, Pin-Gao, Douglas NC Lin, and Peter H Bodenheimer (2003). “The effect of tidal inflation instability on the mass and dynamical evolution of extrasolar planets with ultrashort periods”. In: *The Astrophysical Journal* 588.1, p. 509.

Hahn, Joseph M (2003). “The secular evolution of the primordial Kuiper Belt”. In: *The Astrophysical Journal* 595.1, p. 531.

Haisch Jr, Karl E, Elizabeth A Lada, and Charles J Lada (2001). “Disk frequencies and lifetimes in young clusters”. In: *The Astrophysical Journal Letters* 553.2, p. L153.

Hansen, Carl J, Steven D Kawaler, and Virginia Trimble (2012). *Stellar interiors: physical principles, structure, and evolution*. Springer Science & Business Media.

Hartmann, Lee (2008). “Masses and mass distributions of protoplanetary disks”. In: *Physica Scripta* 2008.T130, p. 014012.

Hashimoto, Jun et al. (2012). “Polarimetric imaging of large cavity structures in the pre-transitional protoplanetary disk around PDS 70: Observations of the disk”. In: *The Astrophysical Journal Letters* 758.1, p. L19.

Hayashi, Chushiro (1981). “Structure of the solar nebula, growth and decay of magnetic fields and effects of magnetic and turbulent viscosities on the nebula”. In: *Progress of Theoretical Physics Supplement* 70, pp. 35–53.

Henrard, J (1982). “Capture into resonance: an extension of the use of adiabatic invariants”. In: *Celestial Mechanics and Dynamical Astronomy* 27.1, pp. 3–22.

– (1993). “The adiabatic invariant in classical mechanics”. In: *Dynamics Reported* 2, pp. 117–235.

Henrard, J and A Lemaitre (1983). “A second fundamental model for resonance”. In: *Celestial Mechanics and Dynamical Astronomy* 30.2, pp. 197–218.

Henrard, Jacques (1991). “Temporary capture into resonance”. In: *Predictability, Stability, and Chaos in N-Body Dynamical Systems*. Springer, pp. 193–196.

Herbst, W (n.d.). “Eislöofffe, l J., Mund, t R., & Scholz, A. 2007”. In: *Protostars and Planets V, eds. B. Reipurth, D. Jewitt, & K. Keil (Tucson: Univ. Arizona Press)*, pp. 297–311.

Herczeg, Gregory J and Lynne A Hillenbrand (2008). “UV excess measures of accretion onto young very low mass stars and brown dwarfs”. In: *The Astrophysical Journal* 681.1, p. 594.

Hillenbrand, Lynne A (2008). “Disk-dispersal and planet-formation timescales”. In: *Physica Scripta* 2008.T130, p. 014024.

Huang, Chelsea, Yanqin Wu, and Amaury HMJ Triaud (2016). “Warm Jupiters Are Less Lonely than Hot Jupiters: Close Neighbors”. In: *The Astrophysical Journal* 825.2, p. 98.

Huber, Daniel et al. (2013). “Stellar spin-orbit misalignment in a multiplanet system”. In: *Science* 342.6156, pp. 331–334.

Irwin, Jonathan et al. (2008). “The Monitor project: rotation of low-mass stars in NGC 2362–testing the disc regulation paradigm at 5 Myr”. In: *Monthly Notices of the Royal Astronomical Society* 384.2, pp. 675–686.

Jackson, John David (1998). “Classical Electrodynamics”. In: *Classical Electrodynamics, 3rd Edition, by John David Jackson, pp. 832. ISBN 0-471-30932-X. Wiley-VCH, July 1998.* P. 832.

Jensen, Eric LN and Rachel Akeson (2014). “Misaligned protoplanetary disks in a young binary star system”. In: *Nature* 511.7511, pp. 567–569.

Jijina, J, PC Myers, and Fred C Adams (1999). “Dense cores mapped in ammonia: a database”. In: *The Astrophysical Journal Supplement Series* 125.1, p. 161.

Johansen, Anders et al. (2012). “Can planetary instability explain the Kepler dichotomy?” In: *The Astrophysical Journal* 758.1, p. 39.

Johns-Krull, Christopher M (2007). “The magnetic fields of classical T Tauri stars”. In: *The Astrophysical Journal* 664.2, p. 975.

Jontof-Hutter, Daniel et al. (2016). “Secure mass measurements from transit timing: 10 Kepler exoplanets between 3 and 8 M with diverse densities and incident fluxes”. In: *The Astrophysical Journal* 820.1, p. 39.

Kant, I (1755). *General History of Nature and Theory of the Heavens*.

Karim, Md Tanveer et al. (2016). “The Rotation Period Distributions of 4–10 Myr T Tauri Stars in Orion OB1: New Constraints on Pre-main-sequence Angular Momentum Evolution”. In: *The Astronomical Journal* 152.6, p. 198.

Kaula, William M (1962). “Development of the lunar and solar disturbing functions for a close satellite”. In: *The Astronomical Journal* 67, p. 300.

Kley, Wilhelm and RP Nelson (2012). “Planet-disk interaction and orbital evolution”. In: *Annual Review of Astronomy and Astrophysics* 50, pp. 211–249.

Knutson, Heather A et al. (2014). "Friends of hot Jupiters. I. A radial velocity search for massive, long-period companions to close-in gas giant planets". In: *The Astrophysical Journal* 785.2, p. 126.

Koenigl, Arieh (1991). "Disk accretion onto magnetic T Tauri stars". In: *The Astrophysical Journal* 370, pp. L39–L43.

Koresko, Chris D (1998). "A Circumstellar Disk in a Pre-main-sequence binary Star". In: *The Astrophysical Journal Letters* 507.2, p. L145.

Kozai, Yoshihide (1962). "Secular perturbations of asteroids with high inclination and eccentricity". In: *The Astronomical Journal* 67, p. 591.

Krasnopolsky, Ruben, Hsien Shang, and Zhi-Yun Li (2009). "Topologies of Current-free Axisymmetric Magnetospheres in Star-Disk Systems". In: *The Astrophysical Journal* 703.2, p. 1863.

Kraus, Adam L et al. (2011). "Mapping the shores of the brown dwarf desert. II. Multiple star formation in Taurus-Auriga". In: *The Astrophysical Journal* 731.1, p. 8.

Kretke, KA et al. (2012). "A method to constrain the size of the protosolar nebula". In: *The Astronomical Journal* 143.4, p. 91.

Lada, Charles J (1985). "Cold outflows, energetic winds, and enigmatic jets around young stellar objects". In: *Annual Review of Astronomy and Astrophysics* 23.1, pp. 267–317.

Lai, D. and B. Pu (2017). "Hiding Planets behind a Big Friend: Mutual Inclinations of Multi-planet Systems with External Companions". In: *The Astronomical Journal* 153, 42, p. 42. DOI: 10.3847/1538-3881/153/1/42. arXiv: 1606.08855 [astro-ph.EP].

Lai, Dong (1999). "Magnetically Driven Warping, Precession, and Resonances in Accretion Disks". In: *The Astrophysical Journal* 524.2, p. 1030.

– (2012). "Tidal dissipation in planet-hosting stars: damping of spin–orbit misalignment and survival of hot Jupiters". In: *Monthly Notices of the Royal Astronomical Society* 423.1, pp. 486–492.

– (2014). "Star–disc–binary interactions in protoplanetary disc systems and primordial spin–orbit misalignments". In: *Monthly Notices of the Royal Astronomical Society* 440.4, pp. 3532–3544.

Lai, Dong, Francois Foucart, and Douglas NC Lin (2011). "Evolution of spin direction of accreting magnetic protostars and spin–orbit misalignment in exoplanetary systems". In: *Monthly Notices of the Royal Astronomical Society* 412.4, pp. 2790–2798.

Laplace, PS (1796). "Exposition du systéme du monde, vol. II". In: *De l?Imprimierie du Circle Social Paris*.

Larwood, JD et al. (1996). “The tidally induced warping, precession and truncation of accretion discs in binary systems: three-dimensional simulations”. In: *Monthly Notices of the Royal Astronomical Society* 282.2, pp. 597–613.

Laskar, Jacques (1996). “Large scale chaos and marginal stability in the solar system”. In: *Chaos in Gravitational N-Body Systems*. Springer, pp. 115–162.

Laughlin, Gregory (2009). “Planetary science: The Solar System’s extended shelf life”. In: *Nature* 459.7248, pp. 781–782.

Laughlin, Gregory, Peter Bodenheimer, and Fred C Adams (2004). “The core accretion model predicts few Jovian-mass planets orbiting red dwarfs”. In: *The Astrophysical Journal Letters* 612.1, p. L73.

Laughlin, Gregory, John Chambers, and Debra Fischer (2002). “A dynamical analysis of the 47 Ursae Majoris planetary system”. In: *The Astrophysical Journal* 579.1, p. 455.

Le Verrier, UJJ (1856). “Ann. Obs. Paris, II”. In:

Lee, C. W., P. C. Myers, and M. Tafalla (1999). “A Survey of Infall Motions toward Starless Cores. I. CS (2-1) and N_2H^+ (1-0) Observations”. In: *The Astrophysical Journal* 526, pp. 788–805. DOI: 10.1086/308027. eprint: astro-ph/9906468.

Lee, Eve J and Eugene Chiang (2016). “Breeding super-Earths and birthing super-puffs in transitional disks”. In: *The Astrophysical Journal* 817.2, p. 90.

Li, Gongjie and Joshua N Winn (2016). “ARE TIDAL EFFECTS RESPONSIBLE FOR EXOPLANETARY SPIN–ORBIT ALIGNMENT?” In: *The Astrophysical Journal* 818.1, p. 5.

Lichtenberg, Allen J and Michael A Lieberman (1992). “Regular and Chaotic Dynamics, vol. 38 of”. In: *Applied Mathematical Sciences*.

Lin, DNC and John Papaloizou (1986). “On the tidal interaction between protoplanets and the protoplanetary disk. III-Orbital migration of protoplanets”. In: *The Astrophysical Journal* 309, pp. 846–857.

Lin, Douglas NC, Peter Bodenheimer, and Derek C Richardson (1996). “Orbital migration of the planetary companion of 51 Pegasi to its present location”. In:

Lissauer, Jack J, Daniel C Fabrycky, et al. (2011). “A closely packed system of low-mass, low-density planets transiting Kepler-11”. In: *Nature* 470.7332, pp. 53–58.

Lissauer, Jack J, Daniel Jontof-Hutter, et al. (2013). “All six planets known to orbit Kepler-11 have low densities”. In: *The Astrophysical Journal* 770.2, p. 131.

Lissauer, Jack J, Darin Ragozzine, et al. (2011). “Architecture and dynamics of Kepler’s candidate multiple transiting planet systems”. In: *The Astrophysical Journal Supplement Series* 197.1, p. 8.

Lithwick, Yoram and Yanqin Wu (2012). “Resonant repulsion of Kepler planet pairs”. In: *The Astrophysical Journal Letters* 756.1, p. L11.

Littlefair, SP et al. (2010). “Rotation of young stars in Cepheus OB3b”. In: *Monthly Notices of the Royal Astronomical Society* 403.2, pp. 545–557.

Livio, M and JE Pringle (1992). “Dwarf nova outbursts–the ultraviolet delay and the effect of a weakly magnetized white dwarf”. In: *Monthly Notices of the Royal Astronomical Society* 259.1, 23P–26P.

Long, Min, MM Romanova, and RVE Lovelace (2005). “Locking of the rotation of disk-accreting magnetized stars”. In: *The Astrophysical Journal* 634.2, p. 1214.

Malmberg, Daniel et al. (2007). “Close encounters in young stellar clusters: implications for planetary systems in the solar neighbourhood”. In: *Monthly Notices of the Royal Astronomical Society* 378.3, pp. 1207–1216.

Marcy, Geoffrey W and R Paul Butler (1996). “A planetary companion to 70 Virginis”. In: *The Astrophysical Journal Letters* 464.2, p. L147.

Marks, Michael and Pavel Kroupa (2012). “Inverse dynamical population synthesis-Constraining the initial conditions of young stellar clusters by studying their binary populations”. In: *Astronomy & Astrophysics* 543, A8.

Matt, Sean and Ralph E Pudritz (2004). “Does disk locking solve the stellar angular momentum problem?” In: *The Astrophysical Journal Letters* 607.1, p. L43.

– (2005). “The spin of accreting stars: dependence on magnetic coupling to the disc”. In: *Monthly Notices of the Royal Astronomical Society* 356.1, pp. 167–182.

Mayor, Michel and Didier Queloz (1995). “A Jupiter-mass companion to a solar-type star”. In: *Nature* 378, pp. 355–359.

Mazeh, Tsevi et al. (2015). “Photometric Amplitude Distribution of Stellar Rotation of KOIs?Indication for Spin-Orbit Alignment of Cool Stars and High Obliquity for Hot Stars”. In: *The Astrophysical Journal* 801.1, p. 3.

McKee, Christopher F and Eve C Ostriker (2007). “Theory of star formation”. In: *Annual Review of Astronomy and Astrophysics* 45.

McLaughlin, DB (1924). “Some results of a spectrographic study of the Algol system.” In: *The Astrophysical Journal* 60.

McQuillan, Amy, Tsevi Mazeh, and Suzanne Aigrain (2013). “Stellar rotation periods of the Kepler Objects of Interest: A dearth of close-in planets around fast rotators”. In: *The Astrophysical Journal Letters* 775.1, p. L11.

Mestel, Leon (1963). “On the galactic law of rotation”. In: *Monthly Notices of the Royal Astronomical Society* 126.6, pp. 553–575.

Millholland, Sarah, Songhu Wang, and Gregory Laughlin (2016). “On the Detection of Non-transiting Hot Jupiters in Multiple-planet Systems”. In: *The Astrophysical Journal Letters* 823.1, p. L7.

Mills, Sean M et al. (2016). "A resonant chain of four transiting, sub-Neptune planets". In: *Nature* 533.7604, pp. 509–512.

Mohanty, Subhanjoy and Frank H Shu (2008). "Magnetocentrifugally Driven Flows from Young Stars and Disks. VI. Accretion with a Multipole Stellar Field". In: *The Astrophysical Journal* 687.2, p. 1323.

Morbidelli, Alessandro (2002). *Modern celestial mechanics: aspects of solar system dynamics*. Vol. 1.

Morbidelli, Alessandro and Aurélien Crida (2007). "The dynamics of Jupiter and Saturn in the gaseous protoplanetary disk". In: *Icarus* 191.1, pp. 158–171.

Morbidelli, Alessandro, Kleomenis Tsiganis, et al. (2012). "Explaining why the uranian satellites have equatorial prograde orbits despite the large planetary obliquity". In: *Icarus* 219.2, pp. 737–740.

Moriarty, John and Sarah Ballard (2016). "The Kepler dichotomy in planetary disks: Linking Kepler observables to simulations of late-stage planet formation". In: *The Astrophysical Journal* 832.1, p. 34.

Morton, Timothy D, Stephen T Bryson, et al. (2016). "False positive probabilities for all Kepler objects of interest: 1284 newly validated planets and 428 likely false positives". In: *The Astrophysical Journal* 822.2, p. 86.

Morton, Timothy D and Joshua N Winn (2014). "Obliquities of Kepler stars: Comparison of single-and multiple-transit systems". In: *The Astrophysical Journal* 796.1, p. 47.

Murray, Carl D and Stanley F Dermott (1999). *Solar system dynamics*. Cambridge university press.

Myers, PC and GA Fuller (1992). "Density structure and star formation in dense cores with thermal and nonthermal motions". In: *The Astrophysical Journal* 396, pp. 631–642.

Nagasawa, M, S Ida, and T Bessho (2008). "Formation of hot planets by a combination of planet scattering, tidal circularization, and the Kozai mechanism". In: *The Astrophysical Journal* 678.1, p. 498.

Naoz, Smadar, Will M Farr, Yoram Lithwick, et al. (2011). "Hot Jupiters from secular planet-planet interactions". In: *Nature* 473.7346, pp. 187–189.

Naoz, Smadar, Will M Farr, and Frederic A Rasio (2012). "On the formation of hot Jupiters in stellar binaries". In: *The Astrophysical Journal Letters* 754.2, p. L36.

Nelson, Benjamin E, Eric B Ford, et al. (2014). "The 55 Cancri planetary system: fully self-consistent N-body constraints and a dynamical analysis". In: *Monthly Notices of the Royal Astronomical Society* 441.1, pp. 442–451.

Nelson, Richard P, John CB Papaloizou, et al. (2000). "The migration and growth of protoplanets in protostellar discs". In: *Monthly Notices of the Royal Astronomical Society* 318.1, pp. 18–36.

Nesvorný, David et al. (2012). “The detection and characterization of a nontransiting planet by transit timing variations”. In: *Science* 336.6085, pp. 1133–1136.

Nobili, Anna and Ian W Roxburgh (1986). “Simulation of general relativistic corrections in long term numerical integrations of planetary orbits”. In: *Relativity in Celestial Mechanics and Astrometry. High Precision Dynamical Theories and Observational Verifications*. Vol. 114, pp. 105–110.

Peale, S. J. (1986). “Orbital resonances, unusual configurations and exotic rotation states among planetary satellites”. In: *IAU Colloq. 77: Some Background about Satellites*. Ed. by J. A. Burns and M. S. Matthews, pp. 159–223.

Peale, Stanton J et al. (2014). “Effect of core–mantle and tidal torques on Mercury?s spin axis orientation”. In: *Icarus* 231, pp. 206–220.

Petrovich, Cristobal (2015a). “Hot jupiters from coplanar high-eccentricity migration”. In: *The Astrophysical Journal* 805.1, p. 75.

– (2015b). “Steady-state planet migration by the Kozai-Lidov mechanism in stellar binaries”. In: *The Astrophysical Journal* 799.1, p. 27.

Petrovich, Cristobal and Scott Tremaine (2016). “WARM JUPITERS FROM SECULAR PLANET–PLANET INTERACTIONS”. In: *The Astrophysical Journal* 829.2, p. 132.

Pollack, James B et al. (1996). “Formation of the giant planets by concurrent accretion of solids and gas”. In: *icarus* 124.1, pp. 62–85.

Rafikov, Roman R (2006). “Atmospheres of protoplanetary cores: critical mass for nucleated instability”. In: *The Astrophysical Journal* 648.1, p. 666.

– (2012). “How to build Tatooine: reducing secular excitation in Kepler circumbinary planet formation”. In: *arXiv preprint arXiv:1212.2217*.

Rice, WKM, Philip J Armitage, and DF Hogg (2008). “Why are there so few hot Jupiters?” In: *Monthly Notices of the Royal Astronomical Society* 384.3, pp. 1242–1248.

Ricker, George R et al. (2015). “Transiting exoplanet survey satellite”. In: *Journal of Astronomical Telescopes, Instruments, and Systems* 1.1, pp. 014003–014003.

Rogers, TM and DNC Lin (2013). “On the tidal dissipation of obliquity”. In: *The Astrophysical Journal Letters* 769.1, p. L10.

Rogers, TM, DNC Lin, and HHB Lau (2012). “Internal gravity waves modulate the apparent misalignment of exoplanets around hot stars”. In: *The Astrophysical Journal Letters* 758.1, p. L6.

Romanova, MM et al. (2012). “MRI-driven accretion on to magnetized stars: global 3D MHD simulations of magnetospheric and boundary layer regimes”. In: *Monthly Notices of the Royal Astronomical Society* 421.1, pp. 63–77.

Rossiter, RA (1924). "On the detection of an effect of rotation during eclipse in the velocity of the brigher component of beta Lyrae, and on the constancy of velocity of this system." In: *The Astrophysical Journal* 60.

Sadavoy, Sarah I and Steven W Stahler (2017). "Embedded binaries and their dense cores". In: *Monthly Notices of the Royal Astronomical Society* 469.4, pp. 3881–3900.

Shakura, N I? And Rashid Alievich Sunyaev (1973). "Black holes in binary systems. Observational appearance." In: *Astronomy and Astrophysics* 24, pp. 337–355.

Shu, Frank H (1977). "Self-similar collapse of isothermal spheres and star formation". In: *The Astrophysical Journal* 214, pp. 488–497.

Shu, Frank H, Fred C Adams, and Susana Lizano (1987). "Star formation in molecular clouds: observation and theory". In: *Annual review of astronomy and astrophysics* 25.1, pp. 23–81.

Shu, Frank, Joan Najita, et al. (1994). "Magnetocentrifugally driven flows from young stars and disks. 1: A generalized model". In: *The Astrophysical Journal* 429, pp. 781–796.

Siess, L, E Dufour, and M Forestini (2000). "An internet server for pre-main sequence tracks of low-and intermediate-mass stars". In: *Astronomy and Astrophysics* 358, pp. 593–599.

Sivia, DS (1996). "Data Analysis: A Bayesian Tutorial (Oxford Science Publications)". In:

Spalding, Christopher and Konstantin Batygin (2014). "Early excitation of spin-orbit misalignments in close-in planetary systems". In: *The Astrophysical Journal* 790.1, p. 42.

– (2015). "Magnetic Origins of the Stellar Mass-Obliquity Correlation in Planetary Systems". In: *The Astrophysical Journal* 811.2, p. 82.

– (2016). "SPIN–ORBIT MISALIGNMENT AS A DRIVER OF THE KEPLER DICHOTOMY". In: *The Astrophysical Journal* 830.1, p. 5.

– (2017). "A Secular Resonant Origin for the Loneliness of Hot Jupiters". In: *The Astronomical Journal* 154.3, p. 93.

Spalding, Christopher, Konstantin Batygin, and Fred C Adams (2014). "Alignment of Protostars and Circumstellar Disks during the Embedded Phase". In: *The Astrophysical Journal Letters* 797.2, p. L29.

Stahler, STEVEN W, FRANK H Shu, and RONALD E Taam (1980). "The evolution of protostars. I-Global formulation and results". In: *The Astrophysical Journal* 241, pp. 637–654.

Stapelfeldt, Karl R et al. (1998). “An Edge-on Circumstellar Disk in the Young Binary System HK TauriUsing the NASA/ESA Hubble Space Telescope. Based on observations made with the Canada-France-Hawaii Telescope, operated by the NRC of Canada, the CNRS de France, and the University of Hawaii.” In: *The Astrophysical Journal Letters* 502.1, p. L65.

Steffen, Jason H et al. (2012). “Kepler constraints on planets near hot Jupiters”. In: *Proceedings of the National Academy of Sciences* 109.21, pp. 7982–7987.

Sterne, Theodore Eugene (1939). “Apsidal motion in binary stars”. In: *Monthly Notices of the Royal Astronomical Society* 99, pp. 451–462.

Stevenson, David John (1982). “Formation of the giant planets”. In: *Planetary and Space Science* 30.8, pp. 755–764.

Storch, Natalia I, Kassandra R Anderson, and Dong Lai (2014). “Chaotic dynamics of stellar spin in binaries and the production of misaligned hot Jupiters”. In: *Science* 345.6202, pp. 1317–1321.

Tanaka, Hidekazu, Taku Takeuchi, and William R Ward (2002). “Three-dimensional interaction between a planet and an isothermal gaseous disk. I. Corotation and Lindblad torques and planet migration”. In: *The Astrophysical Journal* 565.2, p. 1257.

Tanaka, Hidekazu and William R Ward (2004). “Three-dimensional interaction between a planet and an isothermal gaseous disk. II. Eccentricity waves and bending waves”. In: *The Astrophysical Journal* 602.1, p. 388.

Touma, JR, S Tremaine, and MV Kazandjian (2009). “Gauss’s method for secular dynamics, softened”. In: *Monthly Notices of the Royal Astronomical Society* 394.2, pp. 1085–1108.

Tremaine, Scott and Subo Dong (2012). “The statistics of multi-planet systems”. In: *The Astronomical Journal* 143.4, p. 94.

Uzdensky, Dmitri A, Arieh Königl, and C Litwin (2002). “Magnetically linked star-disk systems. I. Force-free magnetospheres and effects of disk resistivity”. In: *The Astrophysical Journal* 565.2, p. 1191.

Veras, Dimitri and Philip J Armitage (2004). “The dynamics of two massive planets on inclined orbits”. In: *Icarus* 172.2, pp. 349–371.

Wald, Robert M (2010). *General relativity*. University of Chicago press.

Walsh, Kevin J et al. (2011). “A low mass for Mars from Jupiter/’s early gas-driven migration”. In: *Nature* 475.7355, pp. 206–209.

Wang, Songhu et al. (2017). “Stellar Spin-Orbit Alignment for Kepler-9, a Multi-transiting Planetary system with Two Outer Planets Near 2: 1 Resonance”. In: *arXiv preprint arXiv:1712.06409*.

Ward, William R (1981). “Solar nebula dispersal and the stability of the planetary system: I. Scanning secular resonance theory”. In: *Icarus* 47.2, pp. 234–264.

Ward, William R (1986). “Density waves in the solar nebula: Diffential Lindblad torque”. In: *Icarus* 67.1, pp. 164–180.

Ward, William R, G Colombo, and FA Franklin (1976). “Secular resonance, solar spin down, and the orbit of Mercury”. In: *Icarus* 28.4, pp. 441–452.

Ward-Thompson, Derek (2002). “Isolated star formation: from cloud formation to core collapse”. In: *Science* 295.5552, pp. 76–81.

Weiss, Lauren M et al. (2017). “New Insights on Planet Formation in WASP-47 from a Simultaneous Analysis of Radial Velocities and Transit Timing Variations”. In: *The Astronomical Journal* 153.6, p. 265.

Williams, Jonathan P and Lucas A Cieza (2011). “Protoplanetary disks and their evolution”. In: *Annual Review of Astronomy and Astrophysics* 49, pp. 67–117.

Winn, Joshua N and Daniel C Fabrycky (2015). “The occurrence and architecture of exoplanetary systems”. In: *Annual Review of Astronomy and Astrophysics* 53.

Winn, Joshua N, Daniel Fabrycky, et al. (2010). “Hot stars with hot Jupiters have high obliquities”. In: *The Astrophysical Journal Letters* 718.2, p. L145.

Winn, Joshua N, Andrew W Howard, et al. (2011). “Orbital orientations of Exoplanets: HAT-P-4b is prograde and HAT-P-14b is retrograde”. In: *The Astronomical Journal* 141.2, p. 63.

Winn, Joshua N, Robert W Noyes, et al. (2005). “Measurement of spin-orbit alignment in an extrasolar planetary system”. In: *The Astrophysical Journal* 631.2, p. 1215.

Winn, Joshua N, Erik A Petigura, et al. (2017). “Constraints on Obliquities of Kepler Planet-Hosting Stars”. In: *arXiv preprint arXiv:1710.04530*.

Wright, Jason T et al. (2011). “The exoplanet orbit database”. In: *Publications of the Astronomical Society of the Pacific* 123.902, p. 412.

Wu, Yanqin and Yoram Lithwick (2011). “Secular chaos and the production of hot Jupiters”. In: *The Astrophysical Journal* 735.2, p. 109.

Wu, Yanqin and Norm Murray (2003). “Planet migration and binary companions: The case of HD 80606b”. In: *The Astrophysical Journal* 589.1, p. 605.

Xiang-Gruess, M and JCB Papaloizou (2014). “Evolution of a disc–planet system with a binary companion on an inclined orbit”. In: *Monthly Notices of the Royal Astronomical Society* 440.2, pp. 1179–1192.

Zanni, Claudio and Jonathan Ferreira (2013). “MHD simulations of accretion onto a dipolar magnetosphere-II. Magnetospheric ejections and stellar spin-down”. In: *Astronomy & Astrophysics* 550, A99.